Master Thesis, Department of Geosciences

Reservoir Quality of Lower-Middle Jurassic Sandstones within the Johan Castberg Field in the SW Barents Sea

Petrographical and Petrophysical approach

Saadullah Nisar

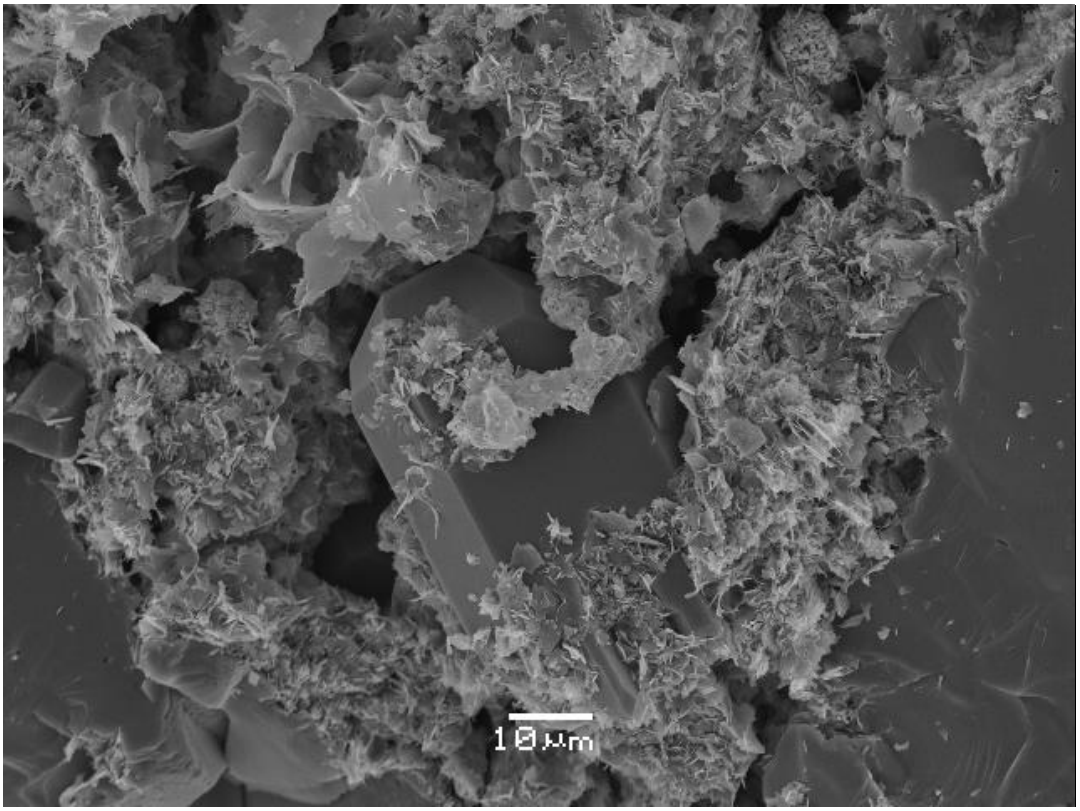

UNIVERSITY OF OSLO

FACULTY OF MATHEMATICS AND NATURAL SCIENCES

Reservoir Quality of Lower-Middle Jurassic Sandstones within the Johan Castberg Field in the SW Barents Sea

Petrographical and Petrophysical approach

Saadullah Nisar

Master Thesis in Geosciences

Discipline: Geology

Department of Geosciences

Faculty of Mathematics and Natural Sciences

University of Oslo

15/06/2015

Tutor: Jens Jahren
This work is published digitally through DUO – Digitale Utgivelser ved UiO
http://www.duo.uio.no
It is also catalogued in BIBSYS (http://www.bibsys.no/english)

DEDICATION

To

My Family

ACKNOWLEDGEMENTS

Glory be to Allah the Lord of Heaven and Earth and Praises to Hazrat Muhammad (P.B.U.H) who is the source of knowledge for all the mankind. I would like to acknowledge the enthusiastic supervision of Jens Jahren and my Co-supervisors Richard Olstad throughout my thesis.

I wish to express my special gratitude to Berit Løken Berg and Maarten Aerts for always being supportive and helpful during SEM & XRD studies. I also express my thanks to Beyene Girma Haile, Oluwakemi Ogebule, Irfan Baig and Muhammad koochak Zahed.

Cordial thanks to all my team in Gamla Raadhus Resturant for their support and motivation during this critical time especially Eirik Strøm Lillebø, Jørn Lie, Uffe Svensson, Jørgen pedersen, Knut Dale Svendsen, Mikael Supertramp, Siv Anita Reime, Mathias Jahr, Hans-Christian Grue, Matilde Paulsrud Curti and Nathalie Svensson.

Special thanks to all my friends in Oslo especially Asad khan Khattak (sakhtee and buzurgi), Qazi Abdul Jabbar , Tauqeer Ahmed saadi(amigo), Moiz pirzada, Russian guy Fahad, Shah Jee, Mohsin Londa, Umair Delta Bhata, Zubair gaam, Mansoor baba jee, Arshad bahi halkay, and all my friends and class fellows for their guidance and support throughout the thesis.

I also like to appreciate Marta Kaer for not giving me any support.

ABSTRACT

The study area is located in the Bjørnøya basin, the southwestern Barents Sea. It is surrounded by the Loppa High and Sub-platform to the east and southeast, the Veslemøy high to the west and to the north by the Bjørnøyrenna Fault Complex. There are two wells included in the study area. Well 7219/8-1 is located in the Bjørnøya Sør area, west of the Loppa high and 7220/7-1 is the other well, located west of the Veslemøy High. The Stø and Nordmela Formations of Lower to middle Jurassic ages are the target reservoirs in the study area where the Stø Formation is the main reservoir. Both petrophysical and petrographical analysis has been carried out using cored intervals from both wells. Well correlation and cross plots have been used in petrophysical analysis and point count analysis, scanning electron microscope, cathode luminescence and X-ray diffraction analysis has been carried out in petrographical analysis.

Sandstone of the Stø Formation is quartz arenite and is texturally and minerlogically mature. On the other hand, the Nordmela Formations is quartz to sub-feldspathic arenite and minerlogically mature. Reservoir quality of the Stø Formation in well 7219/8-1 is poor due to very low porosity but porosity is good in well 7220/7-1 and act as a good reservoir. Porosity in the Nordmela Formation is good but permeability affects its reservoir quality.

Quartz cementation and pressure solution are the factors controlling chemical compaction. Stø formation in well 7219/8-1 is highly compacted due to cementation and pressure solution but the Stø and Nordmela Formation in well 7220/7-1 is slightly affected by quartz cementation and having a well preserved porosity.

Abnormally high intergranular volume in two of the samples from well 7220/7-1 and 7219/8-1 is mainly due to the presence high amount of carbonate cement (siderite). Siderite is present as a detrital grain during early diagenesis and then dissolution and recrystallization at deeper depth causes this increase in IGV value.

Contents

1 INTRODUCTION

1.1 Introduction

The three main provinces on the Norwegian Continental Shelf are shown in Fig. 1.1 (Faleide et al., 2010).

- North Sea
- Mid-Norwegian continental margin
- Western Barents Sea.

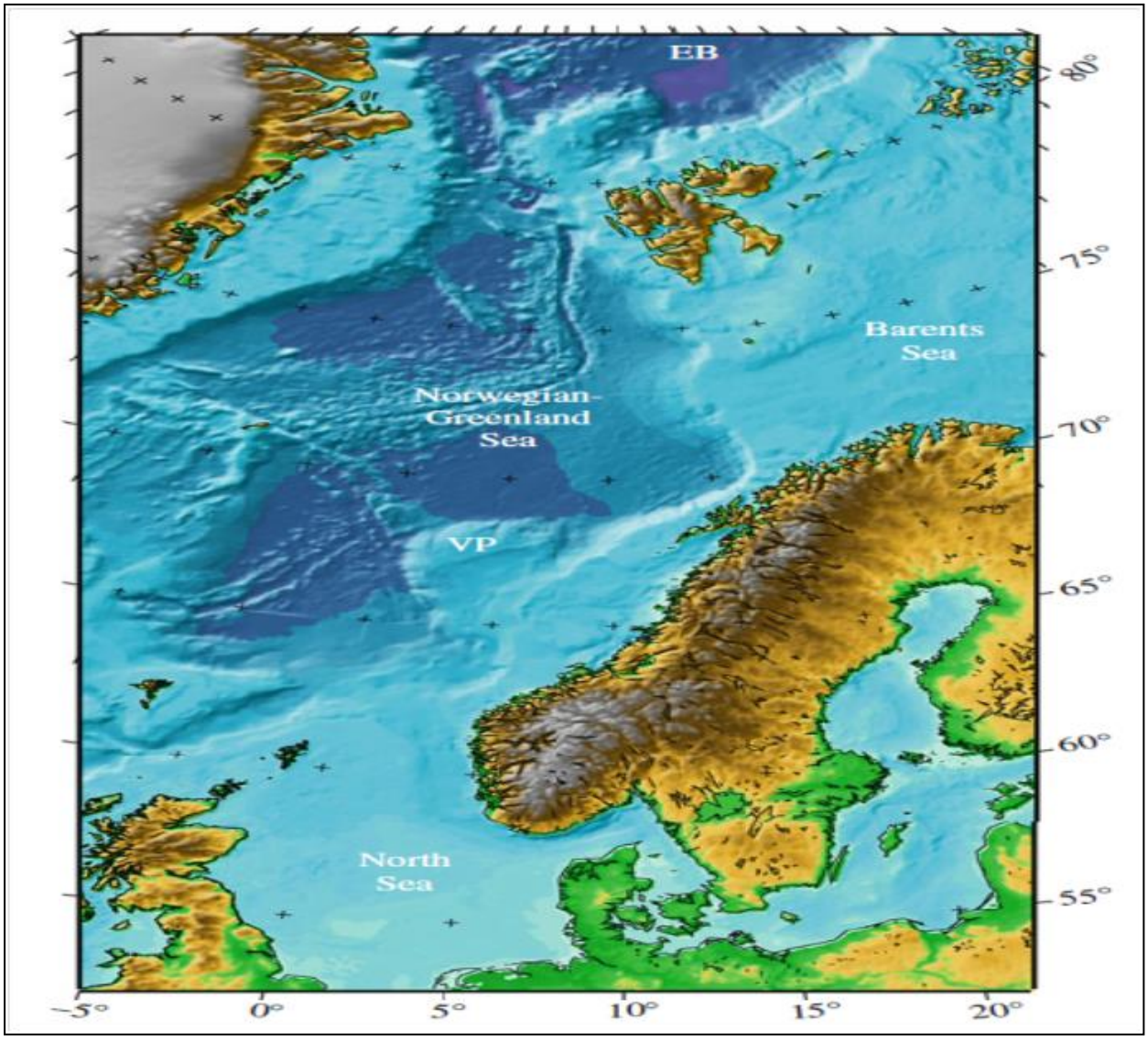

Figure 1.1: Regional setting of Norwegian Continental Shelf and adjoining areas (Faleide et al., 2010).

These three provinces were together in the form of large epicontinental sea which was present between the Fennoscandia, Svalbard and Greenland continental masses before the continental

breakup of the Norwegian-Greenland Sea and beginning of seafloor spreading (Faleide et al., 2010).

1.2 Introduction of the Barents Sea Area

Area covering around 1.3 million square km, the Barents Sea is considered to be one of the largest continental shelf with respect to area surrounded physiographically by the north Norwegian and Russian coasts, the Novaya Zemlya, Franz Josef Land and Svalbard Archipelagos, and the eastern margin of the deep Atlantic Ocean, with average depth of water around 300m (Doré, 1995).

The portion currently available for hydrocarbon exploration of the Barents Sea is itself covers 230 000 square kilometer, that is one and a half times more than the area of the Norwegian sector of the North sea. Reserves of 260-300 billion cubic meters of gas, with minor oil has been estimated after drilling in the Norwegian waters (Dore, 1995) with Jurassic sandstone containing most reserves and Triassic to a lesser extent (Stilwell, 2012).

1.3 Exploration History

On the Norwegian Shelf, petroleum activities commenced about 50 years ago and still many of the early fields are producing. With the discovery of Ekofisk , the Norwegian oil era started in 1969 (NPD, 2014). First offshore drilling in the Barents Sea area took place in early 1980s with the help of geophysical investigation that began during 1970s (Doré, 1995) In the early 1980's exploration on the Norwegian Shelf for assessable hydrocarbon resources increased in the northwards and western Barents shelf. Jurassic succession gained attention where the main geological targets for hydrocarbon exploration are reservoirs of the Lower-Middle Jurassic and source rocks of Upper Jurassic (Smelror, 1994). In the Snøhvit Field (Blocks 7120/6 and 7121/4) the first oil was found in 1984 however the Snøhvit field proved to be mainly a gas field because of the fact that the oil column was thin (Berglund et al., 1986).

In the Barents Sea about 25 discoveries have been made (Faleide et al., 2010) where the Snøhvit, Albatross and Askeladden are the major discoveries and all have the major reservoirs in Lower-Middle Jurassic age deltaic and shallow marine sandstone (Smelror, 1994) particularly in the Stø formation of coastal marine environment commonly has good

reservoir properties. About 85% resources of the Norwegian Barents Sea lie within the Stø Formation (Doré, 1995).

Although the fields discovered so far in the southwestern Barents Sea shelf are mostly gas fields but it still received considerable attention due to expected petroleum potential (Breivik et al., 1998).

In the Barents Sea the year 2011 opened with the news of the 7220/7-1 ("Havis") discovery along with 7220/8-1 ("skrugard") find, which is approximately of the same size makes perspectives exciting for these waters (NPD, 2012) and these discoveries for example the 7220/8-1 Skrugard and 7220/7-1 Havis represent a single project in the planned development of the Johan Castberg that comprises 51 percent of the discovery resources in the Barents Sea (NPD, 2014).

1.4 Exploration Problems

In the western Barents Sea the most significant exploration problem was caused due to the severe uplift and erosion in the Cenozoic era (Faleide et al., 2010). Most of the oil from the traps are expelled as a result of decrease in pressure which causes expansion of the gas, and from oil, exsolution of gas. Seal breaking and oil spillage probably also occurred/took place as a result of uplift. Cooling of source rock ceases effectively most of the hydrocarbon generation which also caused due to a further effect of these late movements in the area. Thus to fill the available trapping space, little new oil was available and hence the predominance of gas over oil is explained by these mechanisms in the Barents Sea (Doré, 1995).

1.5 Research Objectives

The main purpose of this master thesis is to give better understanding of the reservoir quality of Jurassic sandstone , the Stø and Nordmela Formation in the Johan Castberg area (Havis and Skrugard) the southwestern Barents Sea from the cored reservoir interval of given two wells.

During this study 20 thin section samples from each wells 7219/8-1 and 7220/7-1 are made from the cores and observed under microscope.

Moreover both gold coated stubs mounted samples along with carbon coated thin section slides are used for SEM analysis. In order to confirm the mineralogy, XRD analysis has been

performed on all bulk separation samples. By using these above mentioned techniques, depositional environment along with provenance can be interpreted that is a function of lithology, grain size distribution and sorting.

In order to compare the reservoir properties of different reservoir units both mineralogical and petrological analysis of these wells are made. Both core material and geophysical logs will be included in this study and for facies distribution analysis results from logged cores will be compared with released core plug data.

1.6 Study Area

The study area is located in the Bjørnøya Basin in the southwestern Barents Sea surrounded by the Veslemøy High to the west, Loppa High and Sub-platform to the east and southeast and the Bjørnøyrenna Fault Complex to the North. There are two well that are included in the study area where well 7219/8-1 is located in the Bjørnøya Sør area west of the Veslemøy High and 7220/7-1 was drilled in the Barents Sea at the southwest of the 7220/8-1 (Skrugard discovery) and west of Loppa High (NPD) .

At 240 kilometers north-west of the Hammerfest in Norway, approximately 100 kilometers north of the Snøhvit-field, 150 kilometers from the Goliat and nearly 240 kilometers from the Milkoya. The Johan Castberg (PL 532) is located including two main discoveries, the Skrugard from April 2011 and Havis in January 2012 (Fig. 1.2). Around 400-600 million barrels of oil are initial volume estimation and 360-390 meters is the water depth.

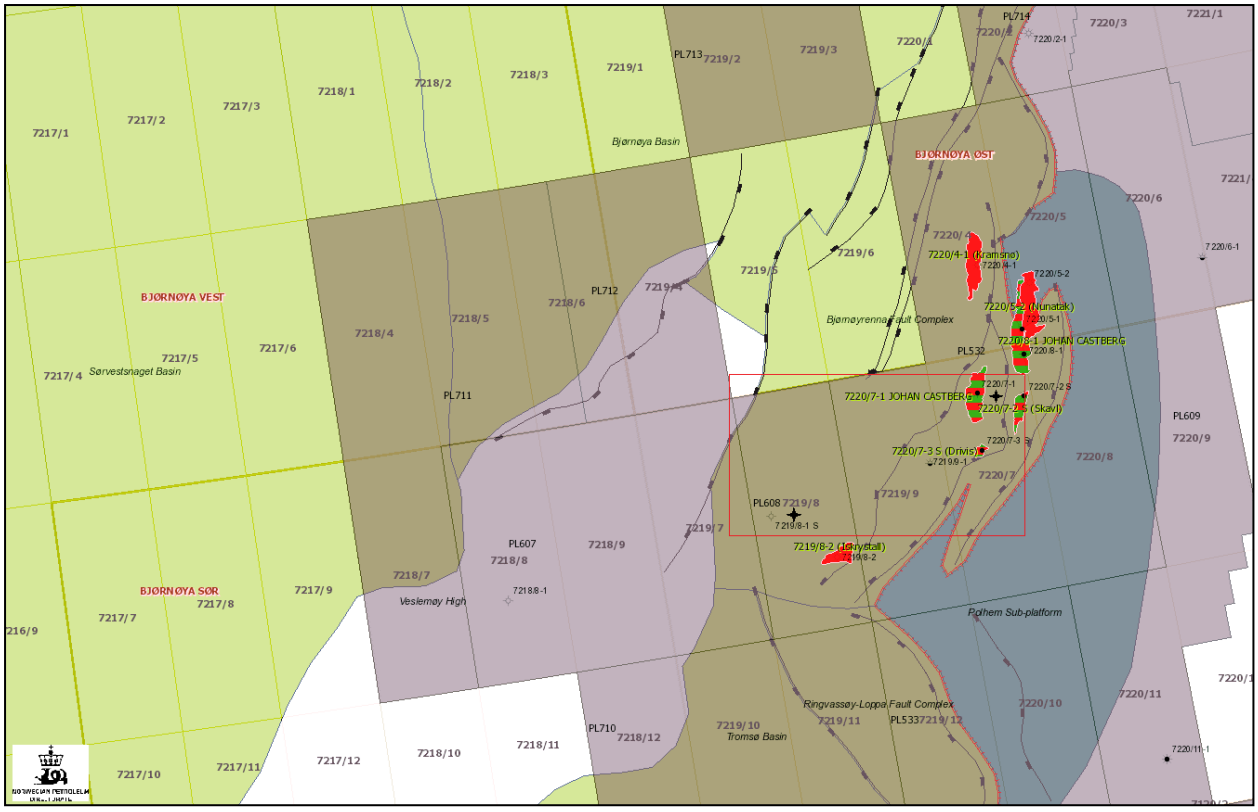

Figure 1. 2 : Location of the JOHAN CASTBERG where wells are represented by ✦ and ▭ showing study area (Modified from NPD).

1.7 Database and Methodology

In this study, two exploration wells have been studied by preparing 20 thin section samples from each well. Both wells were drilled as wild cats and are exploration wells. Saga Petroleum ASA drilled 7219/8-1 in 1992 and it ended up as a dry well .On the other hand In 2011 Statoil Petroleum drilled 7220/7-1 and at 1781m, top of the Stø Formation was encountered which is a target reservoir. Gas-oil-contact (GOC) of a gas bearing reservoir is at 1828m and at 1956 m oil bearing to oil-water-contact (NPD).

By using these methods, the reservoir properties were analyzed from core cuttings, gold coated stub mounted samples along with carbon coated thin sections.

Mineralogical and petrographic analysis approaches used are:

- Optical microscopy
- Scanning electron microscopy (SEM)
- X-Ray Diffraction analysis (XRD).

1.8 Chapter Descriptions

There are seven chapters in this master's thesis

Chapter 1: Introduction, Exploration history, Background and motivation, Research objective and Methodology.

Chapter 2: Geological setting of the Barents Sea and southwestern Barents Sea along with that some description of Basins and Reservoir formations in the study area.

Chapter 3: About the diagenesis of sandstone reservoirs based on the mechanical and chemical compaction and effect on the properties based on that.

Chapter 4: In order to analyze reservoir properties, all the methods and techniques used in this study are discussed.

Chapter 5: Petrophysical analysis including well correlations and marking well tops, porosity predictions and cross plots are discussed.

Chapter 6: All the observations and results collected from both the Stø and Nordmela Formations are discussed based on thin section, SEM and XRD analysis.

Chapter 7: Whole study is discussed in this chapter.

2 GEOLOGICAL BACKGROUND

2.1 Introduction

Area covering around 1.3 million km², the Barents Sea is considered one of the largest continental shelf with respect to area on the globe with average water depth of around 300m (Doré, 1995). Geologically, the Barents Sea is considered as a very complex combination of basins and platforms. (Doré, 1995, Stilwell, 2012) **.** Surrounded by the Norwegian-Greenland Sea to the west, the Svalbard and Franz Josef Land archipelagos to the north, the Novaya Zemlya to the east and the Norwegian and Russian mainland to the south, Barents Sea is located on the continental shelf of the Norway and Russia (Smelror, 1994, Doré, 1995) as shown in (Fig. 2.1).

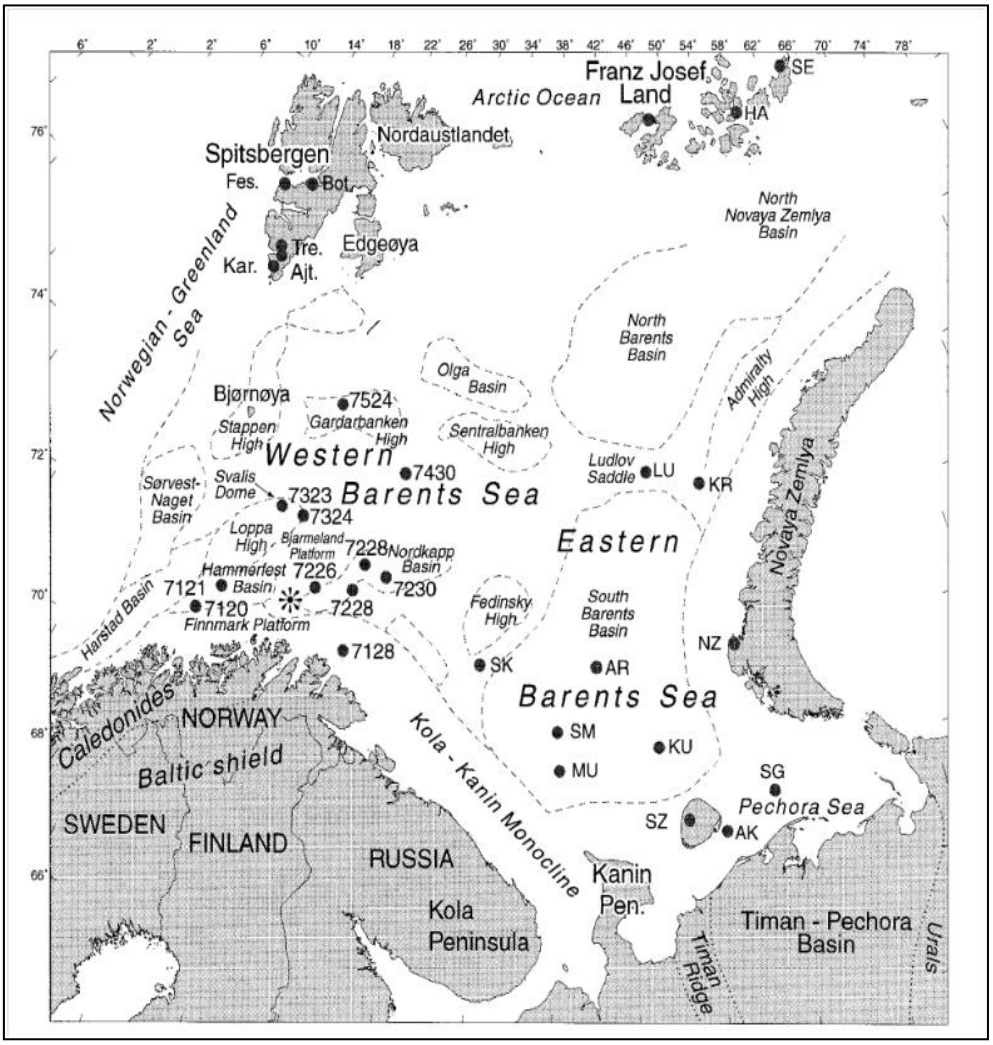

Figure 2. 1: Location map of the Barents Sea and its surrounding areas (Mørk, 1999).

2.2 Tectonic History and Geological Evolution

Dominated by extensional tectonic movement, tectonic history of the Barents Sea from the Late Palaeozoic and Mesozoic begins with the newly formed Caledonian and Uralian orogenic belts collapse, and after that the episodic gradual Pangean super continental break-

up documented in Early-Middle Devonian, Carboniferous, Permian, Triassic and Late Jurassic-Early Cretaceous. (Doré, 1995)

During the first mountain building episode called Caledonian orogeny, plate Laurentia and Precambrian Baltic shield underwent subduction and then collision took place from Ordovician to Early Devonian, (Clark et al., 2014) resulted in the formation of Laurasia continent approximately 400 million years ago that caused the closure of the lapetus Oceans (Doré, 1995). Along the margins of both Laurentia and Baltica, formation of subduction zones, island arcs magmatic activity and other tectonic events took place due to the gradual closure of the lapetus Ocean from the time of late Cambrian to over a period of 80 Myr (Barrère et al., 2009).

As the Caledonian orogenic movements stopped in Early Devonian, the Barents Sea area underwent several tectonic events and presently this area is having an intra-cratonic setting. (Smelror, 1994, Gabrielsen et al., 1990). Caledonian orogeny has impact on the western Barents margin and the structural grains trend of the Svalbard is in N-S and southwestern Barents Sea and Finnmark has NE-SW (Doré, 1995). The structural framework developed in the Caledonian grain is believed to be produced in the later stage of structural development of the area (Clark et al., 2014).

Scandian orogeny began in the Silurian with the major collision between the Baltica and Laurentia and extended until Early Devonian with the formation of plate Larussia. Laurentia was affected by Innuitian or Ellesmerian Orogeny during the time of Silurian to Early Carboniferous and tectonic regime changed from crustal shorting to regional extension. (Barrère et al., 2009)

In Late Devonian to Early Carboniferous times, the Bjørnøya area was effected by regional scale block faulting and the trend prevailing in the western and northwestern areas(Spitsbergen, Bjørnøya and west of Loppa High) were influence by NNW-SSE structural trends (Gabrielsen et al., 1990).

In Permian-Triassic times, a final element in the rejuvenation of most of the worlds land-masses into a single supercontinent Pangea resulted in Uralian orogeny (Doré, 1995). Regional depositional sequences were influenced by subsidence and salt tectonics occurred throughout Triassic period. Rifting and block tilting took place once again during Mid Jurassic and increased through Early Cretaceous.

The NE-SW structural trends developed in the Northeast Atlantic, such as the Bjørnøya Basin was due to the composite rifting episode during Late Jurassic to Early Cretaceous and large regional scale subsidence took place because of this rifting, creating an accommodation space filled with thick Cretaceous strata. During the Mid Cenozoic time, the western Barents Sea Margin developed with the break-up of main continent (Barrère et al., 2009).

2.3 Southwestern Barents Sea

2.3.1 Geological Evolution

In the northern part of the North Atlantic post-Caledonian rift system, the south western Barents Sea is located (Breivik et al., 1998).

Because of episodic rifting, basin formed in four different periods.

- Carboniferous
- Late Permian-Triassic
- Late Jurassic-Early Cretaceous
- Late Cretaceous -Eocene (Clark et al., 2014) as shown in Fig. 2.2.

Large thicknesses of Upper Palaeozoic to Cenozoic sedimentary succession overlay the western Barents Sea and comprising three distinct regions.

1. Mainly Triassic sediments from Upper Palaeozoic and Mesozoic flat-lying succession covering the Svalbard Platform.

2. Number of sub-basins and highs with mainly westwards increasing structural relief represents a basin province between the Svalbard Platform and the Norwegian coast. Sediments of Jurassic-Cretaceous and Paleocene-Eocene in the west are preserved in this basin.

3. There are three main divisions of continental margin.

a. Along the Senja Fractured Zone, a southern sheared margin.

b. Associated with volcanism, a central rifted complex the southwest of Bjørnøya.

c. Along the Hornsund Fault Zone, a northern pre sheared and post rifted margin. (Faleide et al., 2010, Faleide et al., 1993b, Faleide et al., 1984).

Some of the world's deepest sedimentary basins are in the south-western Barents Sea. They formed with in the North Atlantic-Arctic region in response to several episodes of regional

tectonism, that ended up with the Eurasia and Greenland continental separation and gradual development of oceanic crust in the Early Tertiary (Faleide et al., 1993b).

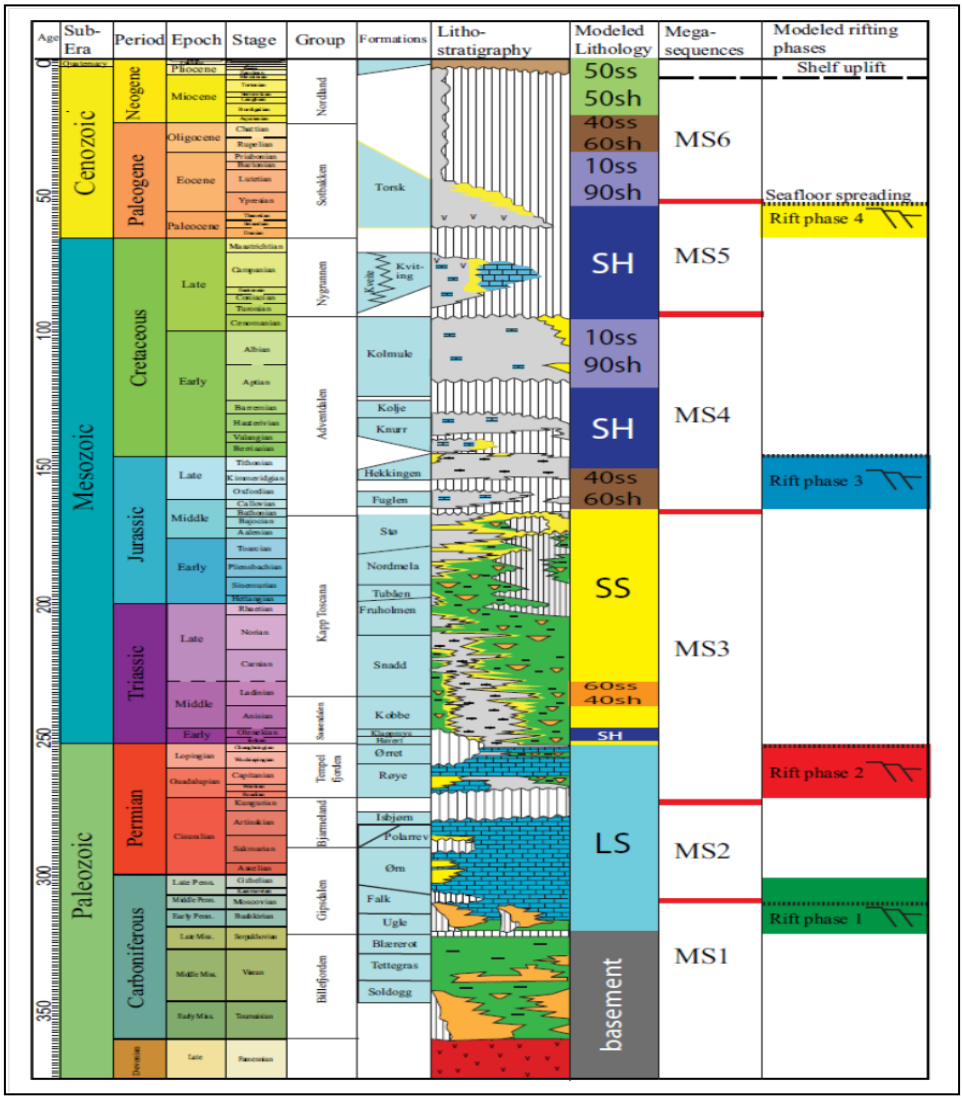

Figure 2.2: Western Barents Sea lithostratigraphic unit showing different rift phases and time periods (Glørstad-Clark et al., 2010).

2.3.2 Palaeozoic

During the late Paleozoic, the Southwestern Barents Sea was dominated by regional extension (Gernigon et al., 2014). From the Late Devonian to Mid-Carboniferous time, the Caledonites collapse followed by rifting are two major tectonic phases in the Barents Sea(Gabrielsen et al., 1990, Clark et al., 2014) and sedimentation are mainly of non-marine origin with relatively uniform thickness in the south-western Barents Sea (Clark et al., 2014). Exhumation and extensive erosion of the hinterlands characterized the Devonian to early Carboniferous time due to the orogeny (Gernigon et al., 2014).

On the southwestern parts of the shelf (i.e., Tromso and Bjørnøya Basin.) thick sequences of evaporites were deposited in the different grabens in late Carboniferous time (Gernigon et al., 2014). Due to the formation of local rift grabens in the southwest Barents Sea, post Carboniferous-post Permian megasequence has been observed with prominent variations in thickness (Clark et al., 2014). Regional sag basin continued to subside in the Late Permian during the deposition of cherty limestones and shales and its initial development is marked by the shift in platform type sedimentation (Faleide et al., 2010).Late Permian and Early Triassic was marine dominated after which shallowing and partial exposure of some areas took place.

2.3.3 Mesozoic

In the Early Triassic a major rift episode has been reported in the southwestern Barents Sea (Gernigon et al., 2014). Shale and sandstones are the dominant lithologies in Triassic strata where the distribution is complex both vertically and laterally (Faleide et al., 2010).Throughout the Barents Sea thick Triassic rocks have coarsening upwards sequences, which present show transgressive - regressive depositional cycles (Faleide et al., 1993b).

In the southwestern Barents Sea, Lower to Middle Triassic succession composes transgressive-transgressive cycles of marine, deltaic, and continental clastics, along with minor tectonic events have been recognized (Gernigon et al., 2014). Regression and erosion ended the Triassic (Faleide et al., 2010). In Late Triassic to Middle Jurassic sequence the cyclic change of shaly continental and sandy shallow marine sediments were controlled by a complex interplay of tectonic subsidence , eustatic sea-level changes and local sediment (Berglund et al., 1986). Throughout the Barents Sea the Lower-Middle Jurassic interval is dominated by sandstones and form the main reservoir in the SW Barents Sea (Faleide et al., 2010).

In Middle Jurassic times the general rise in sea level was initiated led to the deposition of the Stø formation and it continued from Middle Jurassic through the Callovian and into Oxfordian times (Berglund et al., 1986). Since Middle Jurassic time, development of the southwestern Barents Sea comprises two main stages (Breivik et al., 1998) which are rifting in the Mesozoic and basin formation and due to the opening of the Norwegian green land sea, formation of early tertiary margin (Breivik et al., 1998, Faleide et al., 1993b, Faleide et al., 1993a).

In the Southwestern Barents Sea, middle to late Jurassic rifting caused block-faulting along east to north ranging trends, and between tilted fault blocks the deposition of shales took place in restricted basins (Breivik et al., 1998). Initiation of rifting in the southwestern Barents Sea is marked by the Late Middle Jurassic sequence boundary and on the other hand unconformities present within the upper Jurassic sequence indicate interaction between continued faulting and sea level changes (Faleide et al., 2010).

In the Southwestern Barents Sea, the western margin of the Barents Sea shelf is particularly affected by the northern progradation of the Middle Jurassic to Early Cretaceous Atlantic rifting and marine conditions prevailed across the shelf (Gernigon et al., 2014). Formation of deep sedimentary basins from middle Jurassic times give the area much of its present structure (Breivik et al., 1998).Regional extension along with strike-slip movements along old structural lineaments characterize the Late Jurassic-earliest Cretaceous structuring in the SW Barents Sea (Faleide et al., 2010) developing the Bjørnøya, Tromsø and Harstad basins as prominent rift basins (Breivik et al., 1998, Faleide et al., 2010).

Thickest sedimentary packages deposited during 165Ma to 145Ma (Clark et al., 2014). From Valanginian to Cenomanian, Lower Cretaceous Comprises three sedimentary units dominated by clay and silt, with thin interbeds of silt, limestone and dolomite. In deep the SW Barents Sea basins these units make up the main basin fill and the regional subcrop pattern is dominated by these units. Throughout the deposition of these units, marine environment are dominated by distil conditions with periodic restricted bottom circulation. Because of the continuous subsidence as a result of faulting in a pull apart setting the Upper Cretaceous sediments were deposited mainly in the SW Barents Sea. Very deep basins in the SW Barents Sea formed due to the several phases of the Late Mesozoic and Early Cenozoic rifting (Faleide et al., 2010).

Harstad, Tromsø, Bjørnøya and Sørvestsnaget are the deep Cretaceous and Early Tertiary basins of the southwestern Barents Sea basin province separated by intrabasinal highs including the Senja Ridge, Veslemøy High and Stappen High (Faleide et al., 1993b). Throughout the southwestern Barents Sea, depositional break occurred at the Cretaceous-tertiary transition where Palaeogene succession lying unconformable on the Cretaceous. Mesozoic-Cenozoic clastic sedimentary rocks overlain the Upper Palaeozoic characterize by mixed carbonates, evaporites and clastics sedimentation (Faleide et al., 2010) .

2.3.4 Cenozoic

Uplift of broader Barents platform with respect to the Tromsø and Bjørnøya basins indicated by the Paleocene succession during transition between the Cretaceous and Paleocene and this period is marked by hiatus. Development of the Early Paleocene regional hiatus created accommodation space for sediments on Barents platform in post Paleocene (Clark et al., 2014).

Derived from the uplifted areas, thick wedge shaped clastic sediments characterized late Cenozoic evolution by subsidence and burial of the margins. Most of the Cenozoic sediments and even older strata have been eroded due to the late Cenozoic uplift and erosion of the Barents Sea. Erosion which estimates in the SW Barents Sea is in the range 1000 - 1500m.

During the phase of rapid late Paleocene subsidence continental break up and beginning of sea-floor spreading were continued. The Neogene and Quaternary strata thickens dramatically at the margin in the huge sedimentary wedge resting unconformable on the Paleocene and Mesozoic rocks .Sediments of the Late Pliocene to Pleistocene/Holocene age are glacial sediments (Faleide et al., 2010).

2.4 Stratigraphy

2.4.1 Realgrunnen Group

This group is dominated by pale grey sandstone, particularly in its middle and upper parts whereas shale is more common along with thin coal in the lower parts. The age of the preserved section of this group is Early Norian to Bajocian.

Initially the depositional environment in the early Norian began with the transgression which changed in Late Triassic with the development of prograding deltaic systems over the southern parts of the Hammerfest Basin. In the early Jurassic coastal marine environment developed. Deposited in different regimes including shore face, barrier and tidal inlet, sandstone of the Stø Formation is the main reservoir (Dalland et al., 1988).

The Realgrunnen Group consists of:

- Fruholmen Formation(Norian-Rhaetian age)

- Tuben Formation(Rhartian to Hettangian/Sinemurian age)
- Nordmela Formation(Sinemurian to Late Pliensbachian/Toarcian age)
- Stø Formation (Late Pliensbachian to Bajocian/Bathonian age.

These formation are mainly Influenced by sandstone with some shale packages and thin coal seam and showing different Coastal marine environments (Smelror, 1994).

2.4.1.1 Nordmela Formation

The age of the Nordmela Formation is Early Jurassic and the sandstone is very fine to fine grain. The amounts of coarser-grained channel sandstones increase upwards. Thin layers of mudstone are usually interbedded with sandstones having marine bioturbation and plants roots together in the same bed or in alternation beds. Common features are wave ripples, Flasher and lenticular bedding and very thin coal beds. Occasionally herring-bone cross stratification is observed (Olaussen et al., 1984).
The Nordmela Formation is deposited in a paralic system where the environment is low to medium energy (Olaussen et al., 1984) with tidal flat to flood plain facies and individual beds of sandstone indicate estuarine and tidal channels which intercepted this low lying area (Dalland et al., 1988). Generally reservoir quality of the Nordmela Formation is poor but due to the increasing abundance of channel sandstone facies it improves upwards (Olaussen et al., 1984).

2.4.1.2 Stø Formation

The age of the Stø Formation is late Pliensbachian to Bajocian according to the present data (Dalland et al., 1988). Fine to medium grain sandstone of the Stø Formation is mainly classified as quartz arenite. low and high angle large scale cross-stratification with hummocky cross stratification are prominent features (Olaussen et al., 1984). The Stø Formation is dominated with mature sandstone having clear thin beds of shale and siltstone with grain sorting moderately to well-sorted. Phosphatic lag conglomerates may also present particularly in the upper part of the units.

Stø Formation generally thinning towards east and thickness increases in southwestern. There are three division of depositional sequence in the Stø Formation in which base is indicated by transgression sequence and only common in western parts of the Hammerfest Basin. During

the Late Toarcian/Aalenian, the central unit of the area underwent maximum transgression. Due to syn-depositional uplift and winnowing and later due to differential erosion, the topmost Bajocian sequence is extremely variable.

Sand deposited in the Stø Formation was of prograding coastal regimes and characterized with variety of lithofacies of linear clastic coast. Late Toarcian and late Aalenian regional transgressive fluctuation marked by shale/siltstone beds (Dalland et al., 1988). Within an overall transgression or still stand of sea level the lateral extension of these sandstone bodies as progradational unit is very large (Olaussen et al., 1984).

According to (Olaussen et al., 1984) depositional sequence of the Stø Formation is of an upper near shore and inner shelf and Nordmela Formation is coastal plain/tidal flat sequence (Fig.2.3).

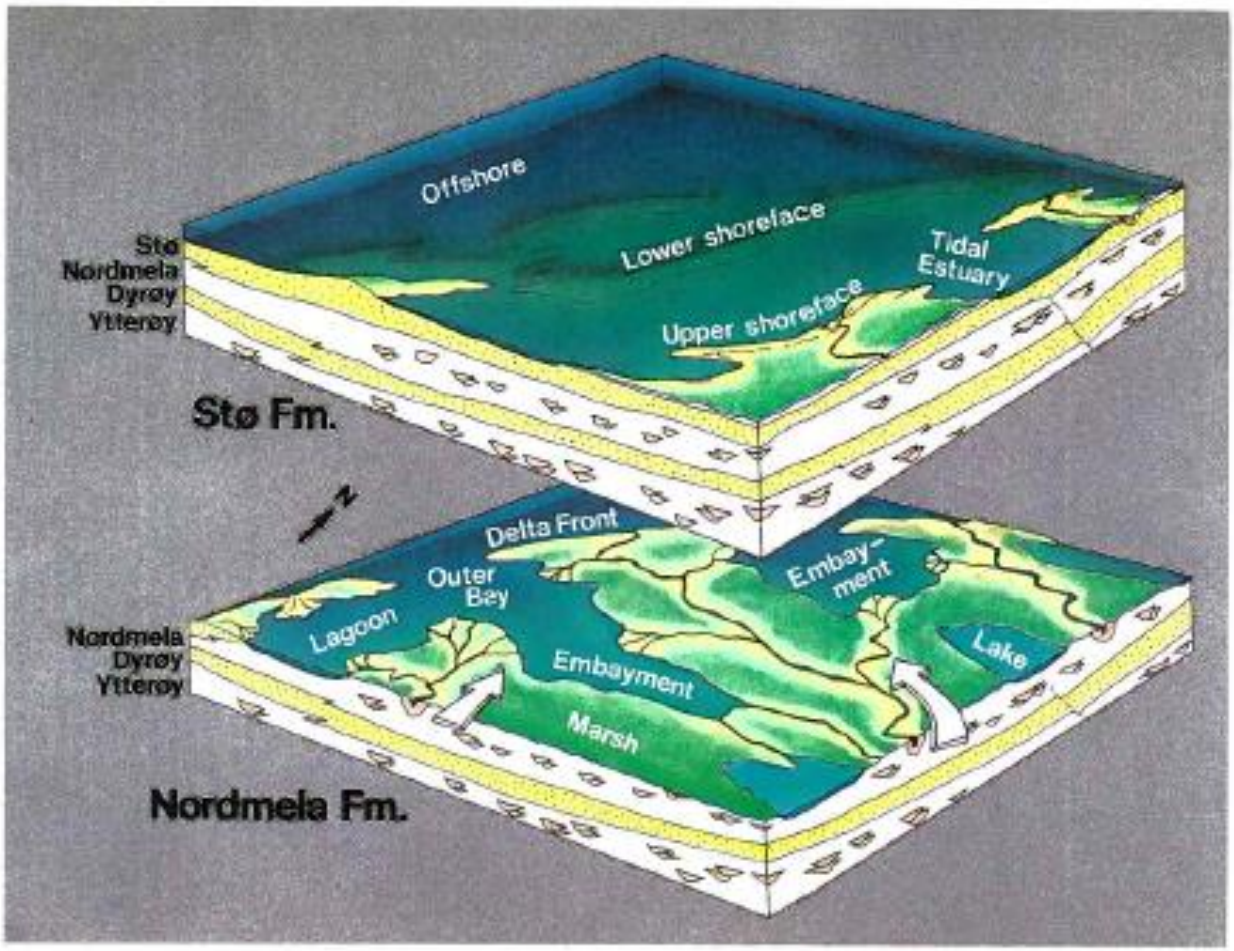

Figure 2.3: Paleogeography and depositional model for the Stø and Nordmela Formation (Taken from Berglund et al., 1986).

2.5 Basin

2.5.1 Bjørnøyrenna Fault Complex

At the south and southeast of Bjørnøya, Bjørnøyrenna is a bathymetrical depression. Bjørnøya Basin has a fault complex called the Bjørnøyrenna Fault Complex which is the southeastern bounding fault of it. Part of this fault complex is related to the Ringvassøy-Loppa Fault Complex. Trends of the Bjørnøyrenna Fault Complex is NE-SW between 72°N,19°E and 73°15'N,22°E. Boundary between the Loppa High and the deep the Bjørnøya Basin is defines by the Bjørnøyrenna Fault Complex in the southwest and divides the Loppa High from the shallow Fingerdjupet subbasin in the northeast (Gabrielsen et al., 1990).

2.5.2 Bjørnøya Basin

Located between 72°30'and 74°N and between 18° and 22°E, trend of the Bjørnøya Basin is NE-SW. The Leirdjupet Fault Complex divides the Bjørnøya Basin into a western deep and eastern shallow part, the Fingerdjupet subbasin(Faleide et al., 1993a). To the southeast, Bjørnøya Basin is bounded by Bjørnøyrenna Fault Complex and from the Stappen High a faulted northwestern boundary slope is dipping down towards the basin (Gabrielsen et al., 1990) and this Bjørnøya Basin has some features of half graben(Gabrielsen, 1984).

Upper sequence of basin fill is eroded (Gabrielsen et al., 1990) and the Early Cretaceous is the age of most of the basin fill and structurally basin appeared as a large half graben downfaulted along the Bjørnøyrenna Fault Complex (Faleide et al., 1993a). Middle part of the basin is structurally simple but deformation is complex at the boundaries as described for the Bjørnøyrenna Fault Complex and the Stappen High.

Large area to the north is affected by the Early Cretaceous subsidence and the Bjørnøya Basin is essentially associated with that. In Tertiary when the Stappen High was uplifted, tilted northern margin of the Bjørnøya Basin was formed at a later stage. With a very thick sedimentary sequence of the Early Cretaceous Bjørnøya Basin form a province along with the Harstad, Tromsø and Sørvestsnaget basins and parts of the Stappen High. Late cretaceous and Tertiary faulting and local inversion related to the Bjørnøyrenna Fault Complex and the Stappen High effected the Bjørnøya Basin (Gabrielsen et al., 1990).

2.5.3 Polhem Sub-platform

According to (Gabrielsen, 1984) the Polhem Subplatform was described as part of the Loppa High.

Between the stable eastern part of the Loppa High and the Bjørnøyrenna and Ringvassøy-Loppa Fault Complexes, the Polhem Sub-platform forms block-faulted area and is located between 72°N and 72°30'N at 20°E.

On the subplatform, Jurassic succession is missing due to erosion and detachment surface of most of the listric faults is below the base of the Triassic. Permian is the starting time where faulting started and remained active in different stages. In the Late Jurassic to Early Cretaceous the listric faults developed but restore again later . At the westernmost part of the Loppa High, Polhem subplatform is located and developed a tectonically active element of the Loppa High in late Palaeozoic. Relative to the crest of the Loppa high it was downfaulted in the Early to Mid-Triassic.

The Triassic and Jurassic cover of the sub-platform move slightly towards the west during the formation of the Ringvassøy-Loppa Fault Complex that caused the development of typical structural pattern of rotated fault blocks (Gabrielsen et al., 1990) .Characteristic structural pattern of rotated fault blocks developed due to the sliding of the Triassic and Jurassic cover of the Sub-platform towards the west during the development of the Ringvassøy-Loppa Fault Complex (Faleide et al., 1993a, Gabrielsen et al., 1990).

2.5.4 Tromsø Basin

From 71° to 72°15'N and 17°30' to 19°50'E, the Tromsø Basin is located north of the town of Tromsø, surrounded by the Ringvassøy-Loppa Fault Complex to the east and Senja Ridge to the west. At present southwestern margin is not well known but it ends up against the Troms-Finn-mark Fault Complex to the southeast. Veslemøy High separate Tromsø Basin from the Bjørnøya Basin in the North (Gabrielsen et al., 1990).

Dominated by salt tectonism, a very deep sedimentary Tromsø Basin contains large amount of sediments from Upper Palaeozoic, Mesozoic and Cenozoic (Olaussen et al., 1984). In the middle Jurassic, faulting may have started along the eastern margin of the Tromsø Basin and separation took place from the Hammerfest Basin to the east during the Early Cretaceous.

In Palaeozoic there is evidence that the Tromsø Basin occurs as a separate basin if we look at its northern extent but later it was combine with the Bjørnøya Basin. Along the Bjørnøyrenna Fault complex, lateral movements took place in the late Cretaceous time before that these two basins were attached. In contrast to the Hammerfest Basin, extreme Cretaceous time subsidence can be explained by halokinesis and structural development of the Tromsø Basin is also influenced by it. As late as the Eocene, fault movements has been reported due to salt movement and continue may be even later.

Large scale extensional and shear movements are related to the Mesozoic and Cenozoic evolution of the Tromsø Basin and the crust in this area came close to break-up (Gabrielsen et al., 1990).

2.5.5 Loppa High

The Loppa High is located north of the Hammerfest Basin and southeast of the Bjørnøya Basin and also includes the Polhem Platform. On the east and southeast, it is surrounded by a monocline towards the Hammerfest Basin and the Bjarmeland Platform and on the south, by the Asterias Fault Complex. Ringvassøy-Loppa and Bjørnøyrenna Fault Complex bounded the Loppa High to the west. (Gabrielsen et al., 1990).

Since Devonian time, the western crest of the Loppa High has been restored at least four times as a high but the Late Jurassic to Early Cretaceous and Late Cretaceous - Tertiary tectonism describes the present High (Gabrielsen et al., 1990). In Late Carboniferous to Early Permian, an easterly tilting of the Loppa High and Hammerfest Basin was caused by this tensional system with rejuvenation of underlying basement fault trends. Along the crest of the high, deep erosion is caused by a reactivated easterly tilting of the Loppa High that took place in Late Permian and Early Triassic times. Lower Triassic sedimentation was low in the Loppa High, but in middle Triassic times it became a depocenter (Berglund et al., 1986).

The High was part of a regional cratonic platform including the Hammerfest Basin and Bjarmeland platform during Ladinian to Callovian. The pre-Jurassic time of the Bjørnøya and the Stappen High are related to that of the Loppa High (Gabrielsen et al., 1990).In Cretaceous time, erosion occurred when the Loppa High was sub-aerially exposed during the post-rifting stage (Berglund et al., 1986).

3 THEORETICAL BACKGROUND

3.1 Introduction

Initial sandstone composition depends on the erosion, transportation and depositional environment of the rock which gives the initiation of the diagenetic processes. Starting from the time of deposition, reservoir properties are constantly changing until the sediments have undergone greater burial depth or uplifted afterwards. Sandstone properties at any given burial depth depends on its shallow depth composition, their temperature and stress history during burial. Porosity and permeability are the most important reservoir properties and are dependent on initial composition which is controlled by the (provenance) textural and minerological composition, of the depositional environment and near surface and during burial diagenetic processes.. Primary clastic composition and the depositional environment are the most important factors in predicting reservoir quality at depth (Bjørlykke and Jahren, 2010). Some of the sedimentary environments have been shown in Fig. 3.1.

Main Diagenetic processes according to (Bjørlykke and Jahren, 2010) are:

1) Near surface Diagenesis.
2) Mechanical compaction
3) Chemical compaction
4) Cementation

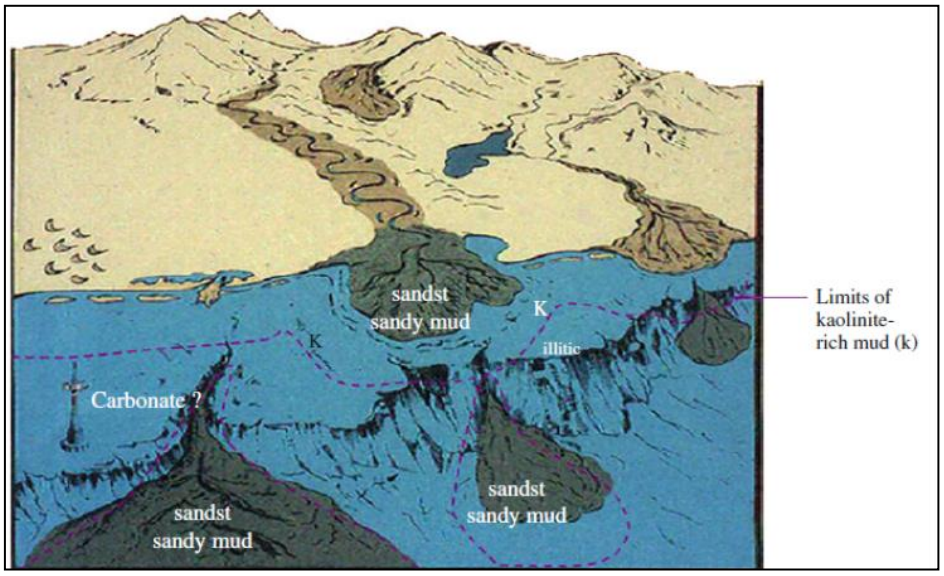

Figure 3.1: Diagrammatic explanation of a sedimentary basin on a continental margin. Provenance, transportation and depositional environment control the initial sediment composition (Bjørlykke and Jahren, 2010).

3.2 Near Surface Diagenesis

Early diagenetic reactions start to change the composition of primary sediments as soon as sediments are deposited. Sediments have the maximum chance to react with the atmosphere or water at very low burial depth (<1-10 m), both by fluid flows and diffusion. Near surface diagenesis is caused by meteoric water. Carbonates will first be dissolved by meteoric water when it seeps down and flow along the most permeable beds into the basin and then slowly dissolve unstable minerals like feldspar and mica as shown in Fig. 3.2 (Bjørlykke and Jahren, 2010).

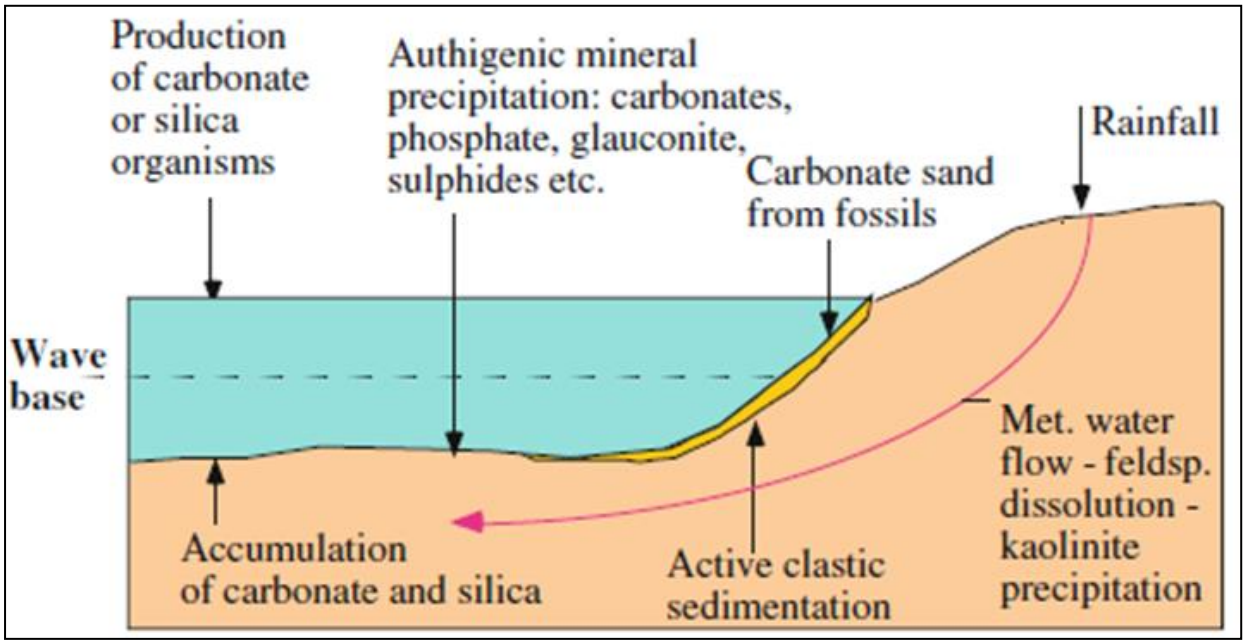

Figure 3.2: Schematic description of diagenetic processes in shallow marine environment (Bjørlykke and Jahren, 2010).

The distribution of carbonate cement and opal A is controlled by the biogenic components like calcareous and siliceous organisms, which that will be change to opal CT and quartz. In sandstone, Carbonate cement is derived mostly from biogenic carbonate, particularly from the aragonite bearing organisms and due to the dissolution and reprecipitation of biogenic carbonate (Bjørlykke and Jahren, 2010). At higher temperatures very little dissolution and reprecipitation of carbonate cementation took place and probably occurred early at temperatures less than 60-70°C (Saigal and Bjørlykke, 1987).

Dissolution of feldspar and precipitation of kaolinite form secondary porosity and effect the reservoir properties significantly (Bjørlykke et al., 1992). At about 130°C reaction between K-feldspar and kaolinite occurs and above this temperature these two minerals are thermodynamically no longer stable together. Permeability of rock is affected by the conversion of kaolinite into illite while secondary porosity is increased by the leaching of K-feldspar.

Kaolinite precipitation and leaching rate of minerals like feldspar and mica are dependent on the amount of groundwater flowing through each rock volume per unit of time. Silicate minerals like feldspar and mica stripped Na^+ and K^+ cations from them and brought into solution. Feldspar and mica reactions with water can be written as follows (Bjørlykke and Jahren, 2010).

$$2K\,(Na)\,AlSi_3O_8 + 2H^+ + 9H_2O \longrightarrow Al_2Si_2O_5(OH)_4 + 4H_4SiO_4 + 2K^+\,(2Na^+)$$

Feldspar — Kaolinite — disolved silica — disolved cations

$$2KAl_3Si_3O_{10}(OH)_2 + 2H^+ + 3H_2O \longrightarrow 3Al_2Si_2O_5(OH)_4 + 2K^+$$

Muscovite — Kaolinite

3.3 Mechanical Compaction

Due to mechanical compaction and pressure solution porosity decreases and it dependents on the grain parameters including sorting, packing, composition and net overburden stress (Bjørlykke et al., 1989). Intergranular volume (IGV) is measured as the initial space between the sand grains which is determined by shape of the grain, size, sorting and matrix content (Paxton et al., 2002, Ajdukiewicz and Lander, 2010) . Intergranular volume is the porosity before quartz cementation and is typically around 25-30% for well sorted quartz-rich sandstones and mechanical compaction is important to determine (IGV). Intergranular volume is determined by the amount of porosity loss during mechanical compaction at the beginning of chemical compaction (Bjørlykke and Jahren, 2010).

IGV equals to IGP in clean sands with no matrix and cement. Initially IGV and IGP decrease with burial due to overburden as a function of mechanical compaction during which grains become more closely packed as shown in Fig. 3.3 (Ajdukiewicz and Lander, 2010).

Loose sand with an initial porosity 40-42% under the experimental compaction shows that the porosity may be reduced to 35-25% depending on the grain strength and size at stresses of 20-30 MPa corresponding to 2-3km of burial for normal pressured rocks (Chuhan et al., 2003, Bjørlykke and Jahren, 2010).

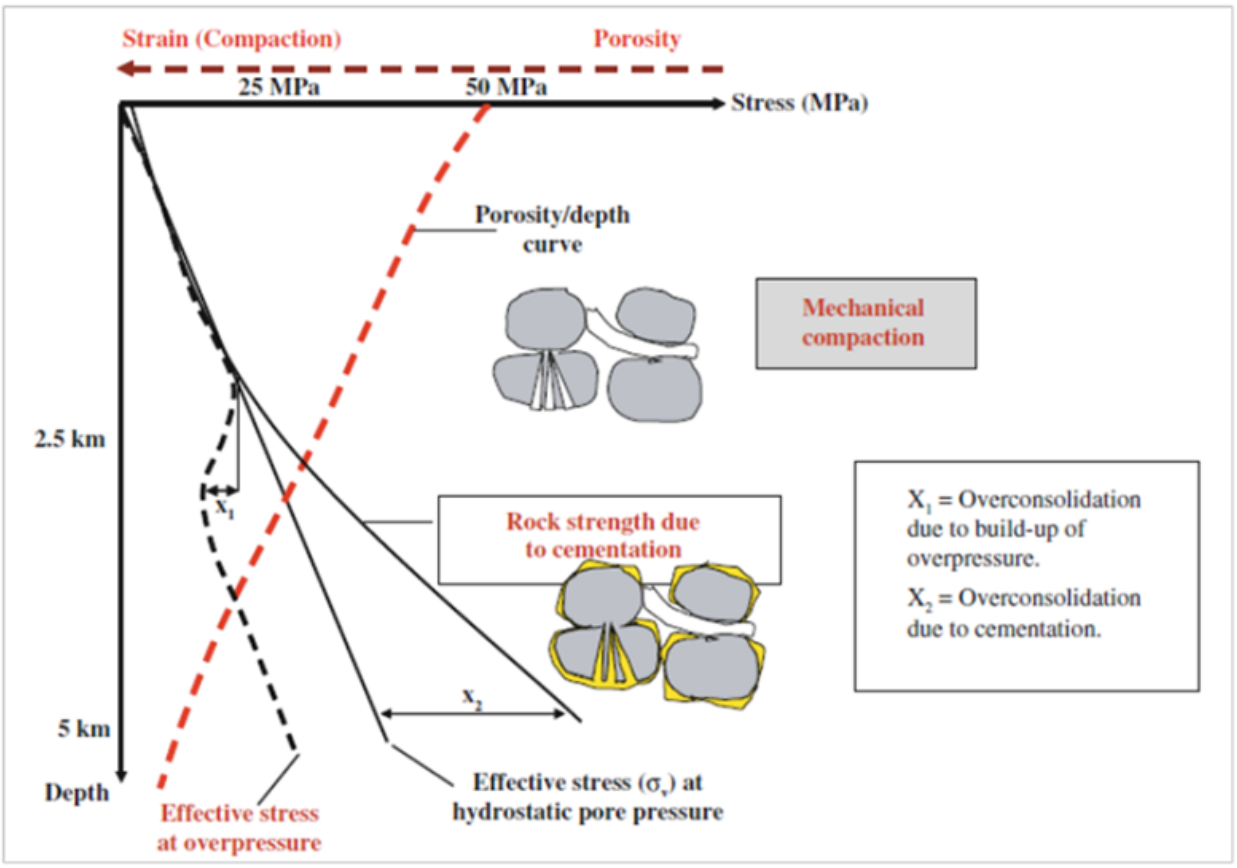

Figure 3.3: Mechanical compaction of sandstone caused due to effective stress by grain packing and breakage, before getting cemented at around 80°C - 100°C (Bjørlykke and Jahren, 2010).

3.3.1 Reservoir Sandstone at Intermediate Burial Depth (2.0 - 3.5 Km, 50 - 120 C)

Rocks get more compacted at a faster rate by quartz cementation rather than by increase in vertical stress from over burden. Mechanical compaction seize further effectively in most cases by only 2-4% quartz cement in sandstone and then compaction is further controlled chemically by rate of mineral dissolution and precipitation (Bjørlykke and Jahren, 2010).

Quartz cement at temperature of around 60 to 80 °C in sandstones takes over kinetic restrictions and starts to precipitate on available surface of quartz grain based on the time , temperature, quartz grain, surface area and nucleation domain size as shown in Fig. 3.4

(Ajdukiewicz and Lander, 2010). At 2.5 to 3.5 km of burial depth , beginning of quartz cementation significantly influences the porosity reduction along with the start of pressure solution and stylolitization (Bjørlykke et al., 1989).

In sandstone, processes of albitization causes K-feldspar or plagioclase to be replace by albite and is often observed at a burial depth of about 3 km or more. Albite form as a result of a reaction between K-feldspar with Na^+ and release of K^+ (Bjørlykke and Jahren, 2010). This reaction is as under.

K AlSi3O8 $+ Na^+$ = NaAlSi308 + K^+
Feldspar Albite (Saigal et al., 1988)

At a Burial dept of 2-3 Km, albitization starts (Saigal et al., 1988)and at this depth around 30-50 % of K-feldspar is converted into albite (Aagaard et al., 1990).

3.3.2 Deeply Buried Sandstones (greater than 3.5 - 4 Km, Higher than 120°C)

Quartz cementation does not stop once it started and has formed quartz overgrowth unless the temperature drops below 70-80 C and almost all porosity is lost. In sandstone reservoirs strong porosity and permeability reduction is observed in most sedimentary basins from a burial depth of around 3-3.5 km to 4-4.5 with a temperature range from about 120°C to 160°C due to quartz cement and diagenetic illite precipitation in most cases (Bjørlykke and Jahren, 2010).

At burial depths of about 3.7 to 4 Km (120°C-140°C) illitization starts only if kaolinite and k-feldspar are present together in reservoir (Chuhan et al., 2000).

Thermodynamically K-feldspar and kaolinite are unstable when present together and illite forms at temperature (120°C-140°C) where activation energy of illitization become suppressed by this sufficiently high temperatures. This reaction will not proceed in the absence of K-feldspar or kaolinite and the reservoir properties will be less affected. Along with quartz cementation, illitization is probably the most important reason for reduction of reservoir properties (Bjørlykke et al., 1992). Equation showing reaction between illitization and Kaolinite:

$$2K(Na)AlSi_3O_8 + Al_2Si_2O_5(OH)_4 \longrightarrow KAl_3Si_3O_{10}(OH)_2 + SiO_2 + 2H_2O$$

Feldspar Kaolinite illite Quartz (Bjørlykke and Jahren, 2010)

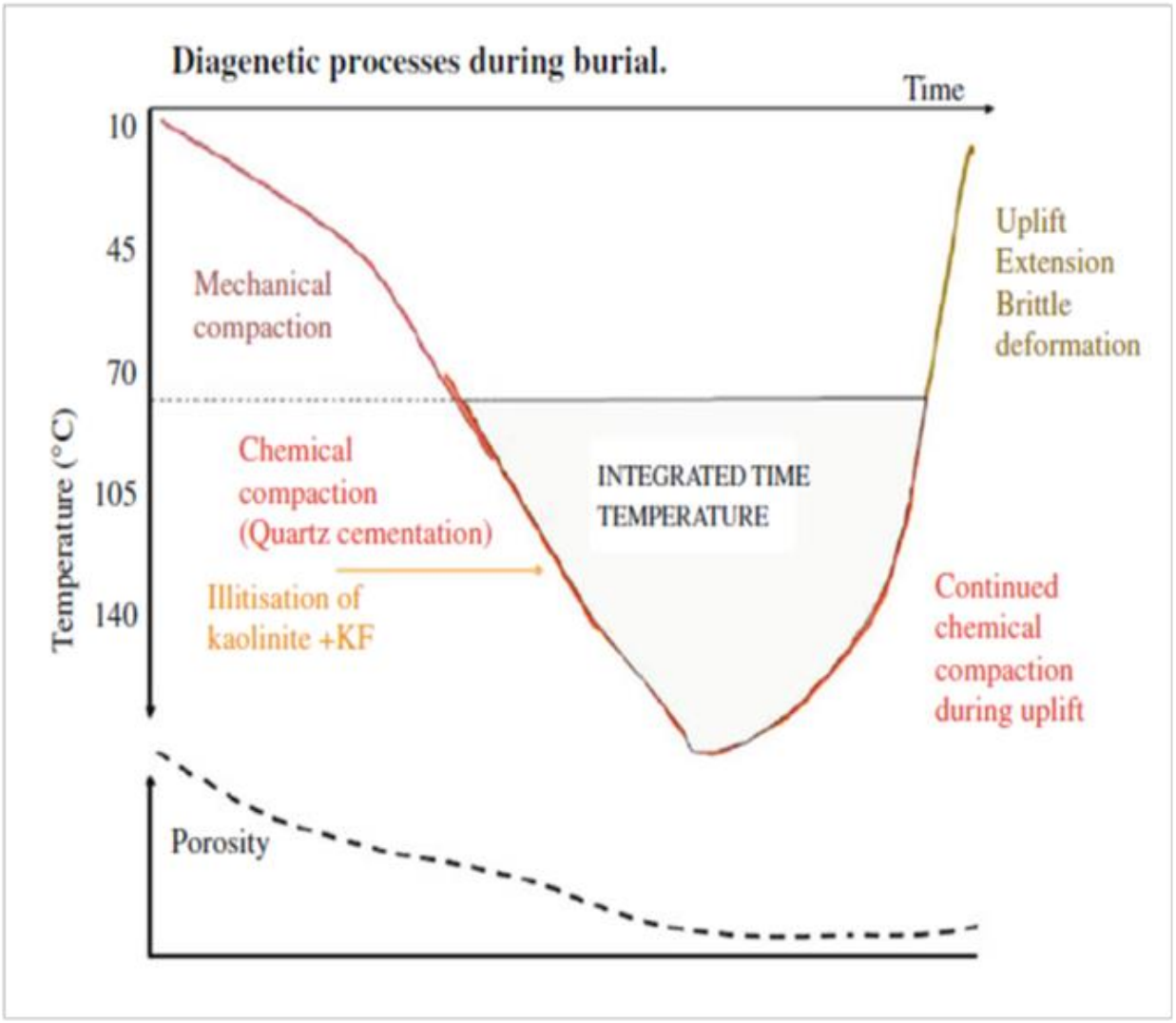

Figure 3.4: Diagenetic processes, mainly quartz cementation, as a function of temperature and time. Note that quartz cementation will continue also during uplift as long as the temperature exceeds 70°C-80°C (Bjørlykke and Jahren, 2010).

3.4 Quartz Cementation

There are three factors according to (Worden and Morad, 2009) that affect reservoir quality:

1) Porosity and permeability (factors which influenced these two parameters are: sorting, grain size, and grain morphology and sand/mud matrix ratio)

2) Amount of mechanical and chemical compaction

3) Amount and type of pour filling cement.

Temperature, time and surface area available for quartz cementation are the main functions required to reduce the porosity (Bjørlykke and Jahren, 2010). In sandstone quartz cementation is controlled by rate of precipitation which is temperature dependent (Taylor et al., 2010). At 2.5 to 3.5 km of burial depth , initiation of quartz cementation significantly influences the porosity reduction along with the start of pressure solution and stylolitization (Bjørlykke et al., 1989). Quartz cementation does not stop once it started and has formed quartz overgrowth unless the temperature drops below 70-80 C and almost all porosity is lost (Bjørlykke and Jahren, 2010).

3.4.1 Origin of Quartz Cement in Sandstone

Pressure solution is the process in which stress is required for the dissolution at grain contacts but only moderate amount of stress is needed and temperature is the important factor in case of silicate. Preferred areas of dissolution are the contacts between mica or illitic clay and quartz. The dissolved silica is transported at grain contacts or along stylolites by diffusion to the grain surface where the quartz overgrowth forms as shown in Fig. 3.5 (Bjørlykke and Jahren, 2010).

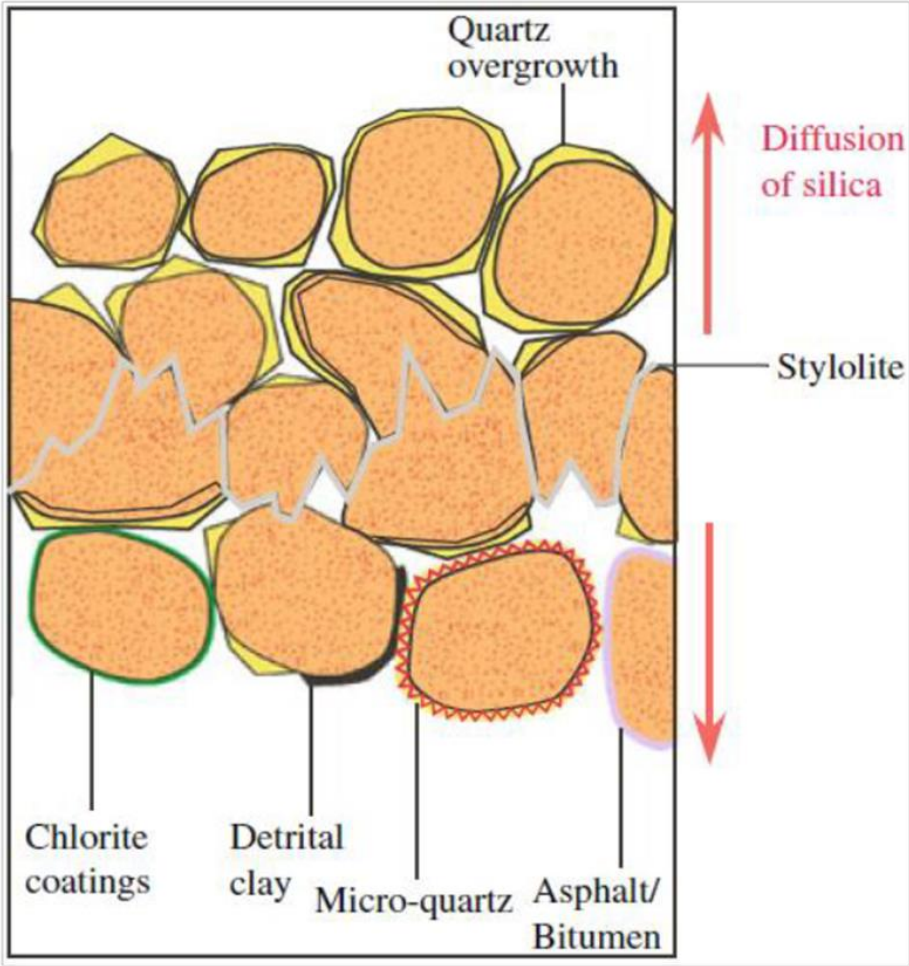

Figure 3.5: Stylolite in a schematic illustratoin. By diffusion,dissolved silica is transported away from clay rich stylolite (Bjørlykke and Jahren, 2010).

At greater depth, sometimes the precipitation of micro-quartz preserves porosity by acting as a coating, preventing quartz cementation. At low temperature (60-80 C) micro quartz precipitated when porewater was highly supersaturated with respect to quartz through the dissolution of opal A or opal CT and while the quartz growth rate was low (Bjørlykke and Jahren, 2010). For quartz precipitation availability of the surface area is also an important factor (Walderhaug, 1996).

3.5 Porosity Preserving Mechanism

At greater depth there are various different porosity preserving mechanisms which has been suggested.

Factors maintaining high porosity in sandstone at greater depth according to (Bloch et al., 2002), are as under.

- Shallow development of fluid overpressure
- Grain coats and grain rims (effect only on detrital quartz rich sandstone).

3.5.1 Grain Coat and Grain Rims

Quartz cementation is retarded by grain coats and grain rims and contribute reduction in porosity and permeability by restricting precipitation of quartz overgrowths on detrital-quartz grains (Bloch et al., 2002). Clay minerals and micro crystalline quartz are the most effective types of grain coats observed in sandstones and detrital clay rims and fine crystalline carbonate (e.g., siderite) are the other types of grain coats. In order to limit quartz cementation, authigenic chlorite is the most important and effective mineral but on the other hand authigenic illite and mixed-layer clays are less frequently reported as grain coatings (Taylor et al., 2010).

3.5.2 Shallow Development of Fluid Overpressure

Amount of fluid pressure which is greater than the hydrostatic gradient for the fluid from the water column top is defined as fluid overpressure. Mechanical compaction is mainly controlled by effective stress so in some cases porosity preservation is helped by fluid overpressure. Mechanical properties of reservoir sandstones as well as timing of fluid overpressure development are the factors that highly control the ability of fluid overpressure to preserve porosity (Bloch et al., 2002).

Fluid overpressure develops 1) where rate of fluid release is low relative to the rate of pore volume reduction. 2) Where rate of pore fluid expansion is fast compared to the rate of fluid release 3) in response to large-scale fluid movement. Porosity preservation at shallow depths is very common and continues throughout the burial history of sandstone where fluid over pressure develops and significantly reduce the effective stress and thus causes the decrease in mechanical compaction (Bloch et al., 2002).

4 METHODS AND DATA

4.1 Well Information and Data Base

Two wells, 7219/8-1 and 7220/7-1 have been used in this project and both are located in the Bjørnøya Basin, southwestern Barents Sea. The information about the wells is taken from the Norwegian Petroleum Directorate website and composes into borehole data sheet (Table 4.1).

Table 4.1. Summary sheet of well bore data (NPD 2014)

Well Name	Well 7219/8-1	Well 7220/7-1
Structural Element	BJØRNØYA SØR	BJØRNØYA ØST
UTM Zone	33	33
Wellbore Contents	DRY	OIL/GAS
RKB Elevation (m)	24	40
Water Depth (m)	369	365
Total Depth (MD)	4611	2230
Average Geothermal Gradient (°C/km)	39.90	36.48
Bottom Hole Temperature [°C]	165	72
Oldest Penetrated Age	EARLY JURASSIC	LATE TRIASSIC
Oldest Penetrated Fm.	STO FORMATION	FRUHOLMEN FM
Maximum Inclination [°]	23.8	6
Final Vertical Depth (TVD) [m RKB]	4404	2229

4.2 Core Logging

Cores from well 7219/8-1 and 7220/7-1 are used for logging and collecting general information from the Stø and Nordmela Formation. Graphic logging has been performed in order to see the variations that are present vertically with in a core sample. Lithology, sedimentary structures, texture, color and grain size are some of the important aspects to consider while doing logging. Hand lens (10 xs), 10% HCl, grain size scale and measuring stick are the equipment used detailed study observation of the core. Samples for thin section preparation as well as for XRD-analysis (Table 4.3) were cut and taken from the core while doing logging.

4.3 Well Correlation

The main purpose of doing well correlation is to look for the thickness variation trend within reservoir sand intervals. In this case, mainly gamma ray log has been used for the correlation. Along with that, density and V-shale logs are also used. Petrel software has been used for well correlation.

4.4 Petrophysical Evaluation

After well correlation, logs are exported from petrel and imported into Interactive Petrophysics (IP) software where different cross-plots and histograms have been generated using these logs. Logs value can be analyze more thoroughly in this software. Density and Gamma ray along with Neutron Porosity and depth Vs porosity and velocity cross plots are used. Histograms of Gamma ray, porosity and density are included.

4.5 Mineralogical And petrographical Analysis

Petrographical analysis has been carried out by using Optical microscopy, X-Ray Diffraction (XRD) and Scanning electron microscopy (SEM).

4.5.1 Optical Microscopy

4.5.1.1 Thin Section Observations

Under a Nikon Optiphot-Pol petrographic microscope, all the thin sections have been studied (Table 4.3). To understand the mineralogy, grain size, shape and sorting, polished thin sections are examined (Fig 4.1). Grain contacts and quartz overgrowth are the parameters related to the sandstone compaction that has also been observed.

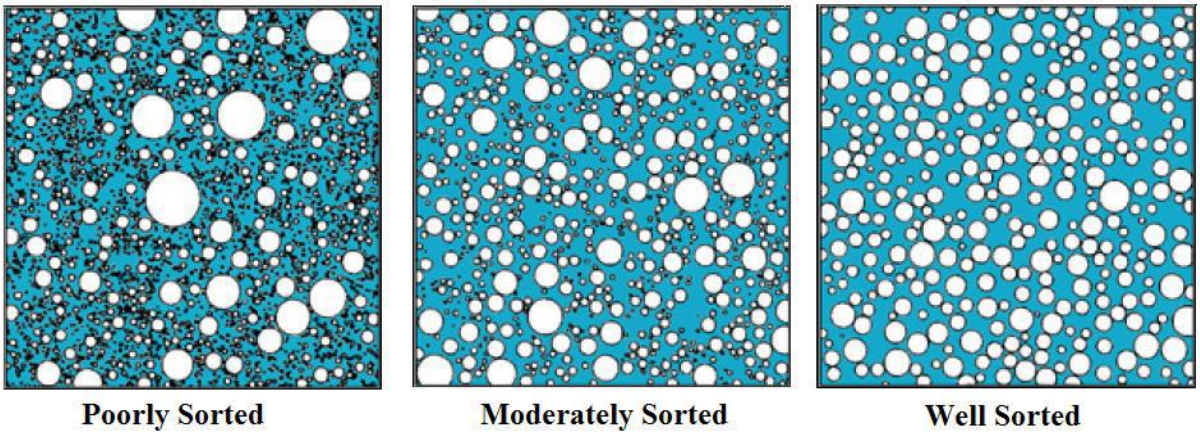

Figure 4. 1:Degree of sorting presented by (Chuhan et al., 2003) and modified after (Longiaru, 1987).

4.5.1.2 Point Counting

In order to estimate the porosity and composition, point counting has been done on all the thin sections. A standard polarization microscope along with an automatic counter and a mechanical stage are used in order to perform point counting. On each thin section 300 point counts have been counted on the basis of set parameters;

1) Quartz 2) Feldspar 3) Matrix 4) Quartz Cement 6) Carbonate Cement 7) Antigenic clay 8) Total Porosity

4.5.1.3 Intergranular Volume (IGV)

According to (Paxton et al., 2002) Intergranular volume is defined as the sum of intergranular porosity, intergranular cement and depositional matrix (Fig 4.2). Depositional silt and clay size particles that fill the space between grains framework is called matrix.

Intergranular Volume (IGV) = cement + depositional matrix + intergranular porosity

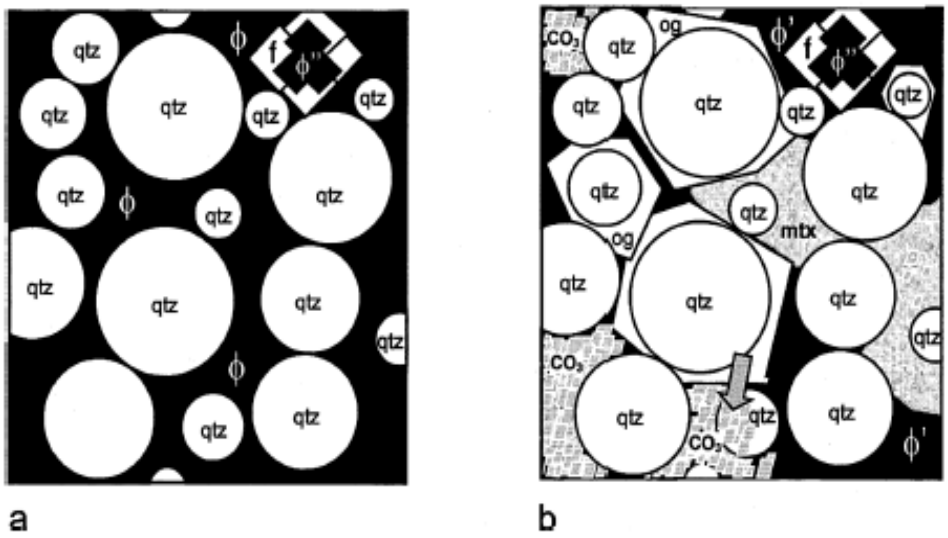

Figure 4.2: IGV in both view a) and b) in same that is 40%, but IGP in b) is less due to the presence of matrix and cement. IGV = intergranular volume, qtz =quartz, f= feldspar grain , mtx = depositional matrix, og = overgrowth quartz, co_3 = carbonate cement, ϕ' or IGP = intergranular porosity, ϕ" = secondary intergranular porosity. (Paxton et al., 2002).

To measure the compaction in sandstone, IGV is used that is calculated from the point counting results.

4.5.2 Scanning Electron Microscopy (SEM)

Using JEO2 JSM-6460LV Scanning Electron Microscope (SEM) with a LINK INKA Energy 300 Energy Dispersive X-Ray (EDX) system, SEM analysis has been performed on the samples (Table 4.3). Under the SEM two types of samples have been studied. Thin section samples that are coated with carbon and gold coated freshly fractured samples taken from core material that are mounted over stubs. 20 samples from each well mounted over stubs are studied and 8 carbon coated thin sections samples in order to look for the quartz over growth and porosity difference between two wells.

Table 4.2: Sample depths of well 7219/8-1 and 7220/7-1

Well Name	**7219/8-1**	**7220/7-1**
Sample Depth	4597.23	1787.65
	4598.33	1792.85
	4598.93	1807.7
	4599.84	1814.37
	4600.15	1815.9
	4601.64	1892.58
	4602.51	1842.32
	4602.87	1848.9
	4603.71	1851.4
	4603.91	1861.4
	4604.26	1871.97
	4604.68	1883.35
	4605.76	1890.4
	4606.35	1905.46
	4607.6	1922.47
	4608.4	1938.63
	4608.76	1948.73
	4609.57	1972.23
	4610.61	1975.37
	4611.05	2017.25

4.5.3 XRD Analysis

XRD analysis gives both qualitative and semi-quantitative analysis. Diffract Eva V4.0 and Profex-3.4.0 software's are used for XRD analysis.

Table 4.3: Total number of samples used in mineralogical and petrographical analysis

Well Name	**Thin Section**	**Carbon Coated(SEM)**	**Stubs(SEM)**	**Bulk Analysis(XRD)**
7219/8-1	20	4	20	20
7220/7-1	20	4	20	20
Total Number of Samples	40	8	40	40

4.5.4 Bulk Analysis

All samples from both wells are used for bulk analysis (Table 4.2). Minerals are identified and then semi-quantified in this analysis.

4.6 Calculating Average Geothermal Gradient

Formula for calculating average geothermal gradient

Geothermal gradient = dt/dz = BHT-MAST/TD

Where BHT is borehole temperature (°C), MAST mean annual surface temperature (°C), TD is total depth in Kilometers and dt/dz is geothermal gradient (°C/km).

5 WELL CORRELATION AND PETROPHYSICAL ANALYSIS

5.1 Introduction

The main purpose of this chapter is to identify different intervals of the Stø and Nordmela Formations based on their lithology and correlate sandstone reservoir interval in the study area. Investigations of petrophysical properties from given core intervals of these formations are also included. This leads to identify the lithology variation in both wells. By using these petrophysical analyses, sand shale ratio and porosity values can be determined and porous and non-porous zones are identified.

5.2 Well correlation and results

Different wells including, 7219/8-1, 7220/7-1 and 7220/8-1 has been correlated, lithostratigraphically on the basis of gamma ray log (Figure 5.1). Correlation of well, 7219/8-1 with other wells is not possible due to the unsufficient data available. Nordmela formation is completely missing and a few portion of the Stø Formation is available. Well 7220/8-1 not included but is used, only to correlate different intervals of the Stø and Nordmela Formations with well 7220/7-1.

In the study area, the Stø Formation is considered as a main reservoir rock but the reservoir quality of the Nordmela FM is poor. Both the Stø and Nordmela Formations are sub divided into upper and lower part based on their difference in depositional environment (figure 5.2). On the basis of gamma ray and density log, different intervals of these formations have been easily correlated in well 7220/8-1 and 7220/7-1. (Figure 5.2). Lower part of the Stø Formation is a well sorted fine to medium grain clean sand. Reservoir properties are good due to the wave and tidal energy environment. Bioturbated, well sorted, fine to medium grain silty sandstone of upper part of the Stø Formation has low reservoir qualities as compared to the lower part. The deposition is influenced by middle to upper shore face environment. According to (Olaussen et al., 1984) depositional environment of the Stø Formation is upper near shore and inner shelf environment.

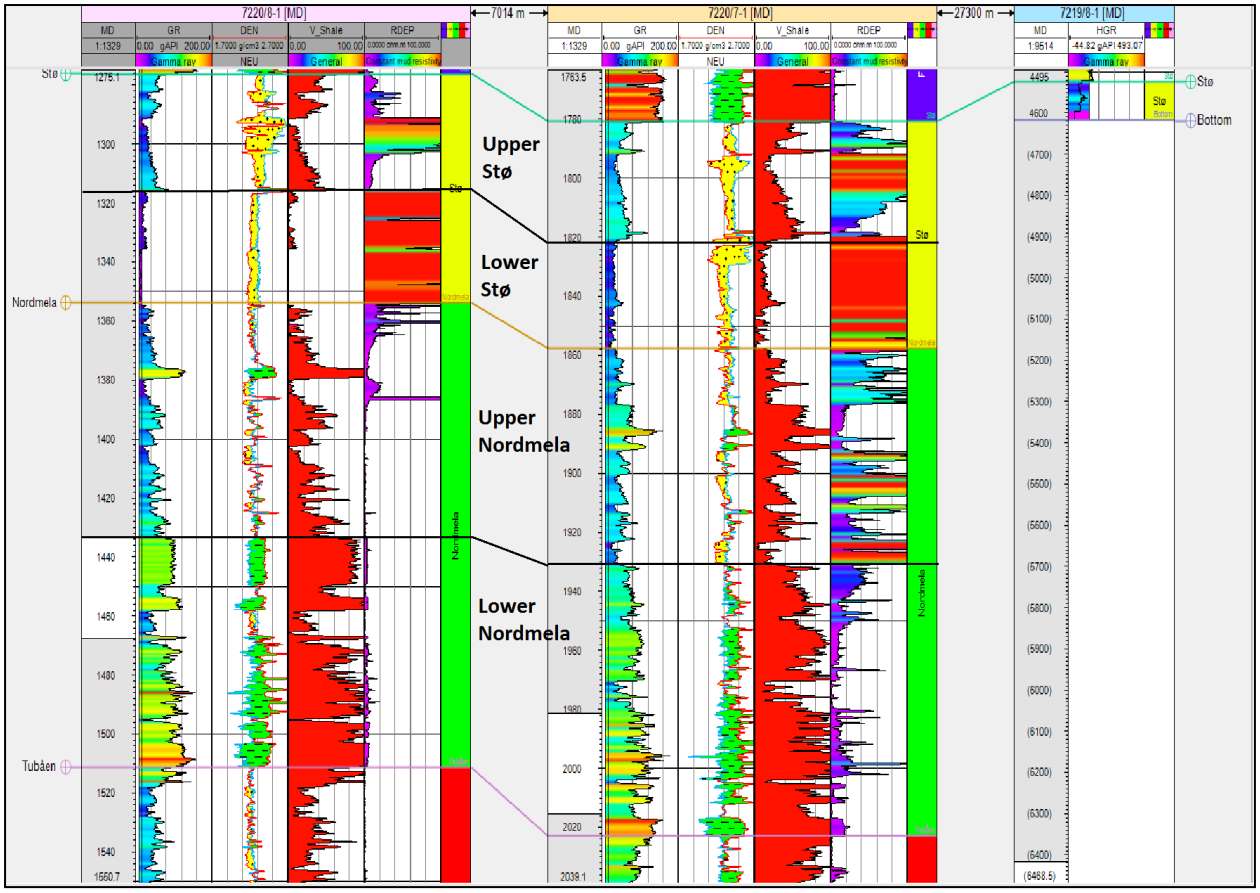

Figure 5.1: Lithostratigraphic correlation of wells 7220/8-1, 7220/7-1 and 7219/8-1 showing different intervals of the Stø and Nordmela Formations (NPD 2014).

The lower part of the Nordmela Formation is fine to medium grain well sorted silty sandstone and mudstone having poor reservoir quality. The upper part of the Nordmela Formation is fine to medium grain sandstone with lenticular to flaser bedding with moderate reservoir quality. Gamma ray value of upper part is low which means it is sandier as compared to the lower part and having a better reservoir quality. (Figure 5.2). Depositional sequence of the Nordmela Formation is coastal plain/tidal flat sequence (Olaussen et al., 1984).

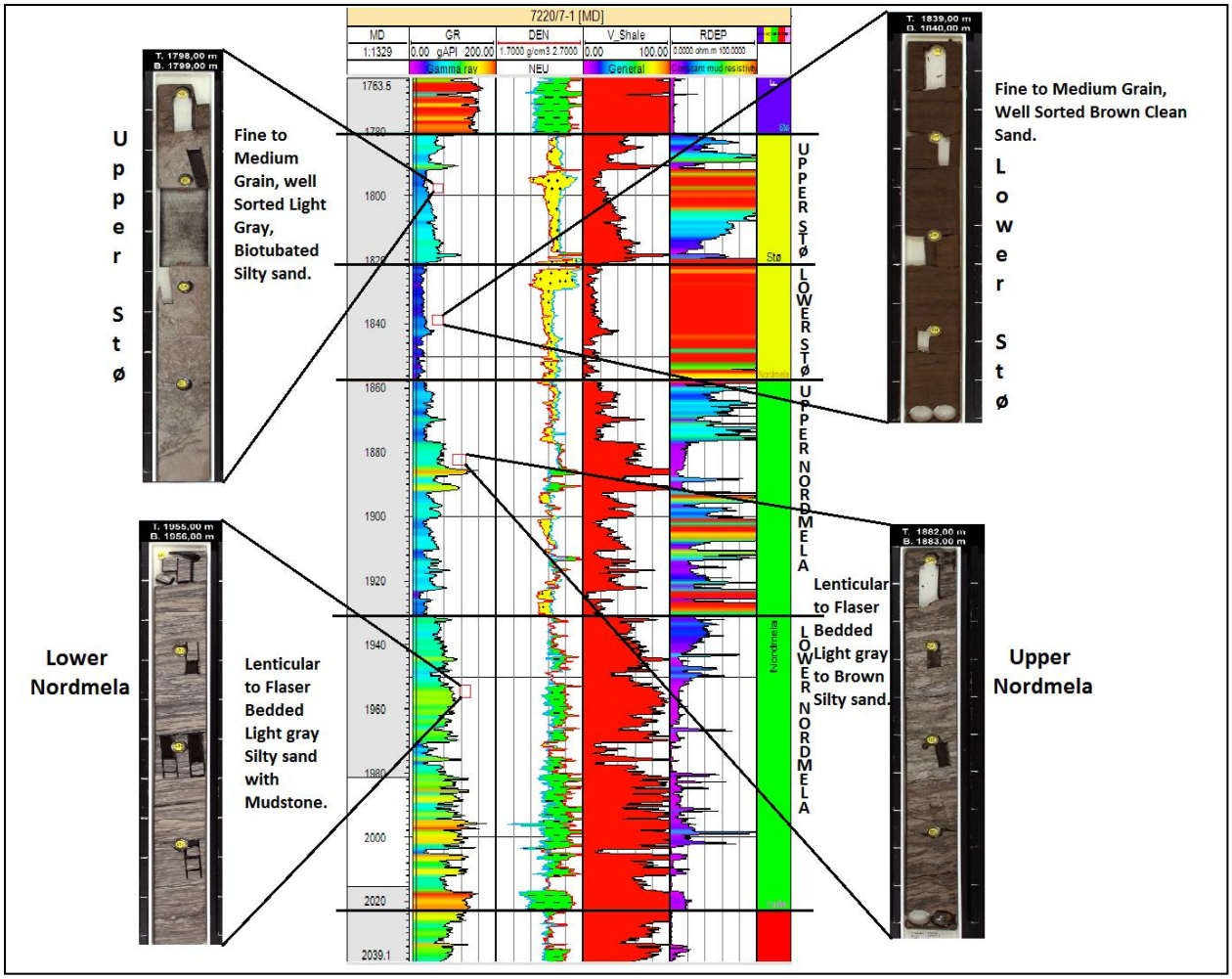

Figure 5.2: Different sedimentary units of the Stø and Nordmela Formations with core photographs from well 7220/7-1. Sedimentary structures are different in different units along with variation in depositional environment.

5.3 Petrophysical Analysis

Petrophysical analysis has been performed in order to have a better understanding of lithology and porosity. Several different cross plots and histograms from well 7219/8-1 and 7220/7-1 are used to compare and understand the lithology and porosity distribution.

5.3.1 Cross plots And Histograms

To have a better overview of the Stø and Nordmela Formations in well 7219/8-1 and 7220/7-1, different cross plots and histograms are plotted against different parameters.

5.3.1.1 Histogram of Gamma Ray

Histogram is showing gamma ray population for the given intervals (Figure 5.3a) and (Figure 5.3b) .Critical point (60 API) which separates the sand and claystone is mark by the black line. Gamma ray value in well 7219/8-1 is high in sand interval but in well 7220/7-1 claystone is having high gamma ray value.

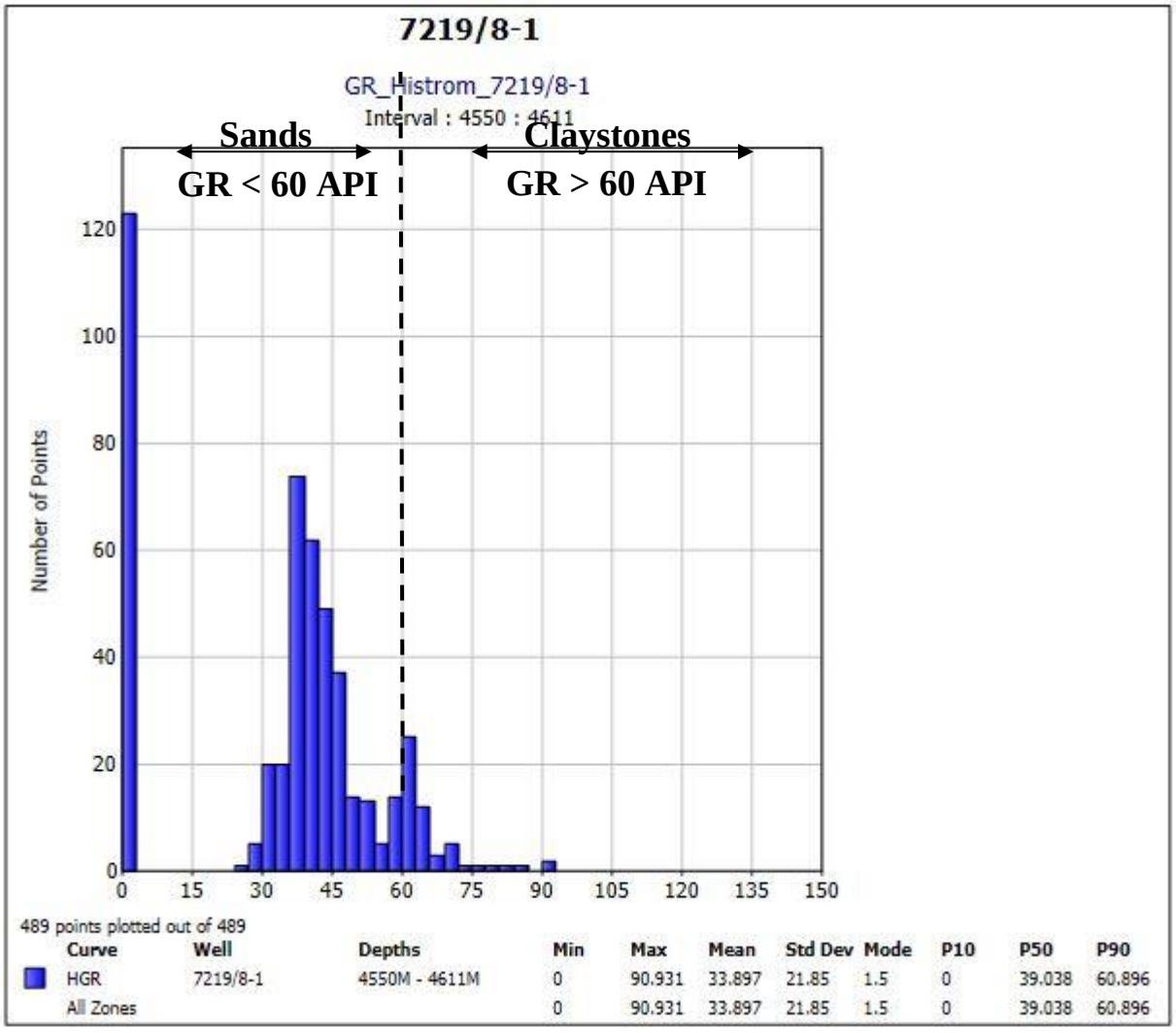

Figure 5.3a: Histogram of gamma ray (API) distribution for the Stø Formation of well 7219/8-1. Sand (GR < 60API) and claystone (GR > 60API) intervals are also showing.

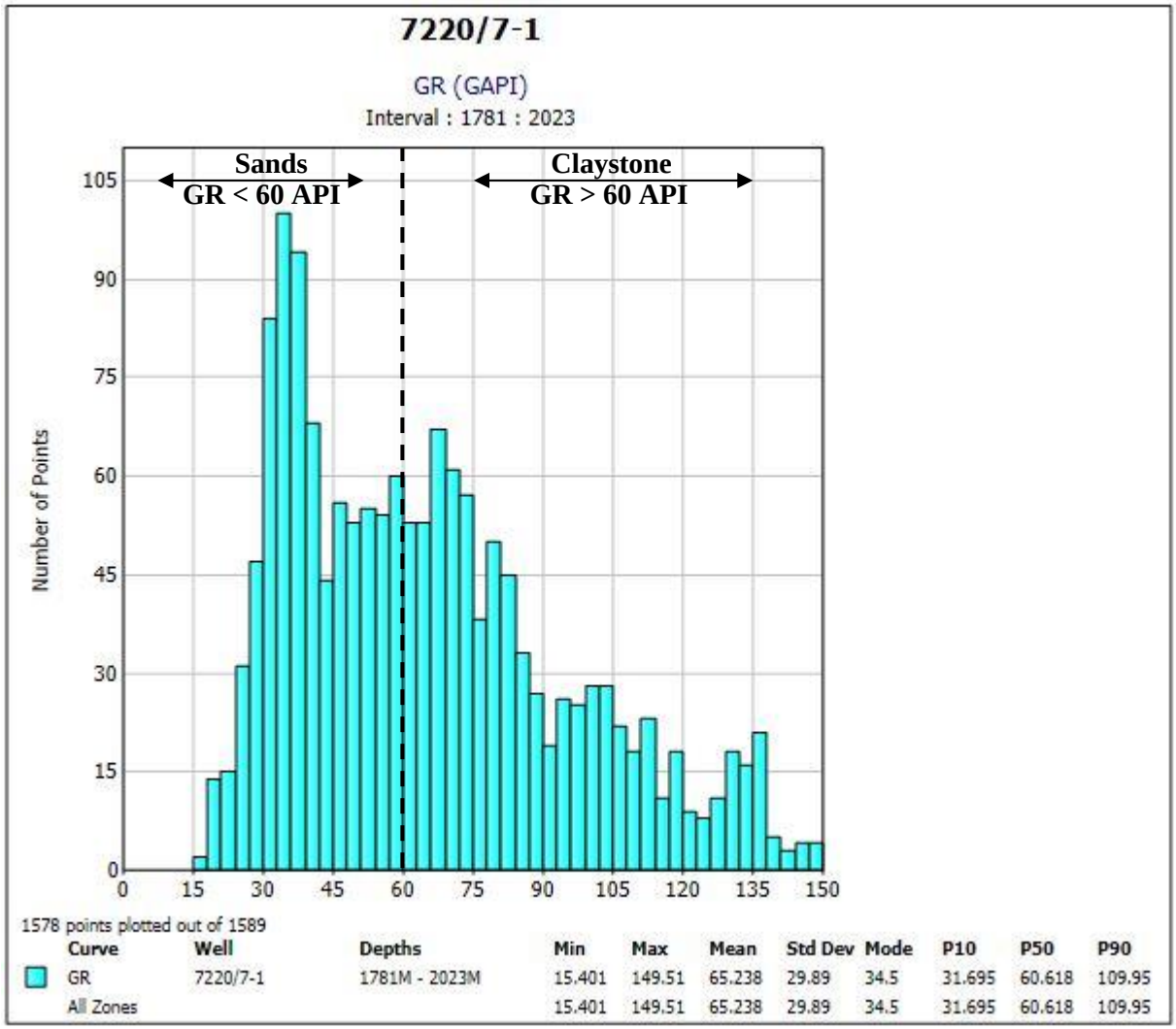

Figure 5.3b: Histogram of gamma ray (API) distribution for the Stø and Nordmela Formations of well 7220/7-1. Sand (GR < 60API) and claystone (GR > 60API) intervals are also showing.

At an interval of 1781m-2023m, minimum and maximum porosity values vary in between 0% and 48% with an average of about 20.5% in well 7220/7-1 (Figure 5.4a). On the other hand, well 7219/8-1 has porosity values that vary from 0.2% to 12.6% with an average porosity of about 7.8% at an interval of 4550m-4611m (Figure 5.4b).

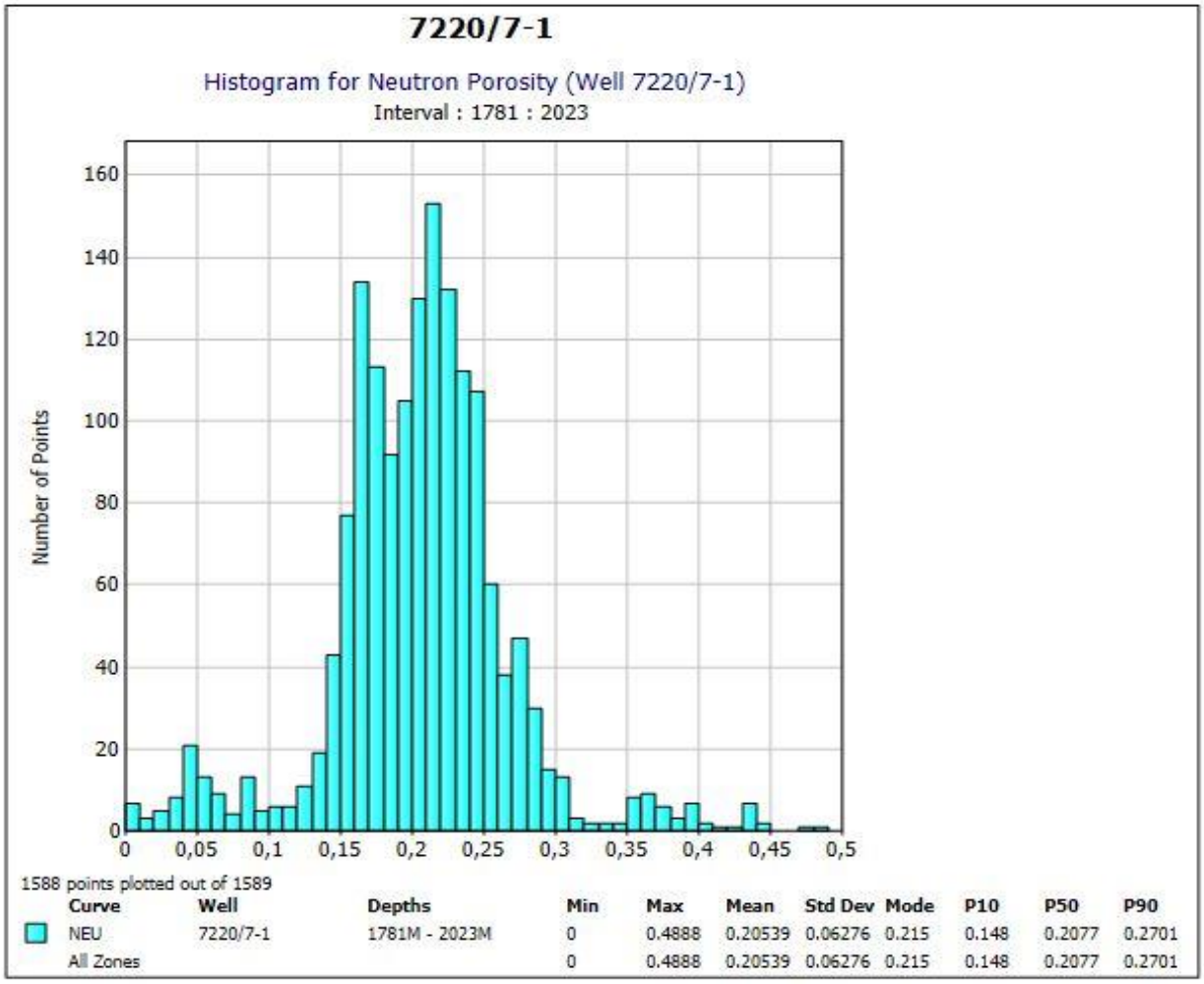

Figure 5.4a: Histogram of Neutron Porosity (%) distribution of the Stø and Nordmela Formations for well 7220/7-1.

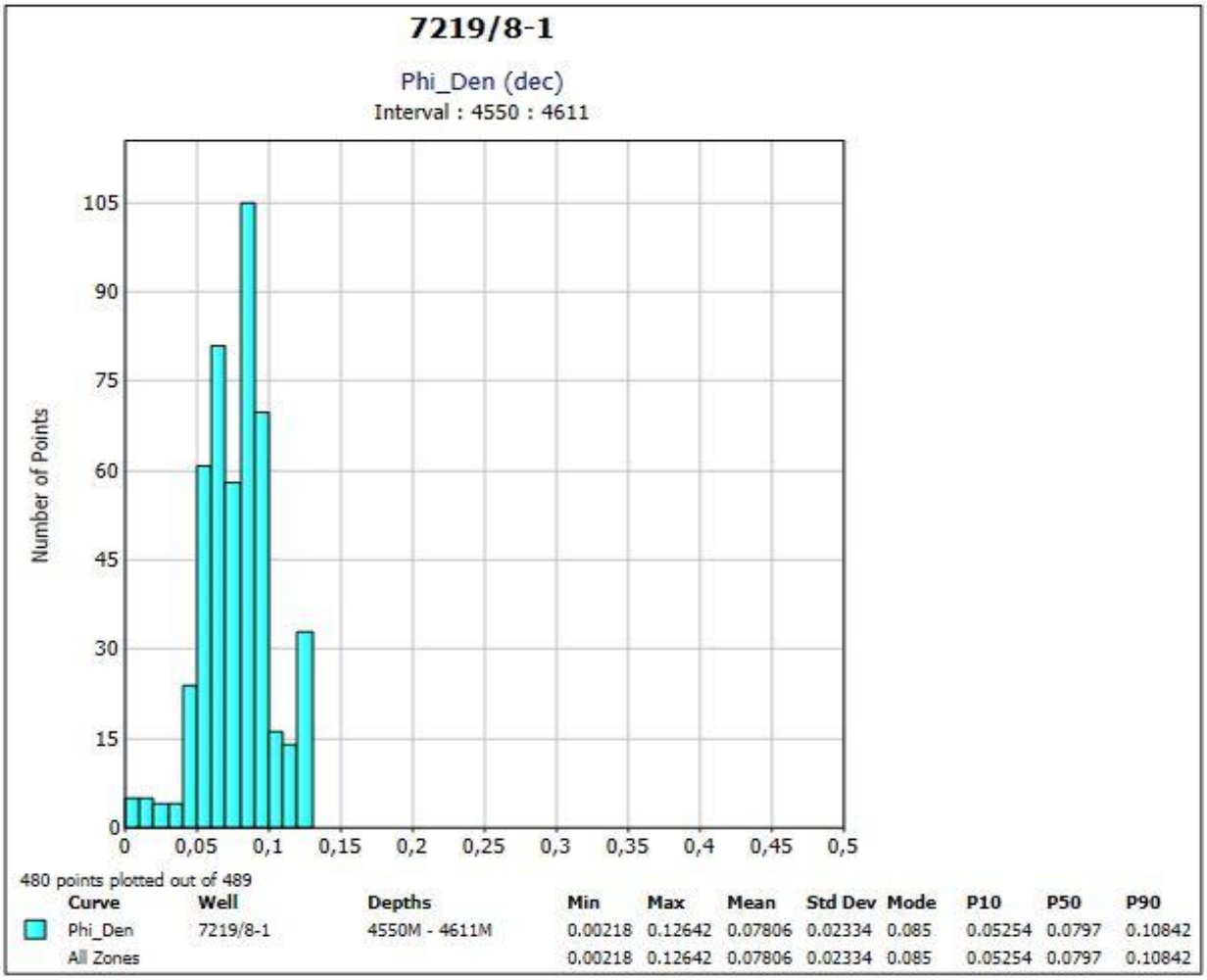

Figure 5.4b: Histogram of neutron porosity (%) distribution of the Stø Formation for well 7219/8-1.

Well 7220/7-1 has an average density of 2.37g/cc with minimum and maximum values varies between 2.07g/cc to 2.99g/cc. On the other hand mean density of the Stø Formation in well 7219/8-1 is 2.52g/cc with a least value of 2.4g/cc and highest of 2.7g/cc.

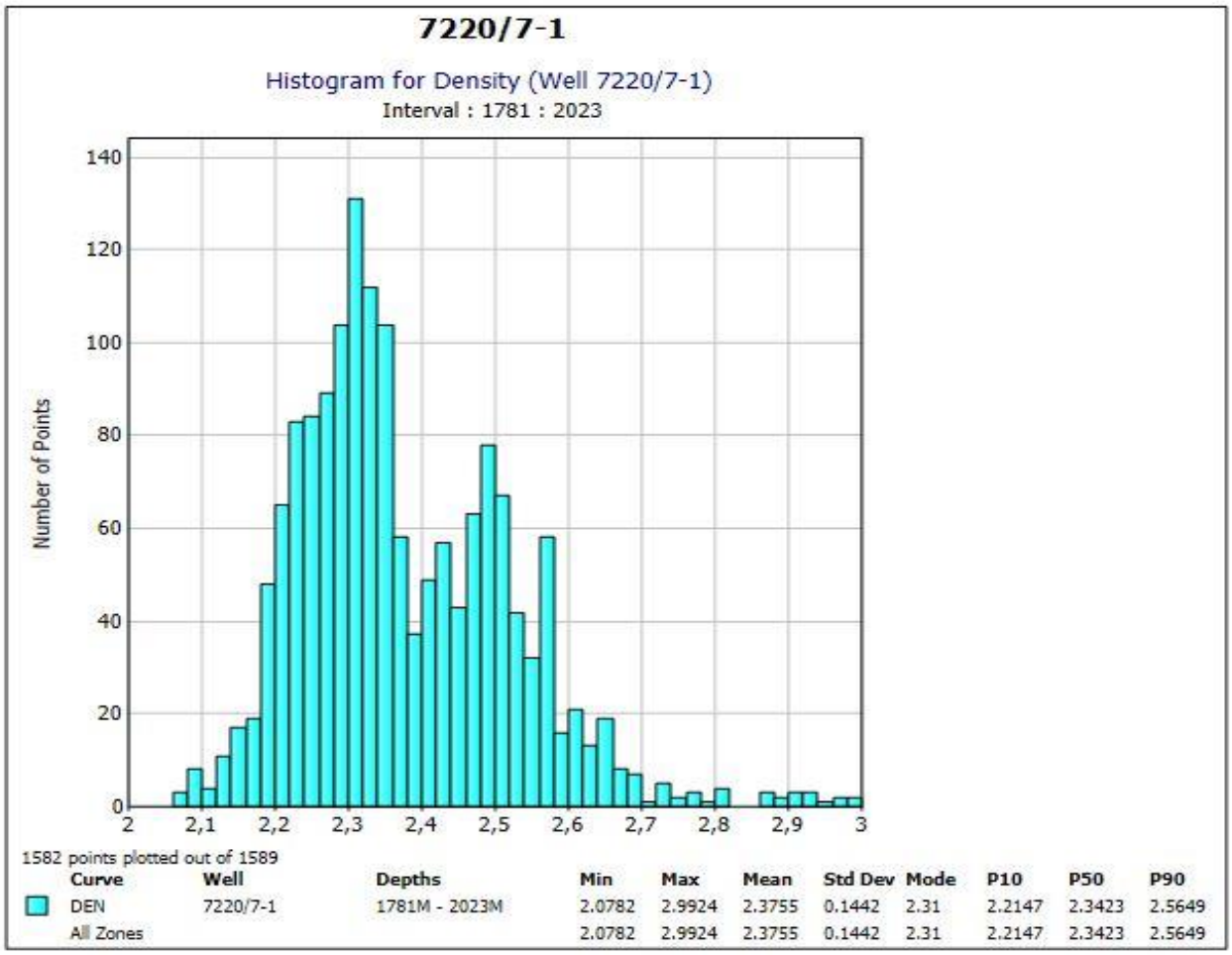

Figure 5.5a: Histogram of density (g/cc) distribution of the Stø and Nordmela Formations for well 7220/7-1. Mean density is 2.37 g/cc.

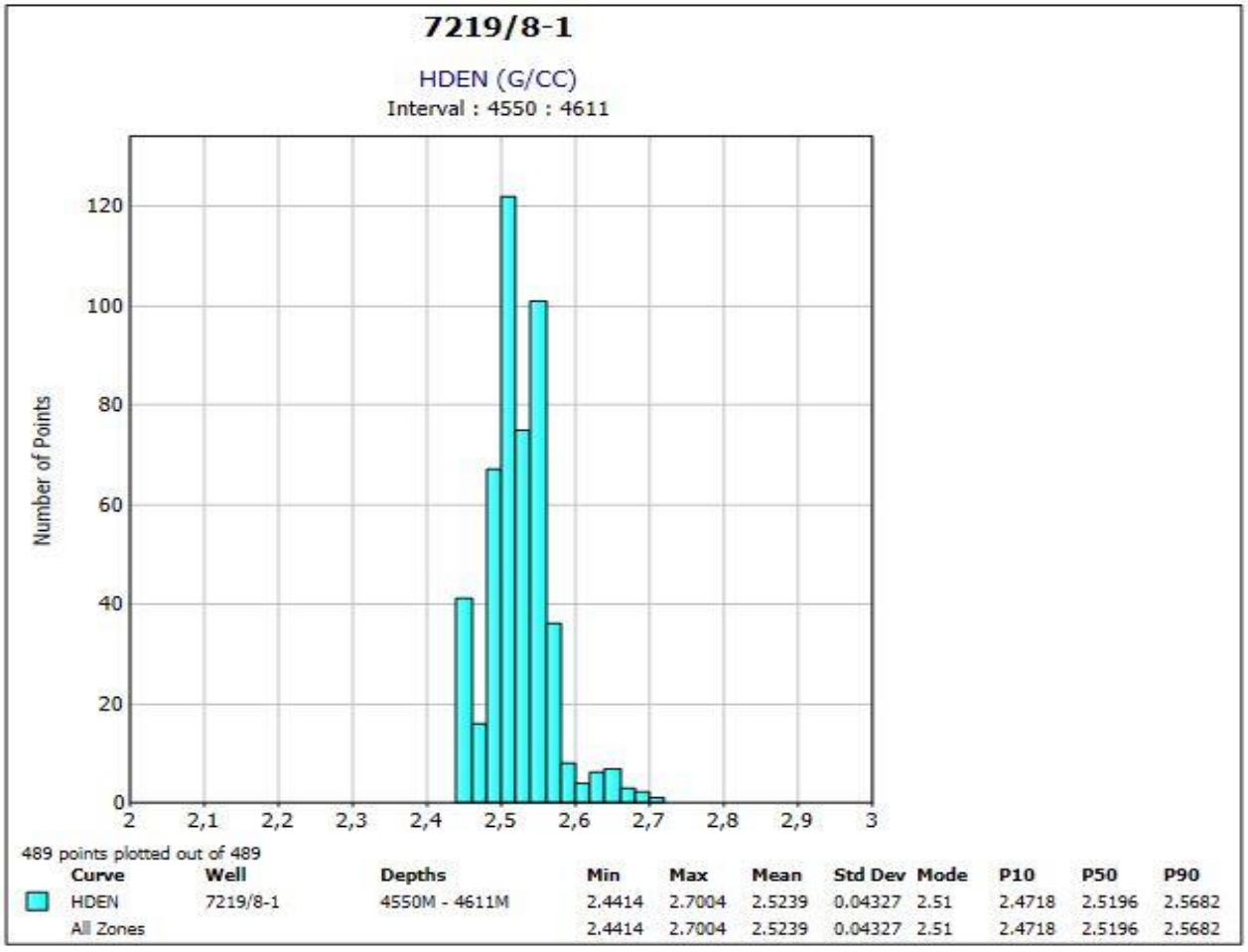

Figure 5.5b: Histogram of density (g/cc) distribution of the Stø Formation for well 7219/8-1. 2.52 g/cc is the mean density.

5.3.1.2 Depth versus Vp (Well 7220/7-1)

Velocity increases with depth and chemically compacted rocks are more dense and having high acoustic impedance. Based on this velocity increment, mechanical and chemical compaction zones can be marked. Stress, temperature and time are the main controlling factors in sediments compaction. Compaction due to stress and temperature effects different rock properties like density, velocity and porosity. Sudden shift in velocity is observed at a transition between mechanical and chemical compaction zone. Based on the Vp-depth trend, both zones are marked in both wells (Fig 5.6a, b). Both the Stø and Nordmela Formations of Jurassic age are in chemical compaction (CC) zone and quartz cementation is probably the main reason for the change in rigidity.

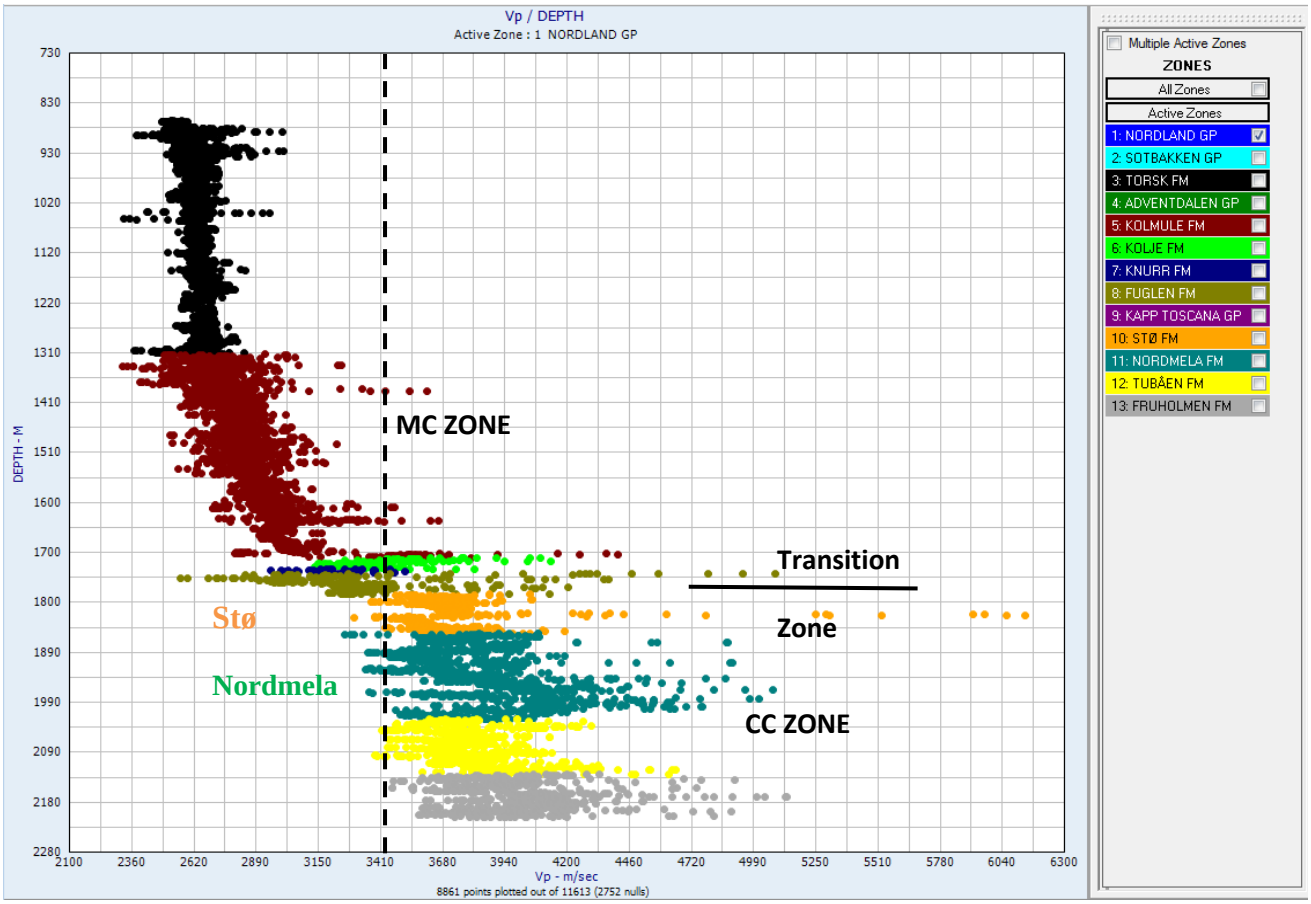

Figure 5.6a: Cross plot between Depth (m) and Vp (m/s) showing compaction trend in well 7220/7-1. Threshold velocity is shown by dotted line.

Velocity increases with depth and chemically compacted rocks are more dense and having high acoustic impedance. Based on this velocity increment, mechanical and chemical compaction zones can be marked. Stress, temperature and time are the main controlling factors in sediments compaction. Compaction due to stress and temperature effects different rock properties like density, velocity and porosity. Sudden shift in velocity is observed at a transition between mechanical and chemical compaction zone. Based on the Vp-depth trend, both zones are marked in both wells (Fig 5.6a, b). Both the Stø and Nordmela Formations of Jurassic age are in chemical compaction (CC) zone and quartz cementation is probably the main reason for the change in rigidity.

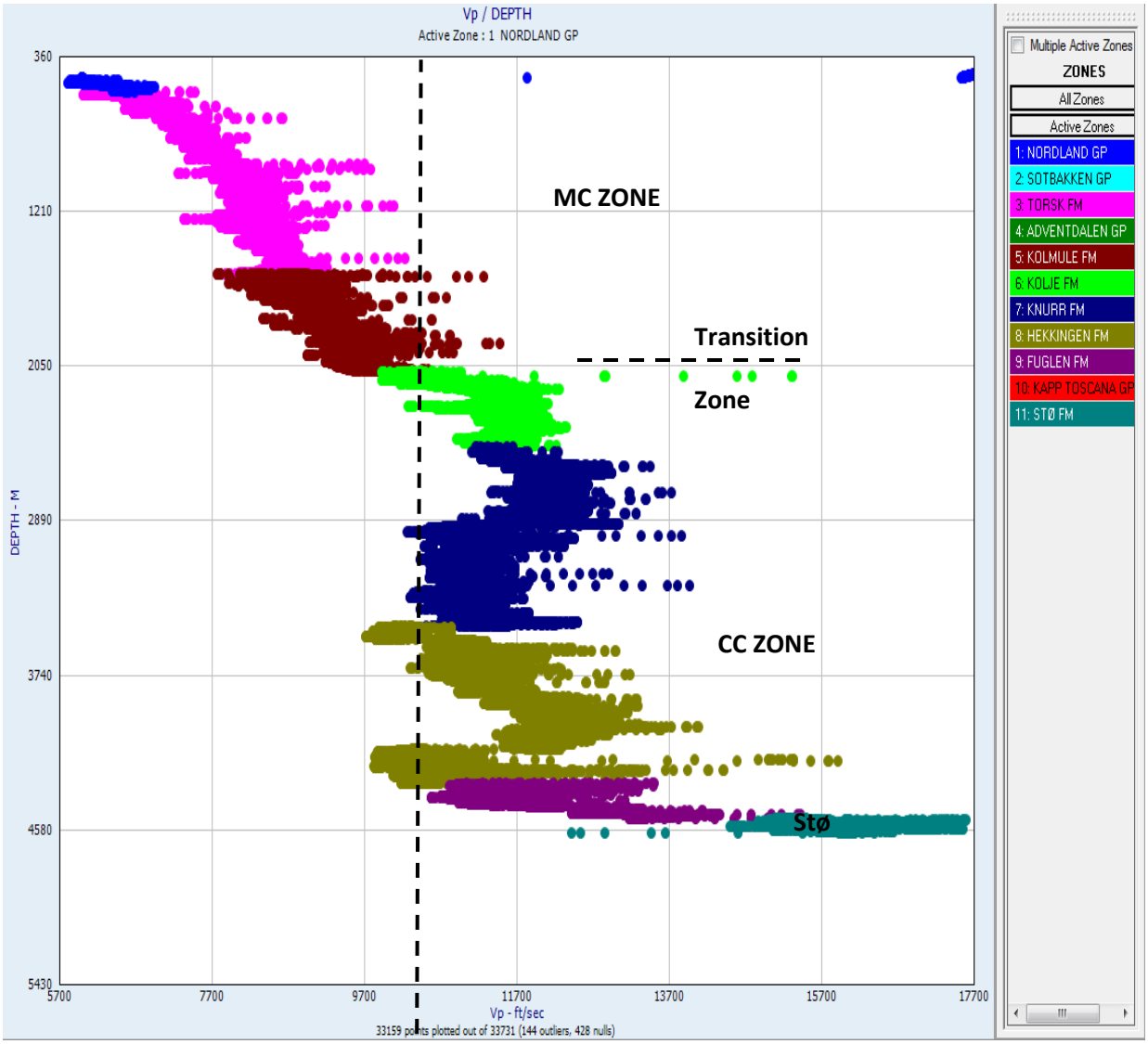

Figure 5.6b: Cross plot between depth (m) and Vp(m/s) showing compaction trend in well 7219/8-1. Dotted line is showing threshold velocity.

Different cross plots of density and gamma ray color code with neutron porosity from well 7220/7-1 and 7219/8-1 showing difference between the Stø and Nordmela Formations. For well 7220/7-1, interval depth is 1781m-2023m and 4550m-4611m for 7219/8-1. Comparison is made within the same well as well as between two wells. For claystone and sandstone separation, gamma ray cut of value is 60 API. Density and porosity of the Stø Formation in both wells is difference. This is due to high quartz cementation at greater depth and low porosity and high stiffness (figure 5.7). The Stø Formation in shallow well is less dense and more porous.

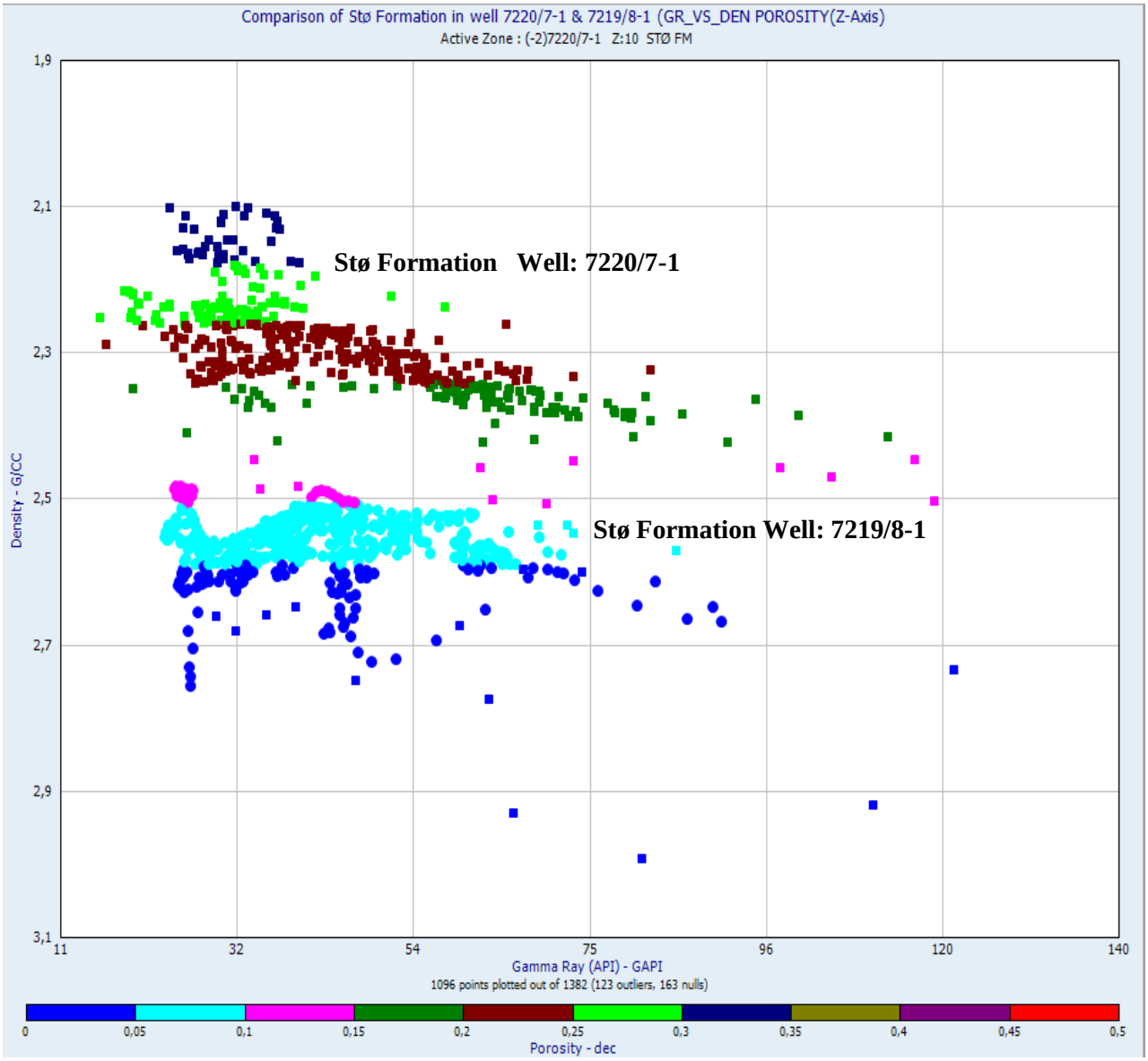

Figure 5.7: Cross plot between density (g/cc) and gamma ray(API) color coded with porosity(%) showing comparison of the Stø Formation between well 7220/7-1 and 7219-8-1.

Porosity cross plot for well 7220/7-1 and 7219/8-1 is plotted with depth for given intervals of the Stø and Nordmela Formations (Figure 5.8).This gives the porosity difference between two wells in the Stø and Nordmela Formations. Porosity difference is significant between the Stø Formation in well 7220/7-1 and 7219/8-1 (Figure5.9).

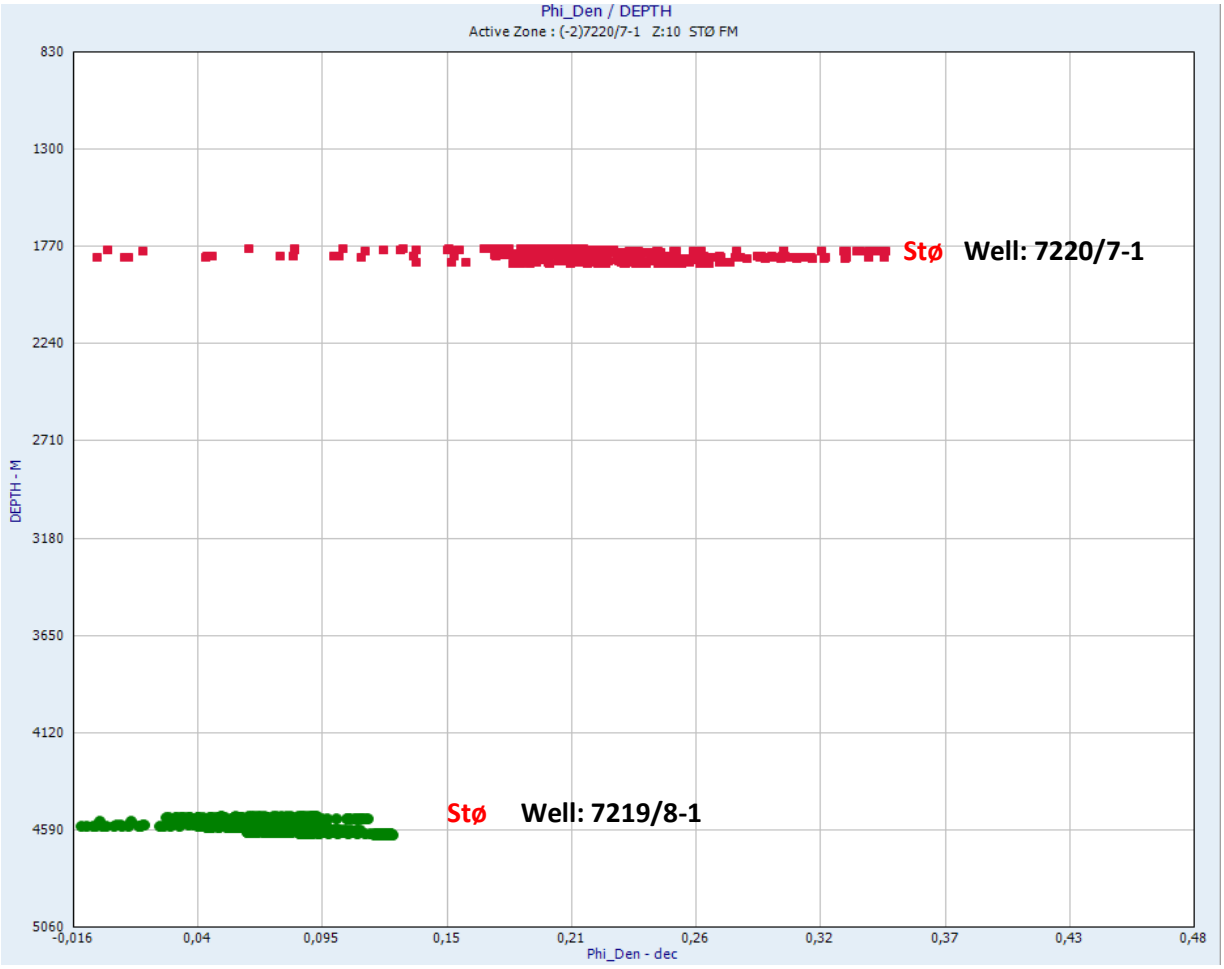

Figure 5.8: Cross plot between Depth (m) and porosity (%) showing comparison of the Stø Formation between well 7220/7-1 and 7219-8-1

6 MINEROLOGICAL AND PETROGRAPHICAL ANALYSIS

6.1 Introduction

Mineralogical and petrographical analysis can be performed in order to understand the mineralogical effects on reservoir properties. Provenance, burial diagenesis, amount of matrix, grain size distribution and cementation are analyzed and estimated based on these analyses.

Samples of both the Stø and Nordmela Formation from well 7210/8-1 and 7220/7-1 have been analyzed. Composition and porosity information of these samples have been point counted under a polarizing microscope.

Point counting results are helpful to find out Intergranular volume, petrographical classification and provenance studies by using thin sections.

In order to find out the results, several different techniques including thin section analysis under the polarizing and scanning electron microscope, gold mounted stubs under scanning electron microscope and XRD analysis has been used.

Using both optical and scanning electron microscopy, estimation of quartz cementation in both wells is the main target to look for. How porosity is influenced with burial depth due to cementation and factors that affect quartz overgrowth at deep burial are also under consideration.

Results

6.2 Thin Section Analysis

6.2.1 Stø and Nordmela Formations

40 Thin sections from both wells have been analyzed under the plan polarizing microscope and collect the porosity and mineralogical information using point counting. IGV calculation, sorting, grain size distribution, provenance and petrographical classification are the parameters that are under consideration.

A total of 29 thin sections from Stø and 11 from Nordmela Formation are studied from both wells. Almost all samples from Stø Formation are well sorted and fine to medium grain apart from sample (4599.84m) that is moderately sorted from both wells (Table 6.1). Samples of Nordmela Formation are well to moderately sorted from well 7220/7-1. Quartz grains are

mostly monocrystalline along with some polycrystalline. Kaolinite and K-feldspar are observed in shallow well (7220/7-1) but not in deep well (7219/8-1). Illite, lithic fragments and muscovite are the other observed minerals. The most dominant cement observed in both well is quartz but calcite, siderite and ankerite are also present in minute amount. Long, concavo-convex and sutured grain to grain contacts are observed (Fig 6.2). The amount of quartz cementation varies with depth. Samples from shallow depth have low quartz cementation as compared to the samples from deeper depth (Fig 6.3). Porosity in Stø Formation is ranging from (2- 8%) in well 7219/8-1 and both Nordmela and Stø Formation has a range in between (20-25%) in well 7220/7-1(Table 6.2). In well 7219/8-1, Stø Formation has quartz cementation that is ranging from (5-8%) but both Stø and Nordmela Formation is from (0-2%) in well 7220/7-1. Overall the amount of detrital quartz in Stø Formation is quite high but values of quartz cementation are low in well 7219/8-1. At this depth, quartz overgrowth is expected to be higher than this. In this well, sample from depth 4607.6m have abnormally high amount of cement due to presence of siderite around 39.3% and high IGV as well as compared to others (Table 6.1). Same from the well 7220/7-1 where sample from depth 1938.63m have comparatively high IGV value around 44.4% because of the high carbonate cement value due to the presence of siderite (Table 6.2).

Table 6.1: Point Counting Results from well 7219/8-1.

Well	Formations	Depth	Rock Composition			Matrix		Other Minerals	Cement		Porosity		IGV	Sorting	Grain size (mm)
			Qtz	Feldspar	Lithic. Frag	Authigenic.Clay	Muscovite		Quartz	Carbonate	Primary	Secondary			
				Plag.Albite											
7219/8-1	Stø	4597.23	79.9		2.1	3.6	0.3	1.2	6.6	0.9	5.1	0.3	16.8	well	0.10
		4598.33	79		1.5	3.9	0.3	0	5.7	1.8	7.2	0.6	19.5	well	0.10
		4598.93	75.7	0.3	1.8	4.2	0.6	0.6	7.5	1.5	6.9	0.9	21.6	well	0.05
		4599.84	76		1.2	3.3	0.3	1.2	7.2	3.9	6.3	0.6	21.6	Moderately	0.15
		4600.15	80.2		2.7	3.3	1.2	0	6.3	1.5	4.8	0	17.1	well	0.07
		4601.64	78.8		2.1	3	0.9	1.2	6	1.7	5.7	0.6	17.9	well	0.07
		4602.51	80.5		1.5	2.7	0.9	0.6	6.9	3	3.9	0	17.4	well	0.10
		4602.87	83.2	1.5	1.8	1.8	0	0.6	5.7	0.9	4.5	0	12.9	well	0.10
		4603.71	84.1		1.5	2.1	0	0	7.5	0.6	3.6	0.6	14.4	well	0.10
		4603.91	84.6	0.6	2.4	2.4	0	1.3	5.7	0	3	0	11.1	well	0.10
		4604.26	83.2	1.5	1.8	2.4	0.3	0.3	7.2	0.6	2.7	0	13.2	well	0.10
		4604.68	83.8		1.5	2.7	0.3	0	7.5	1.2	3	0	14.7	well	0.07
		4605.76	76.9	0.3	2.7	4.2	1.5	1.2	6.9	2.7	3.3	0.3	18.9	well	0.10
		4606.35	81.4		2.1	4.2	0.9	0.6	6.3	1.8	2.7	0	15.9	well	0.05
		4607.6	45.4		1.8	2.1	0.6	0.6	7.2	39.3	2.4	0.6	52.2	well	0.05
		4608.4	81.7		1.5	3.3	1.2	0.3	6.6	2.4	3	0	16.5	well	0.05
		4608.76	82.9		1.2	4.2	2.1	0.3	5.7	0.3	2.7	0.6	15.6	well	0.05
		4609.57	81.4		2.1	3.6	1.8	0.3	6	1.5	3.3	0	16.2	well	0.05
		4610.61	77.2		1.8	5.7	3.3	0	6.6	1.2	4.2	0	21	well	0.05
		4611.05	73.3		2.7	3.3	0.6	3.6	7.2	5.7	3	0.6	20.4	well	0.15

Table 6.2: Point Counting Results from well 7220/7-1.

Well	Formations	Depth	Rock Composition				Matrix		Other Minerals	Cement		Porosity		IGV	Sorting	Grain size (mm)
			Qtz	Feldspar		Lithic. Frag	Authigenic. Clay	Muscovite		Quartz	Carbonate	Primary	Secondary			
				Plag.Albite	K-Feldspar											
7220/7-1	Stø	1787.65	59.9	1.5	1.8	3	6.1	0.6	0.9	0.9	0.3	24.1	0.9	32.9	well	0.10
		1792.85	50.5	2.1	1.5	3.9	8.4	0.6	7.5	0.6	0	23.4	1.5	34.5	well	0.10
		1807.7	56.5	1.5	5.1	3.3	3.3	0.6	3.6	0.6	0.3	24.6	0.6	30	well	0.05
		1814.37	58.9	2.7	3.6	3	3	0	1.2	0.9	2.7	22.8	1.2	30.6	well	0.15
		1815.9	59.4	0.9	4.5	3.3	4.9	1.5	2.7	0.3	0	21.9	0.6	29.2	well	0.05
		1892.58	68.9	0.3	1.2	2.4	0	0	0.3	1.2	0	24.8	0.9	26.9	well	0.10
		1842.32	67.4	0.3	1.2	3.6	1.2	0	1.2	0.6	0	23.9	0.6	26.3	well	0.10
		1848.9	66	0.6	2.1	3.9	0.6	0	0.6	0.9	0	24.4	0.9	26.8	well	0.10
		1851.4	64.8	0.6	1.2	3.3	2.1	0.6	1.2	0.6	0	24.7	0.9	28.9	well	0.10
	Nordmela	1861.4	69.6	0.3	0.6	2.8	0.9	0	0.3	1.2	0	23.4	0.9	26.4	Moderately	0.10
		1871.97	70.9	0.3	0.3	3.3	1.2	0	0	0.9	0	21.9	1.2	25.2	well	0.15
		1883.35	62.1	0	1.8	2.5	6.6	1.2	0.9	1.2	0	22.5	1.2	32.7	well	0.05
		1890.4	55.9	6.6	4.8	1.8	6	0.9	0.9	0.9	0	21.6	0.6	30	Moderately	0.10
		1905.46	63.7	3.9	2.1	2.7	2.7	0	0	0.6	0	24.3	0	27.6	well	0.10
		1922.47	60.4	0.9	5.7	1.8	5.7	0.6	1.2	0.6	0	22.5	0.6	30	well	0.10
		1938.63	47.5	0.3	4.5	2.4	5.7	0.3	0.9	0.3	15.9	21.9	0.3	44.4	Moderately	0.07
		1948.73	65.2	0.3	2.4	1.8	3	0	0	1.2	2.1	23.1	0.9	30.3	Moderately	0.10
		1972.23	69.4	0	0.6	1.8	0.9	0	0	1.8	1.5	22.5	1.5	28.2	very well	0.15
		1975.37	66.1	0.6	2.1	1.5	3.9	0.6	0.9	0.9	0	21.6	1.8	28.8	well	0.15
		2017.25	57.3	0.9	5.7	0.6	11.1	2.4	0	0.9	0	20.5	0.6	35.5	well to Moderately	0.07

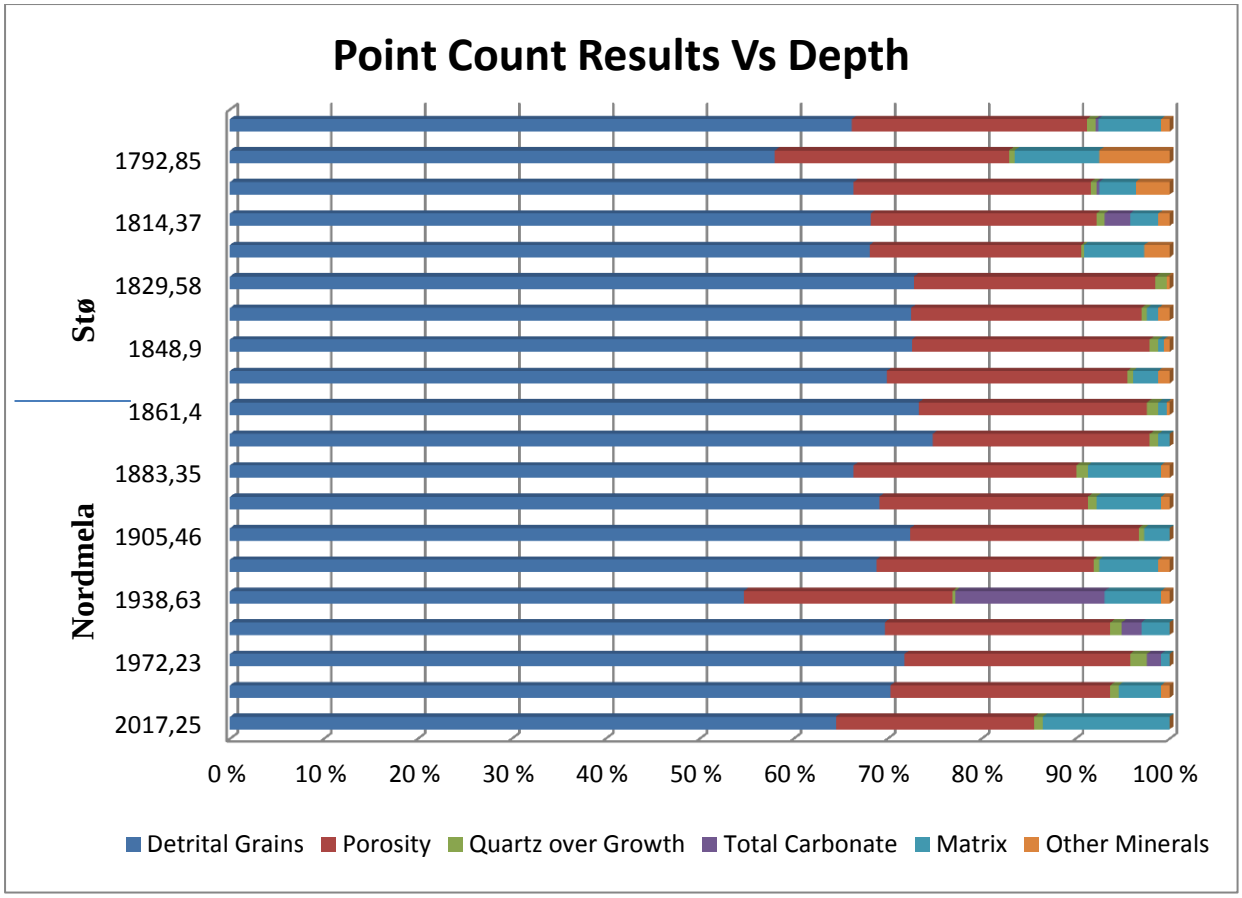

Figure 6.1a: Point count results versus depth from Well 7220/7-1. Stø Formation starts from 1792.85 and an end up at 1851.4 m. Rest is the Nordmela Formation.

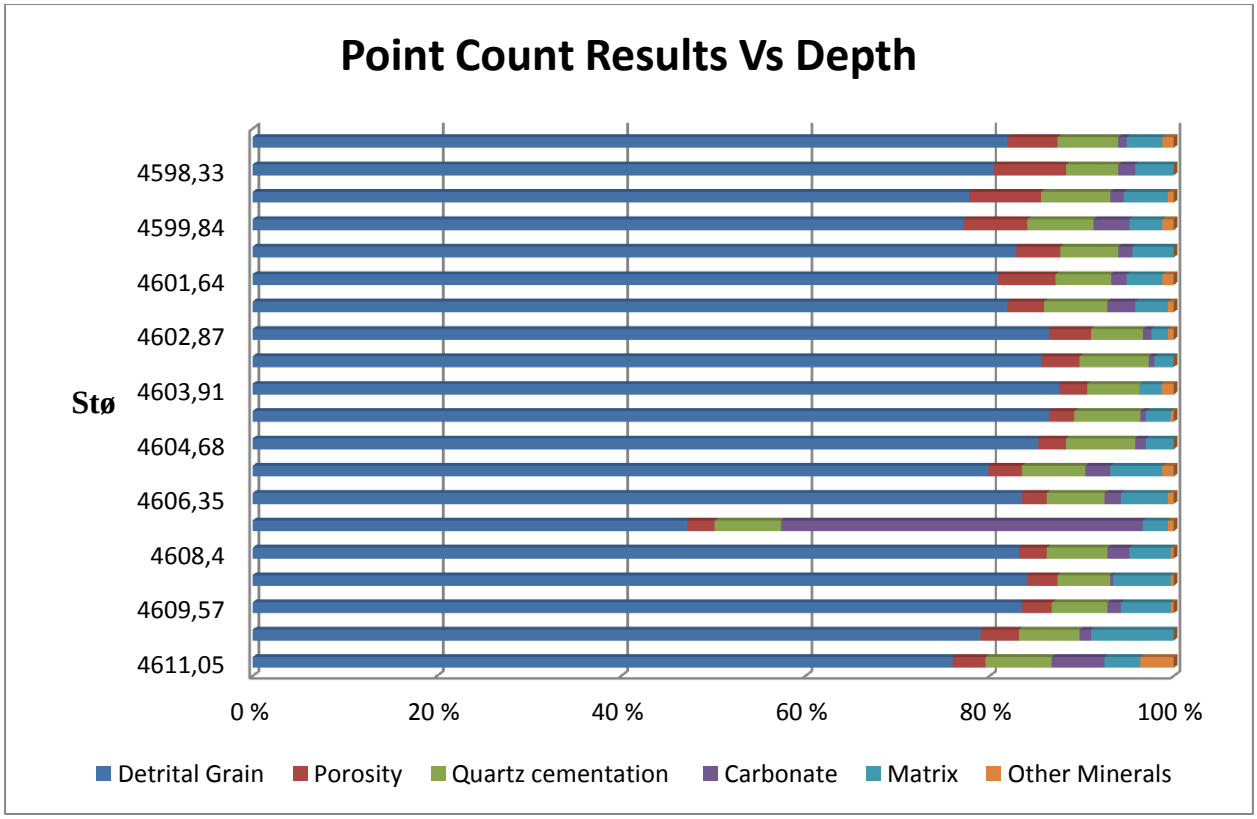

Figure 6.1b: Point Count results Vs depth from Well 7219/8-1. All samples are from the Stø Formation.

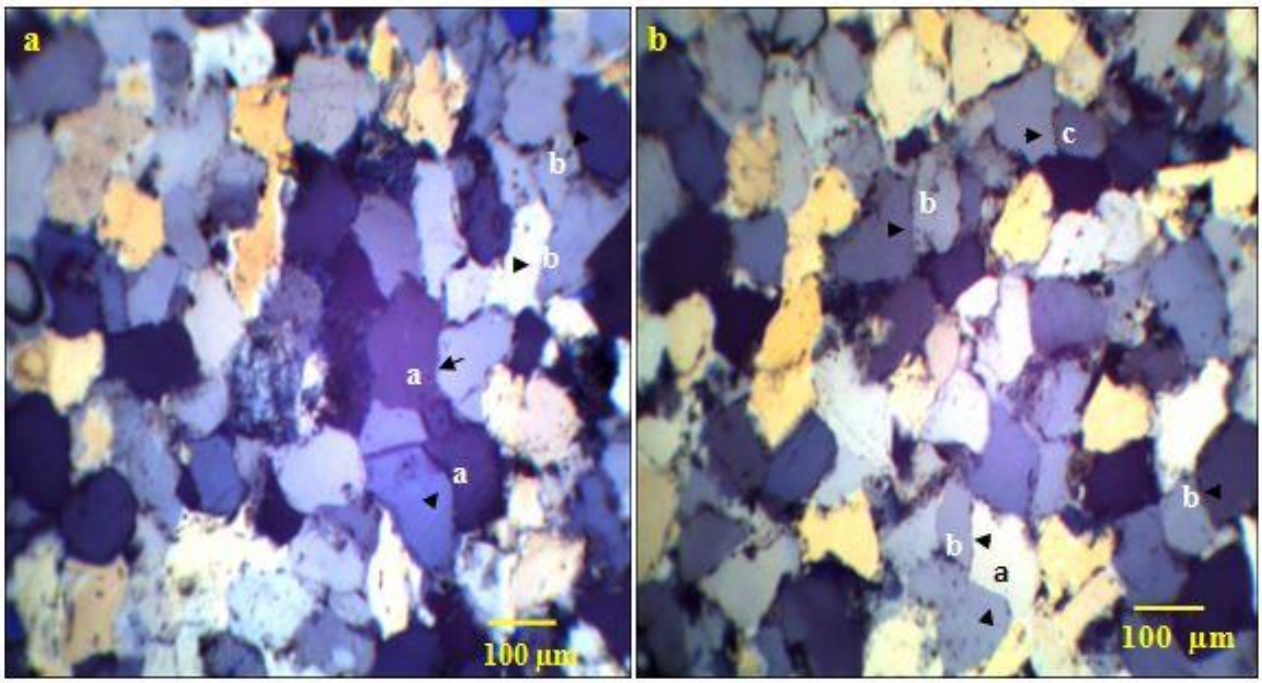

Figure 6.2: Thin section from well 7219/8-1.Contacts between quartz grain and quartz cementation. a) 4602.87m b) 4604.26m a) Concavo-convex b) long c) suture.

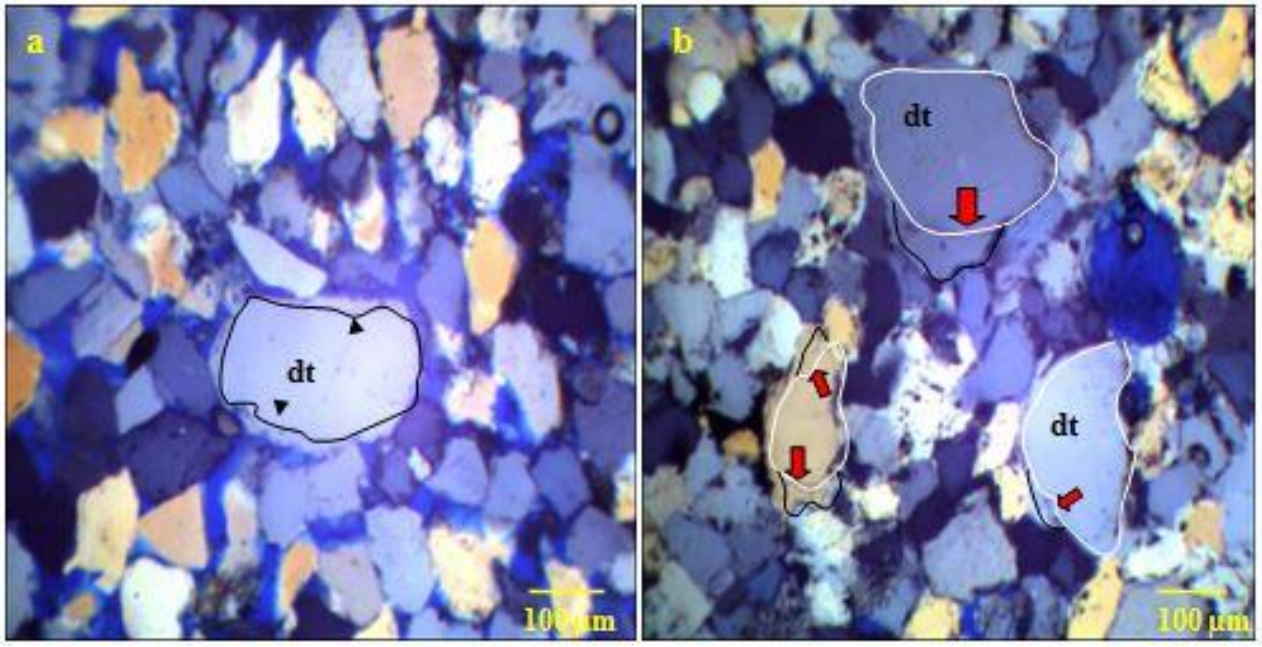

Figure 6.3: Well: 7220/7-1 Depth: 1787.65m a) Showing low quartz Overgrowth around detrital quartz grain. Well: 7219/8-1 Depth: 4599.84 b) and 4597.23. dt = Detrital quartz grain. Indicate low over growth and ➡ show high overgrowth.

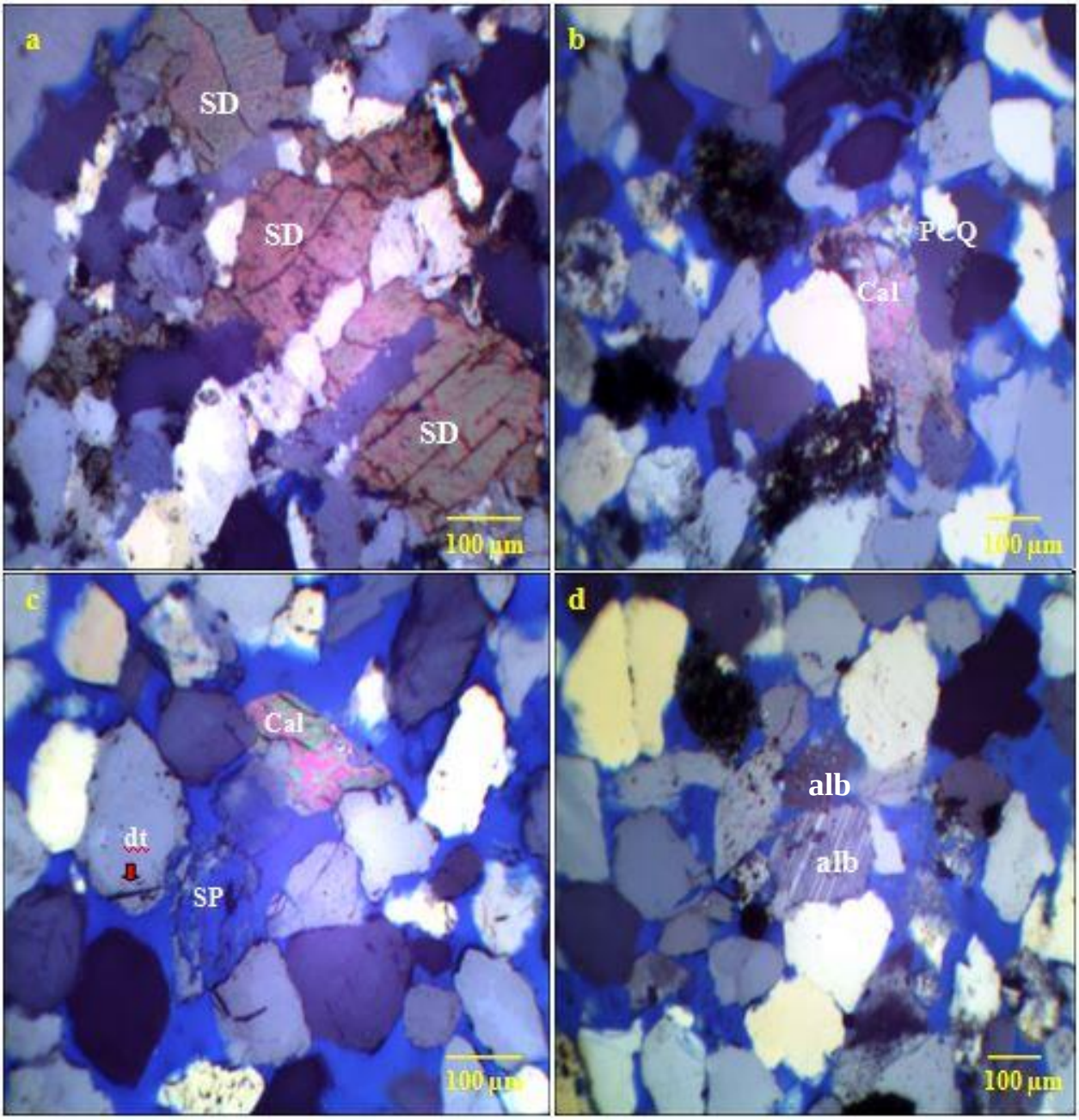

Figure 6.4: a) 7219/8-1 (4611.05m) Siderite cement in between grains b) 7220/7-1 (1814.37m) Calcite cement in between quartz grain. c) 7220/7-1 (1972.23m) K-feldspar grain dissolution (secondary porosity), quartz overgrowth and calcite cement. d) 7220/7-1 (1814.37m) Plagioclase feldspar (Albite). SD=Siderite, Cal=Calcite, PCQ = polycrystaline quartz, dt = detrital grain, SP= secondary porosity, Alb= albite. ➡ Show quartz overgrowth.

6.2.2 Petrographical Classification

In order to find out the sandstone composition, all the detrital grains observed during point counting are divided into three categories; quartz, feldspar and lithic fragments and plotted in a QFL ternary petrographical classification diagram (Fig 6.5a, b)**.** Stø and Nordmela Formation from both wells contain matrix less than 15% and have quite good amount of detrital grain so it fall into a category of arenite. Samples from both wells fall in arenite area defined by Pettijohn (1975). Quartz arenite are the sandstones having more than 95% of quartz and considered as matured mineralogically (Adams et al., 1984). Most of the samples lie in between mature to sub-mature category according to Folk (1951) and this is confirmed from the results obtained by thin section analysis (Table 6.1 & 6.2).

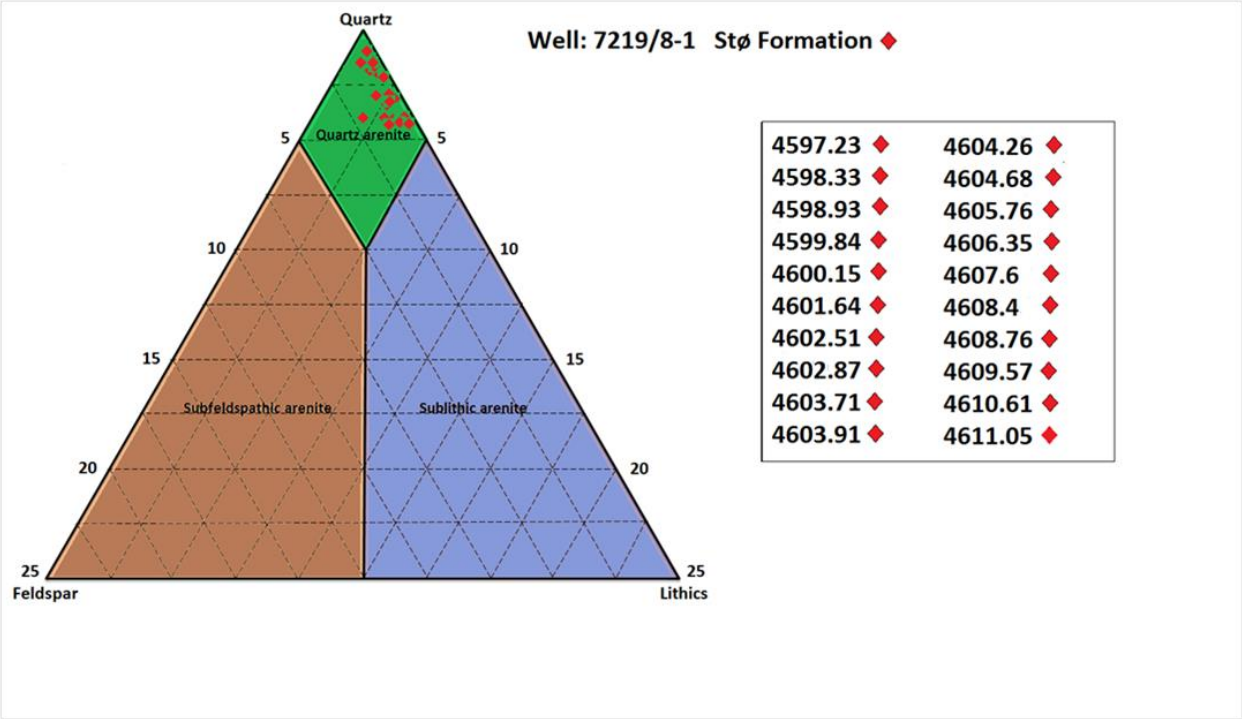

Figure 6.5a: Petrographic Classification of arenites Pettijohn (1975). All samples of Stø Formation from well 7219/8-1 are plotted according to their depth.

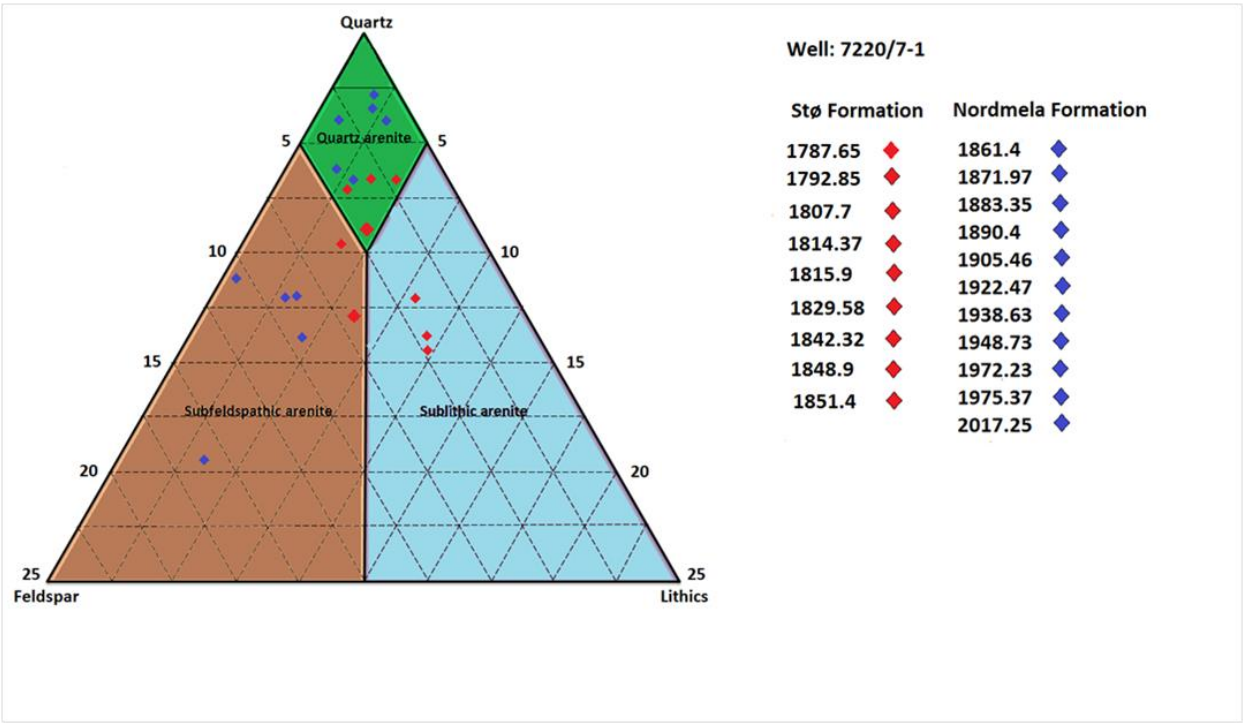

Figure 6.5b: Petrographic classification of arenites Pettijohn (1975). All samples of the Stø and Nordmela Formations from well 7220/7-1 are plotted according to their depths.

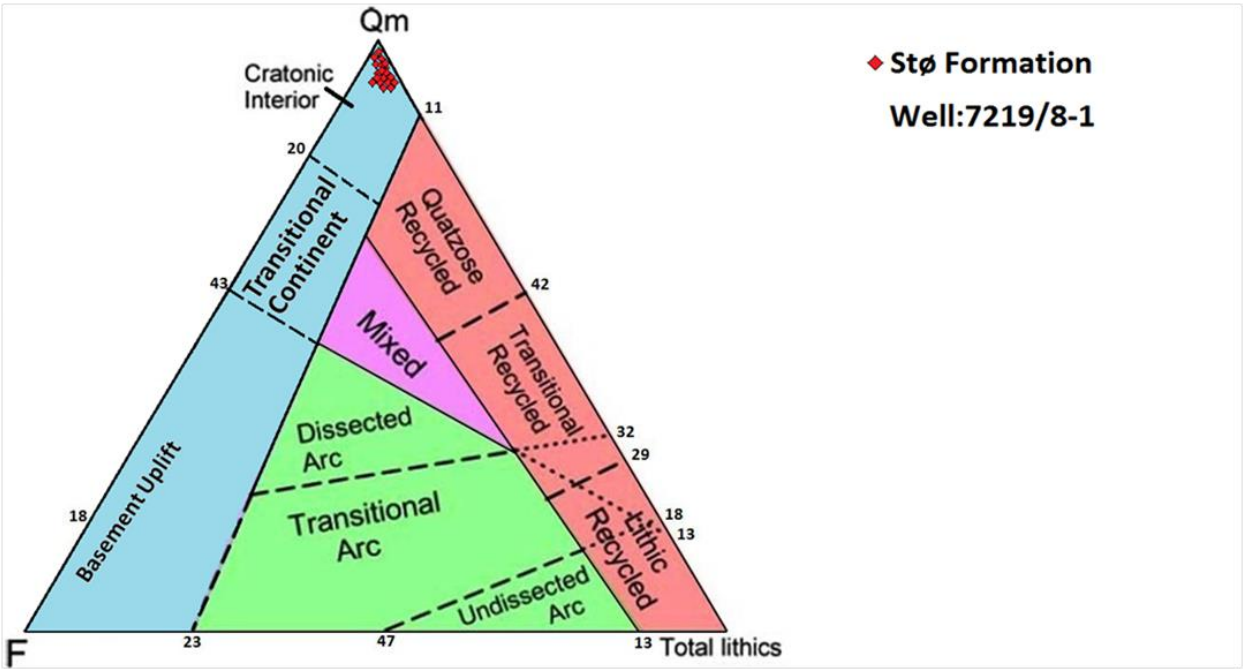

Figure 6.6a: Sandstone composition and provenance interpretation shows a provenance of cratonic interior from the sandstone petrography (Dickinson 1985).

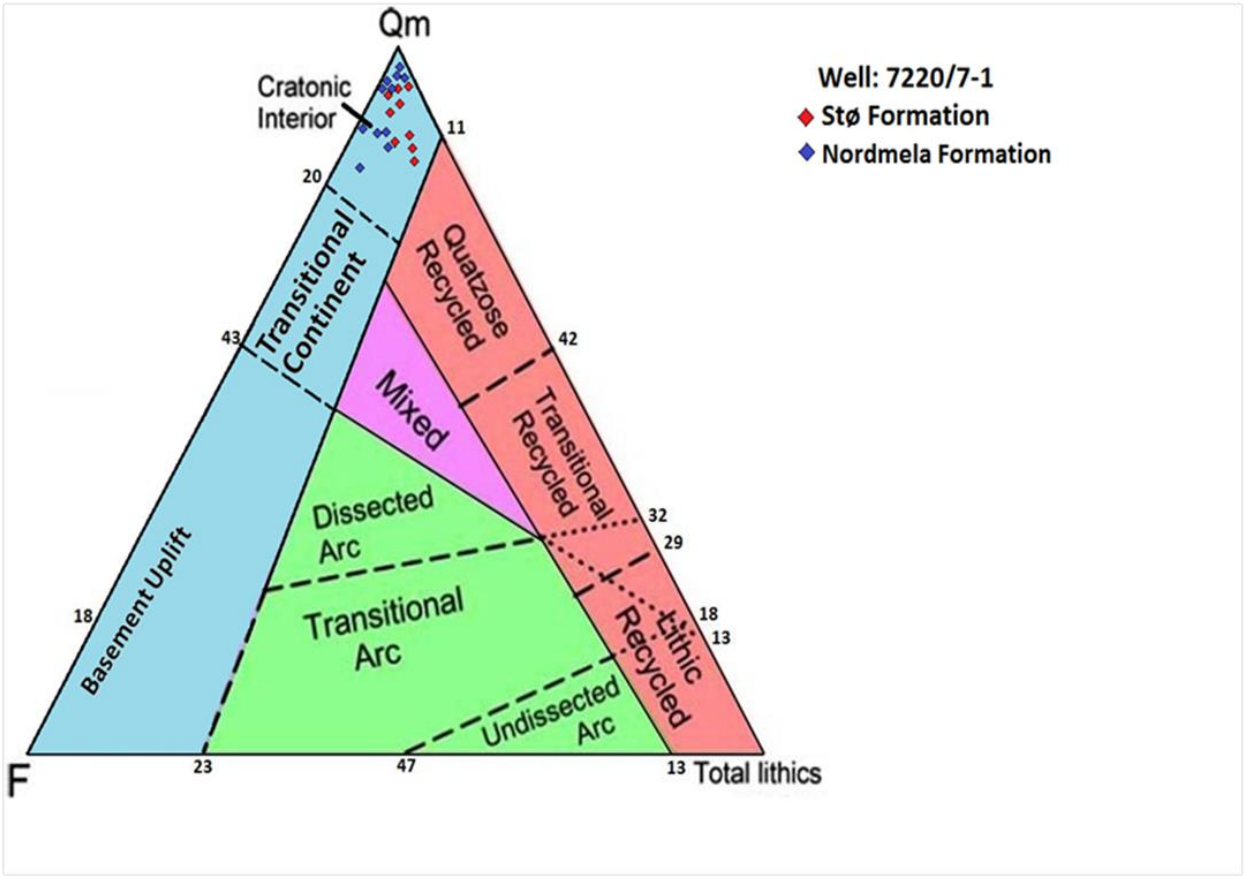

Figure 6.6b: Sandstone composition and provenance interpretation shows a provenance of cratonic interior from the sandstone petrography (Dickinson 1985).

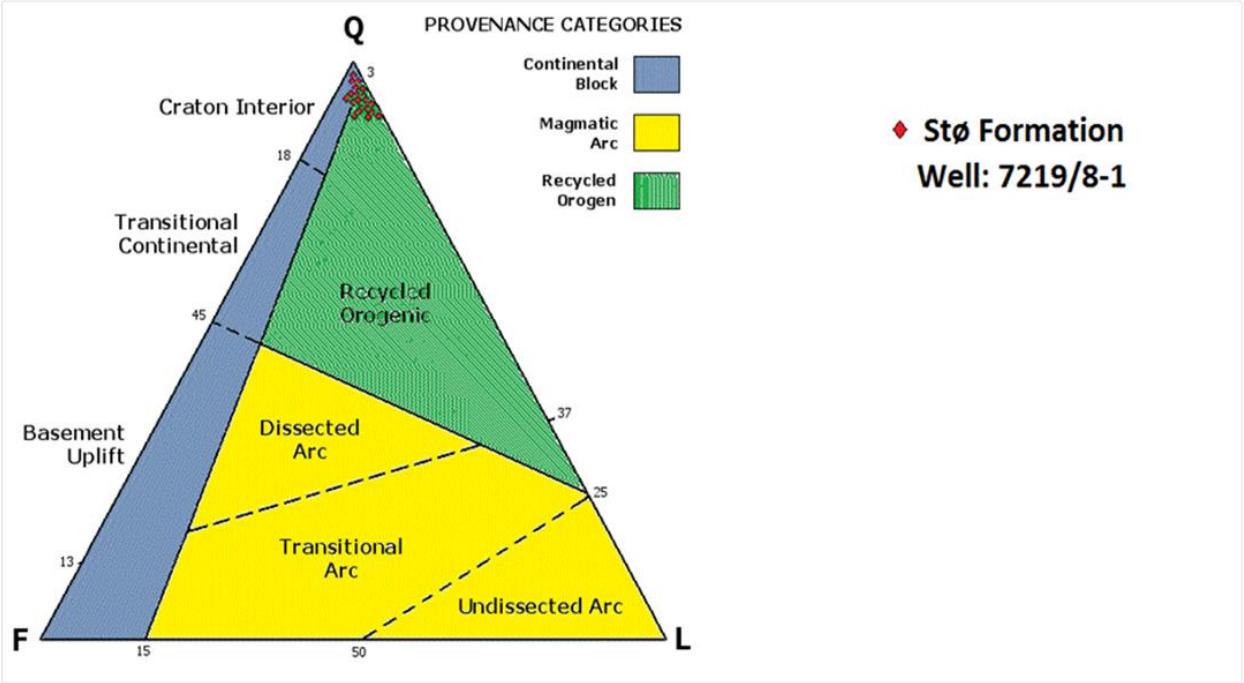

Figure 6.7a: Source of the Stø Formation sandstone shown by detrital mineral composition plot is cratonic interior or recycled orogenic (Dickinson 1985).

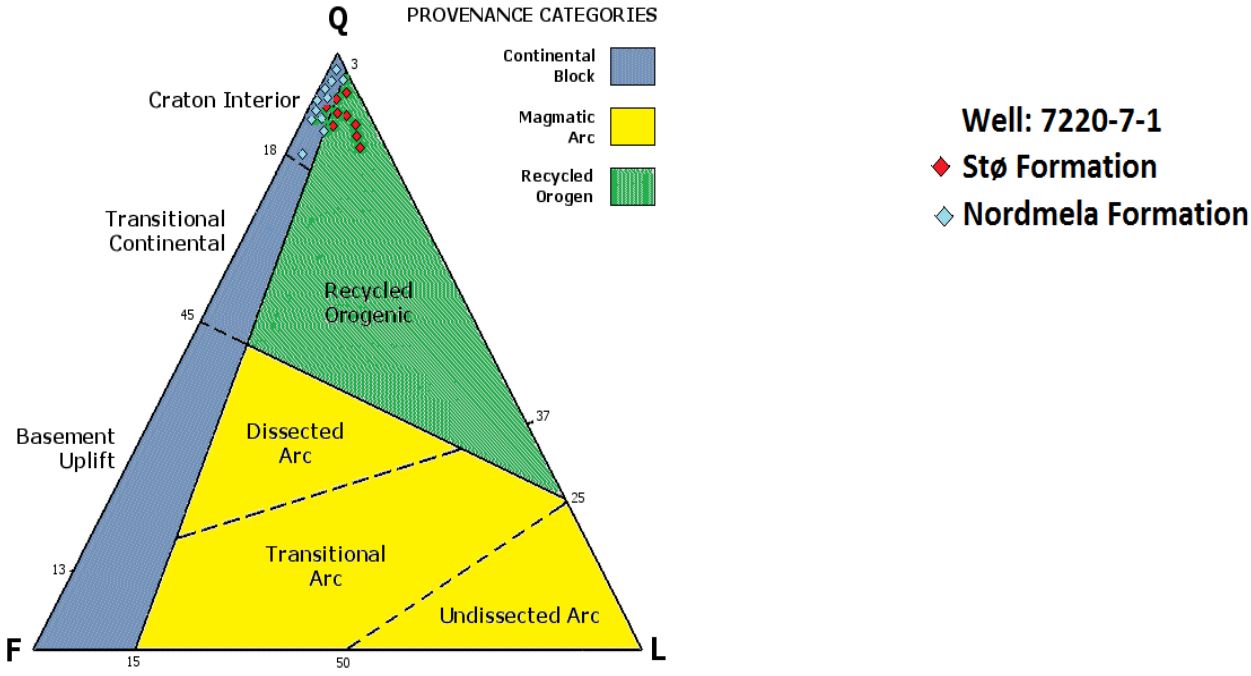

Figure 6.7b: Source of the Stø and Nordmela Formations sandstones shown by detrital mineral composition plot is cratonic interior or recycled orogenic (Dickinson 1985).

6.2.3 Total Porosity

In point counting, total porosity is the parameter that gives both primary and secondary porosity. In these samples, secondary porosity observed is too low. Porosity values vary a lot in histogram in both wells (Figure 6.8)**.** The total porosity varies from 2.7% in deep well to 25.7 in shallow well. After calculating mean porosity of the Stø and Nordmela Formation in both wells (table 6.3) it is quite evident that, overall mean porosity is high in well 7220/7-1 as compared to porosity in well 7219/8-1. There is not a big difference in porosity between Stø and Nordmela Formation in well 7220/7-1 but the mean porosity of the Stø Formation in well 7219/8-1 is 4.335% and 24.74% in well 7220/7-1.

Table 6.3: Calculated mean porosity of the Stø and Nordmela Formations from well 7219/8-1 and 7220/7-1

Mean Porosity (%)		
7219/8-1	**7220/7-1**	
Stø Formation	**Stø Formation**	**Nordmela Formation**
4.335	**24.74**	**23.19**

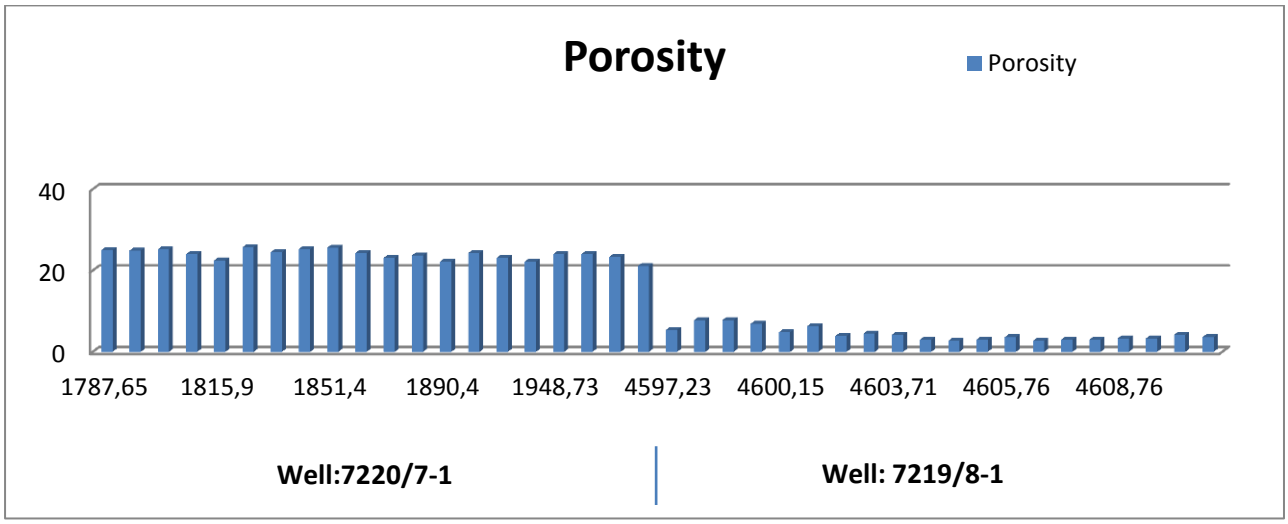

Figure 6.8: Histogram of Total porosity versus depth from both wells.

In sandstones usually low porosity is mainly due to the result of late diagenesis. Quartz cementation controls the porosity reduction at greater depth due to increase in temperature. Quartz cement is plotted against the counted percentage of porosity to find out any relationship existing within the samples. Both wells are plotted simultaneously; where well 7220/7-1 have quite low quartz cementation and high porosity percentage in histogram due to shallow depth (Figure 6.09)**.** This makes a coupled relationship between porosity and quartz cementation where both are inversely proportional to each other. On the other hand quartz cementation in well 7219/8-1 is not as high at this depth as it is supposed to be and both porosity and quartz cementation are not showing any big difference respectively. Generally quartz cementation at this depth is expected to be quite high as compared to the values in well 7219/8-1. This may be due to miss calculation while doing point count analysis. Under the optical microscope, surface of the quartz grains observed in theses samples look homogeneous and smooth so it's really hard to differentiate between the detrital quartz rim and the over growth. Pressure solution is also observed where grains are welding due to grain dissolution.

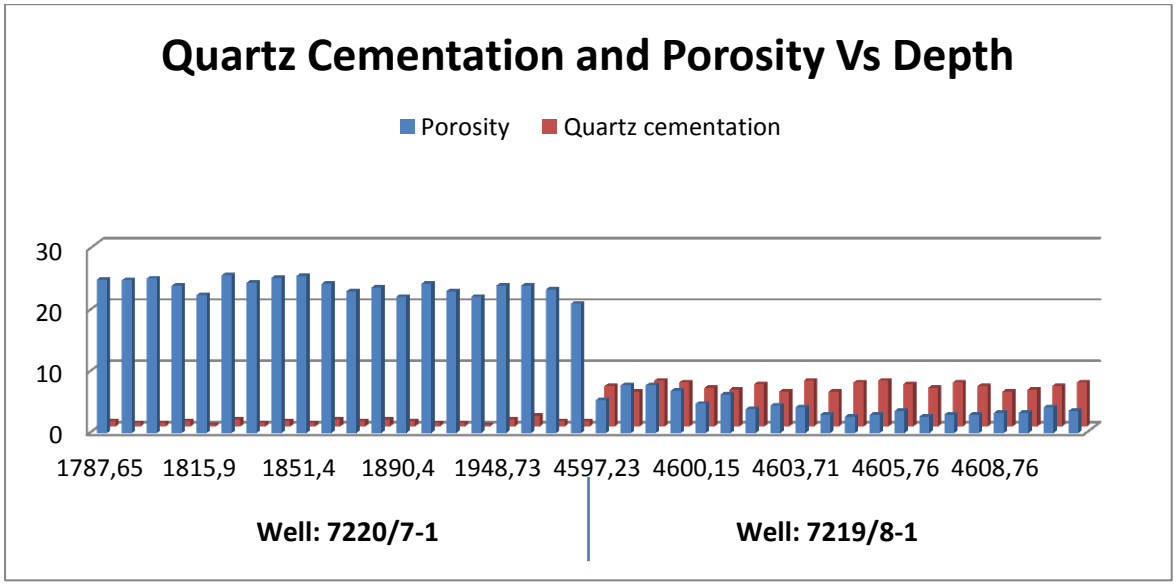

Figure 6.9: Histogram of porosity and quartz cement having a comparison with increasing depth. Both wells are plotted simultaneously.

6.2.4 Authigenic Clays

Most of the clay present within the examined samples in both wells are Pore filling kaolinite and illite and act as porosity reducing agent. The average percentage of clay present in both the Stø and Nordmela Formation are low and varies from 3.3% to 3.4% respectively (Table 6.4). From the figure 6.10 it can be assume that, most of the clay may act as a Pore filling because samples that have high value of clay have comparatively low value of porosity in both wells. Grain coated illite is also observed in SEM in the Stø Formation, well 7219/8-1.

Table 6.4: Calculate mean percentages of clays from both Stø and Nordmela Formation in different wells.

Average clays (%)		
7219/8-1	**7220/7-1**	
Stø Formation	**Stø Formation**	**Nordmela Formation**
3.3	**3.288**	**4.336**

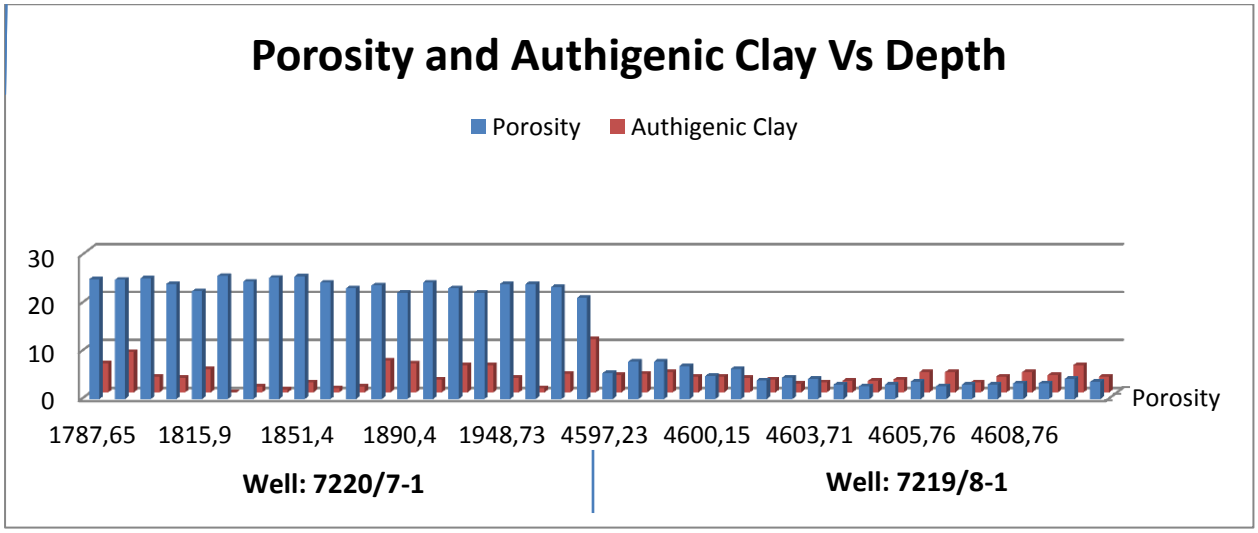

Figure 6.10: Histogram of porosity and authigenic clays comparison with increasing depth. Both wells are plotted together.

6.2.5 Carbonate Cement

In sandstones, carbonate cement is one of the major porosity reducing factors during the early diagenesis. The percentage of carbonate cement present in both well is quite low. Stø

Formation in well 7220/7-1 has the least carbonate cement value. Two samples have relatively very high carbonate value due to the presence of high amount of siderite. Carbonate value in well 7219/8-1 from sample depth 4607.6m is 39.3% and 15.9% from a sample depth of 1938.63m in well 7220/7-1 (Figure 6.11). Mean percentage of carbonate cement ranges from 0.366 to 3.625 (Table 6.5). Carbonate cement other than siderite found in these samples are calcite and ankerite that is also confirmed from SEM and XRD analysis.

Table 6.5: Calculated mean carbonate cement from both Stø and Nordmela Formation.

Carbonate cement (%)		
7219/8-1	**7220/7-1**	
Stø Formation	**Stø Formation**	**Nordmela Formation**
3.625	**0.366**	**1.77**

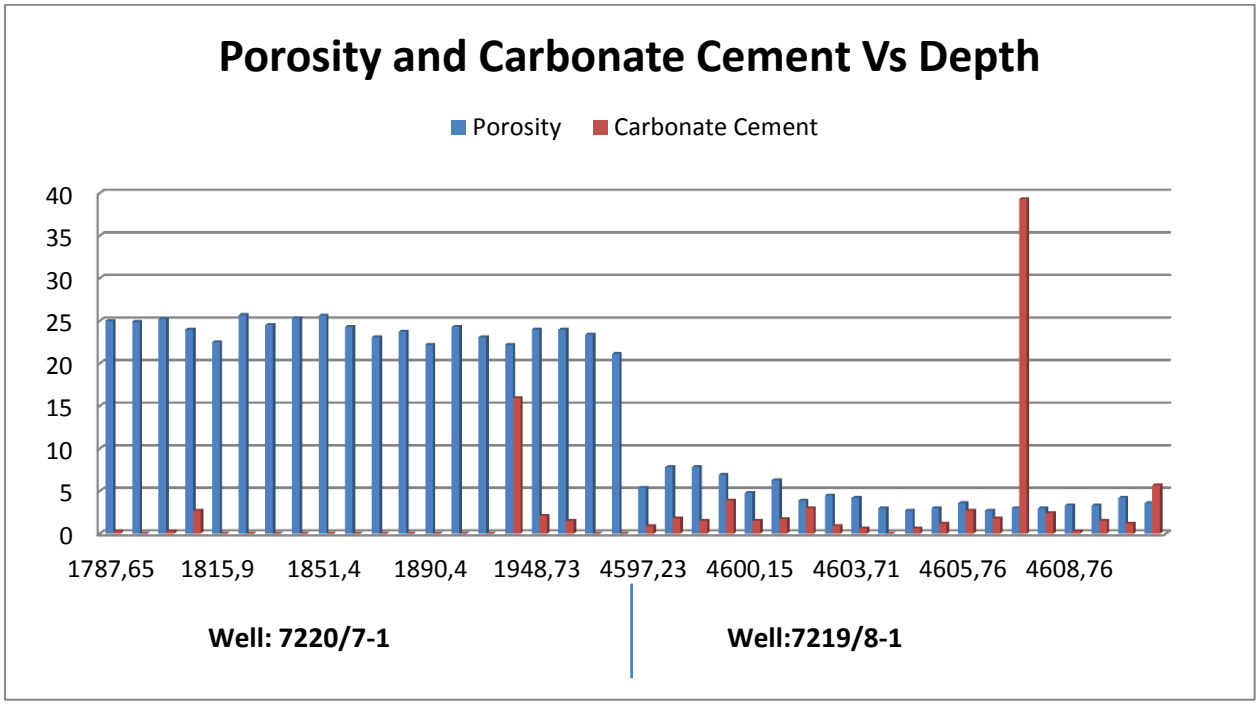

Figure 6.11: Histogram between total porosity and carbonate cement showing comparison.

6.2.6 Intergranular Volume (IGV)

In order to calculate the amount of porosity loss due to compaction and cementation during diagenesis, intergranular volume (IGV) calculation is use and formula for IGV is:

Intergranular volume (IGV) = cement + matrix + porosity.

Intergranular volume is calculated by using point counting results.

Nordmela Formation has the highest IGV value of 30.827% in well 7220/7-1 but the Stø Formation has low IGV value in well 7219/8-1 and that is 18.745%. This is due to the underestimated values of overgrowth measured during point count analysis (Table 6.6).

Table 6.6: Calculated mean IGV of the Stø and Nordmela Formation from both wells

Mean IGV (%)		
7219/8-1	**7220/7-1**	
Stø Formation	**Stø Formation**	**Nordmela Formation**
18.745	**29.566**	**30.827**

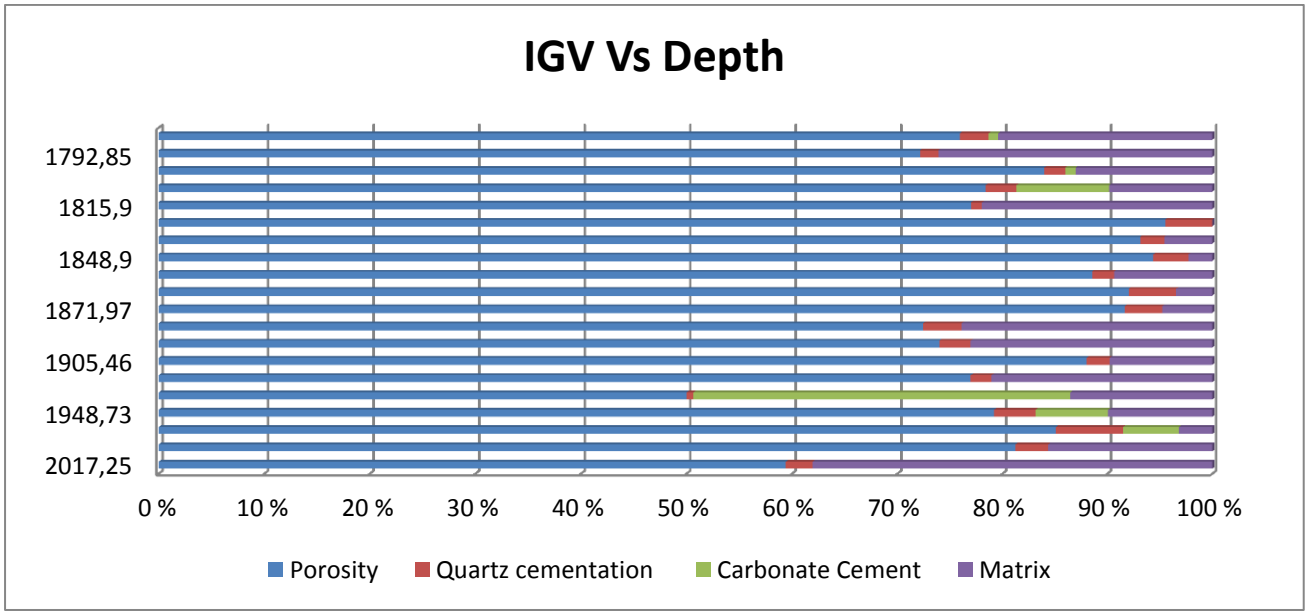

Figure 6.12a : Calculate IGV versus depth from well 7220/7-1.

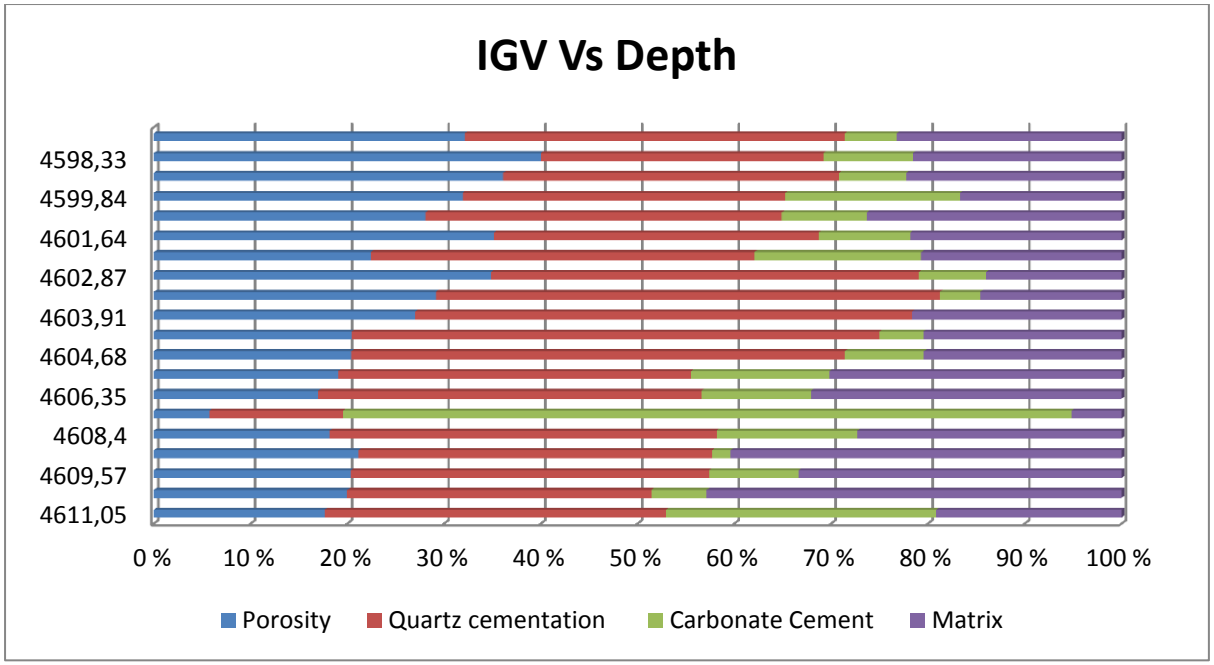

Figure 6.12b : Calculate IGV versus depth from well 7219/8-1.

IGV of both wells have been plotted with increasing depth and IGV at shallow depth is higher than the deeper, mainly due to the high porosity in well 7220/7-1. Matrix also influence a little bit on IGV at the shallow depth. Low IGV at higher depth as compared to the shallow depth is mainly due to low quartz cementation value that is missing calculated during point count analysis. IGV at two sample depths 4607.6m and 1938.63m are extremely high with respect to others. That is due to high amount of carbonate cement, particularly siderite.

6.2.7 Textural Characteristics

In order to understand the variation within the thin section samples of Stø and Nordmela Formation from both deep and shallow wells, a visual estimation is performed on the parameters including, grain size, sorting, and shape against calculated intergranular volume (Figure 6.14a,b,c). Another plot has also been used to see any trend between grain size and sorting (Figure 6.13a,b). Fine grain sediments have better sorting then coarse grain. Same results have been used in order to find the textural maturity of sandstones using the (Folk, 1951) classification (Table 6.7). Most of the samples from Stø Formation are well sorted with varying grain size in both wells but some of the samples from Nordmela Formation are moderately sorted in well 7220/7-1. Generally the trend between IGV and grain size (Figure

6.14b) is showing that the IGV decreases with increasing grain size. Grain shapes also affect the IGV. Rounded grains have more IGV than angular (figure 6.14c). IGV is higher in well 7220/7-1 than in well 7219/8-1 against all the parameters including grain size, shape and sorting. Two samples from both wells have abnormally high IGV due to the presence of high amount of siderite. The amount of quartz overgrowth in well 7219/8-1 during point count analysis is not measured properly, so that's why IGV calculated for deep well is relatively low.

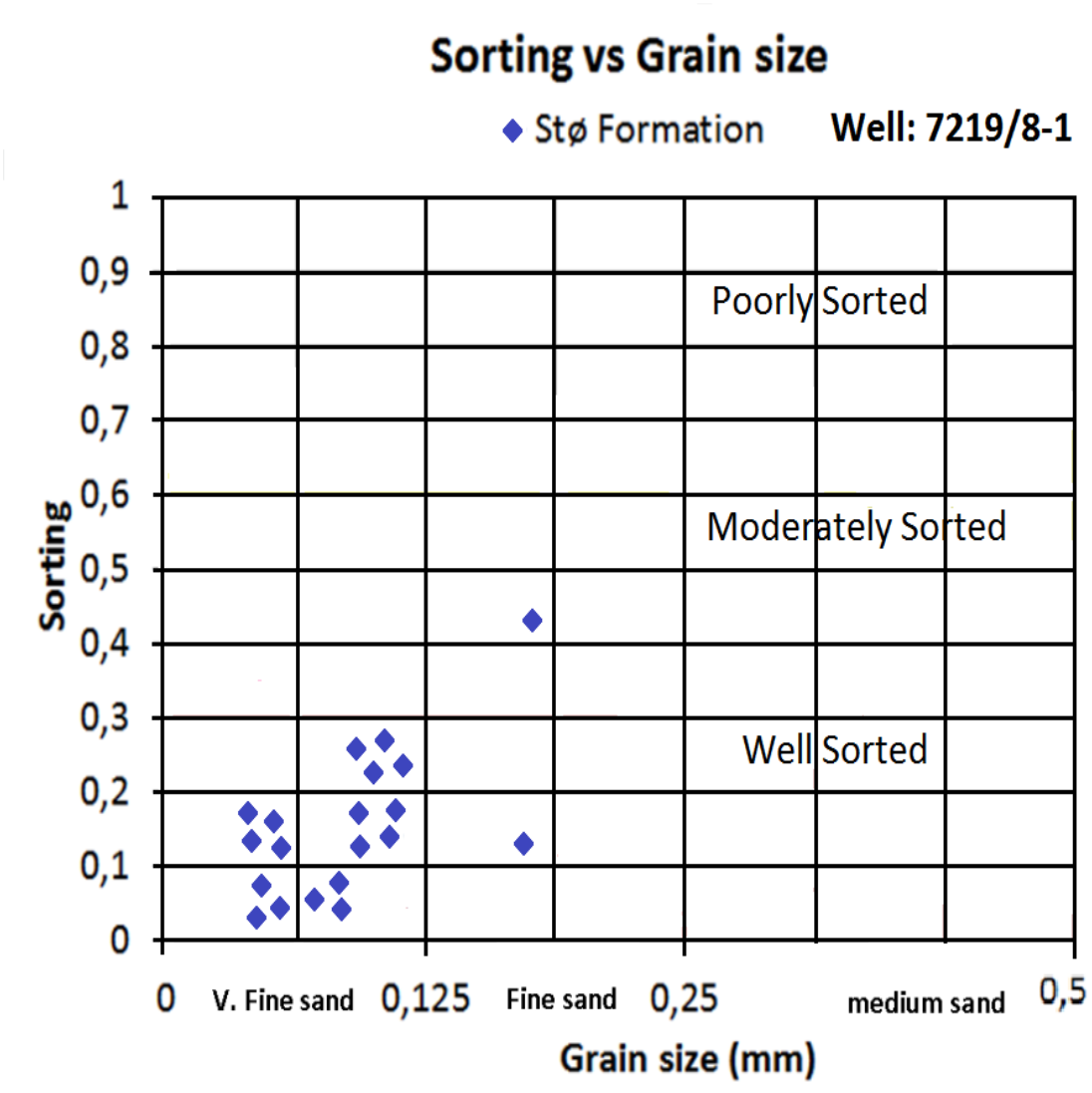

Figure 6.13a:The relationship between the grain size and degree of sorting.

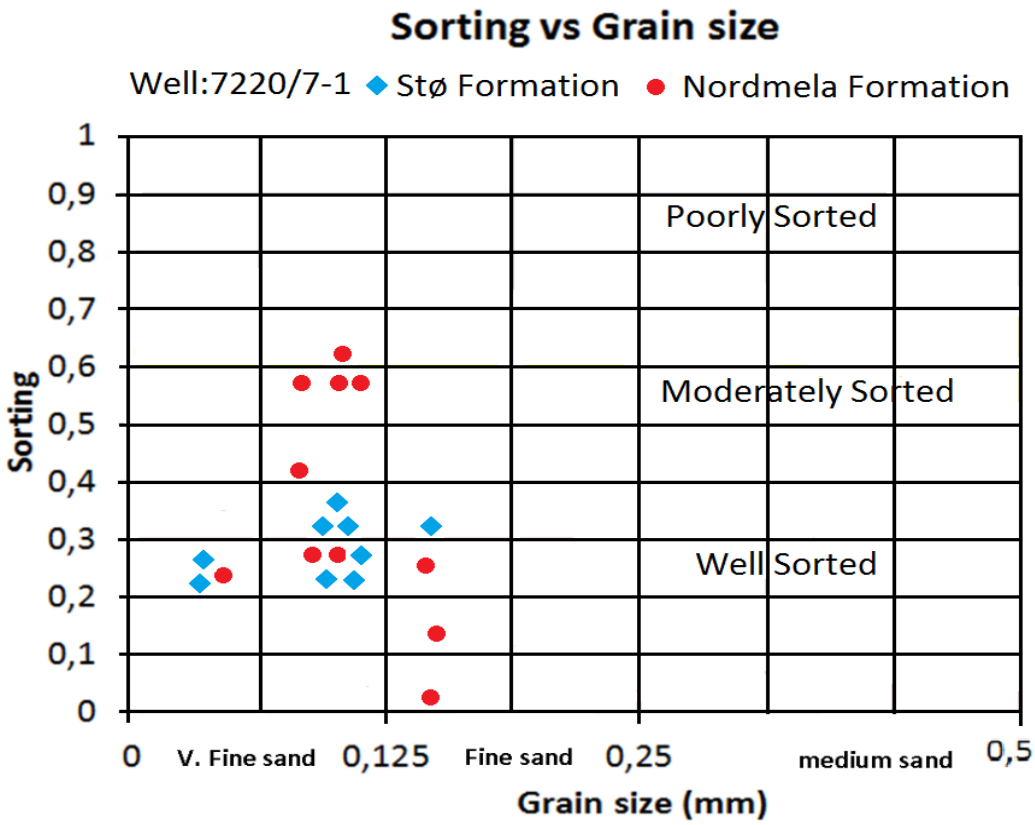

Figure 6.13b: The relationship between the grain size and degree of sorting.

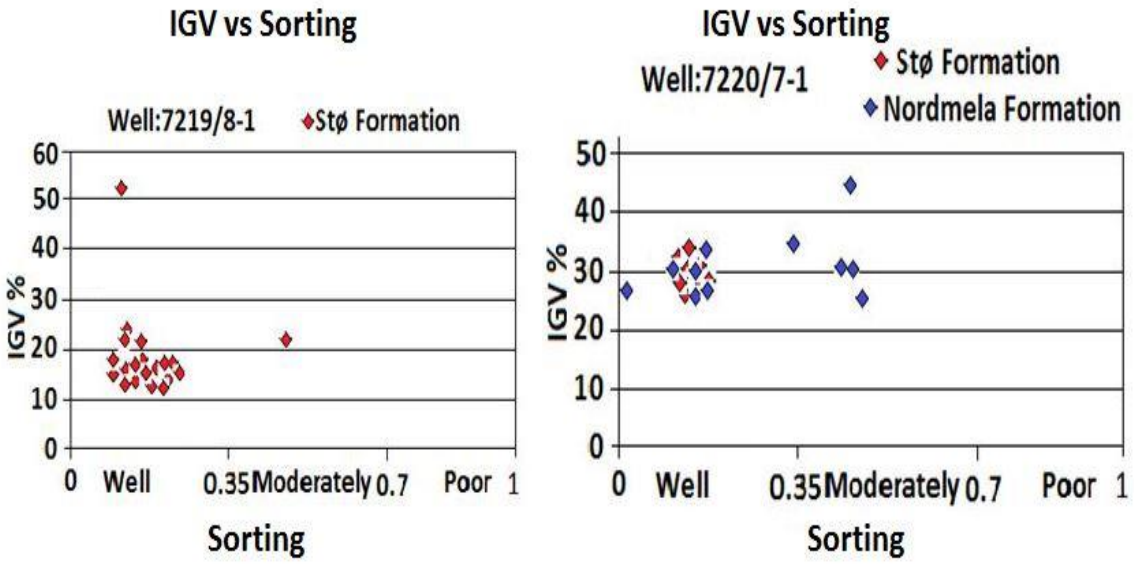

Figure 6.14a: Relationship between Calculated IGV and Grain Sorting.

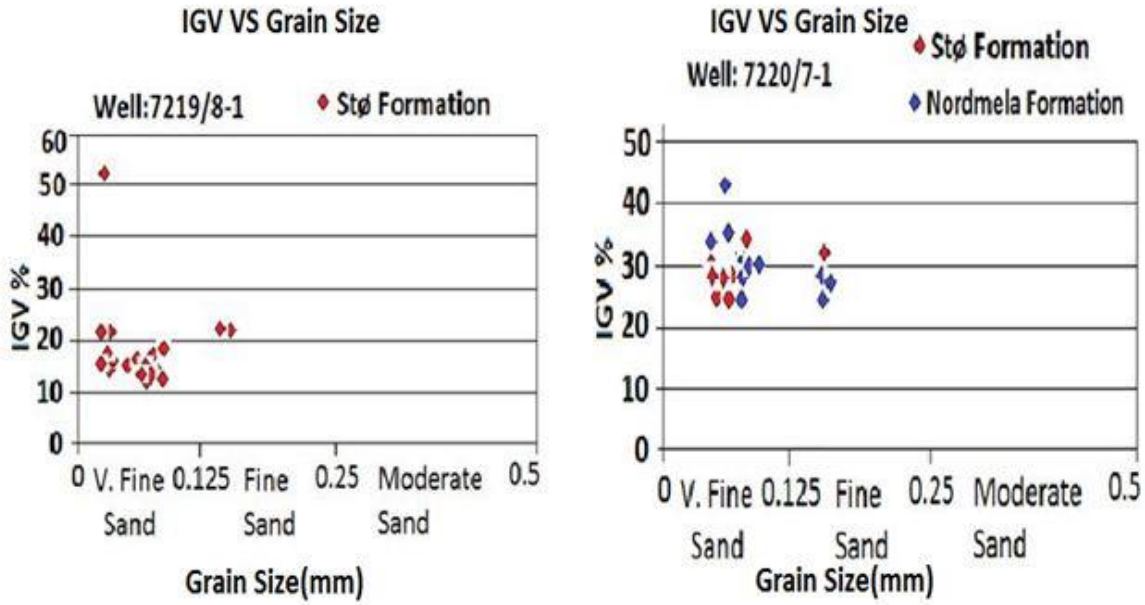

Figure 6.14b: Relationship between Calculated IGV and Grain size (mm).

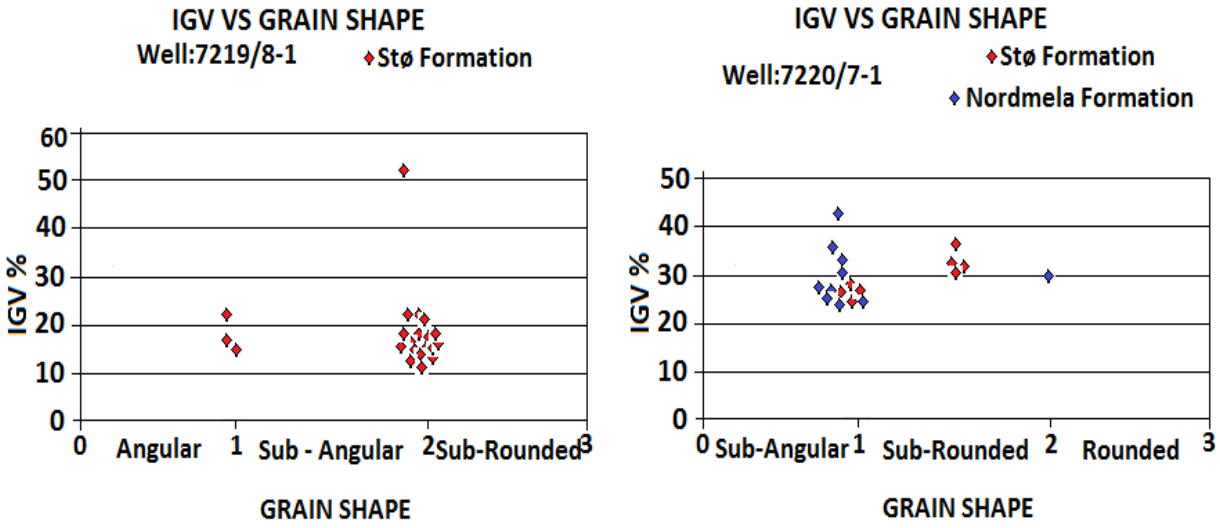

Figure 6.14c: Relationship between Calculated IGV and Grain shape.

6.2.8 Textural Maturity

To find the textural maturity, the results obtained from the visual estimation of grain size, shape and sorting are used.

Table 6.7: Stages of Textural Maturity in sedimentary Rocks are given. Revised from (Folk, 1951).

1. Immature stage	2. Submature stage	3. Mature stage	4. Supermature stage
Grains are angular and poorly sorted and sediments have large amount of clay and fine mica.	Grains are poorly sorted and angular and sediments have little or no clay.	Grains are well sorted but shape is still subangular and sediments have no clay.	Grains are rounded and well sorted and sediments have no clay.

Samples from both the Stø and Nordmela Formations contain insignificant amount of clay content to fall in immature stage, so by this they are out of this category of textural maturity by (Folk, 1951). Now in order to satisfy the definition of maturity by (Folk, 1951) grains should be well sorted and subangular in their shape. Most of the samples from both wells are subangular to subrounded and well sorted apart from some of the samples from the Nordmela Formation that are moderately sorted.

6.3 Scanning Electron Microscopy (SEM)

For further investigation, samples from both wells are analyzed under scanning electron microscope (SEM). Detailed observation has been made in order to look for the amount of quartz cementation in both wells with the help of cathode luminescence. Grain coating, authigenic clays including Pore filling and grain coated illite along with kaolinite; carbonate cements like calcite and siderite with other minor minerals are under observation.

6.3.1 Grain Coatings

In order to find out the coating under the scanning electron microscope, stub mounted samples have been investigated. Very few exceptions in all the samples have been observed with very minute amount. Micro quartz coating is observed in the Nordmela Formation in well 7220/7-1 at a sample depth of 1922.47m (Fig 6.15) and in the Stø Formation at 4606.35m in well 7219/8-1.

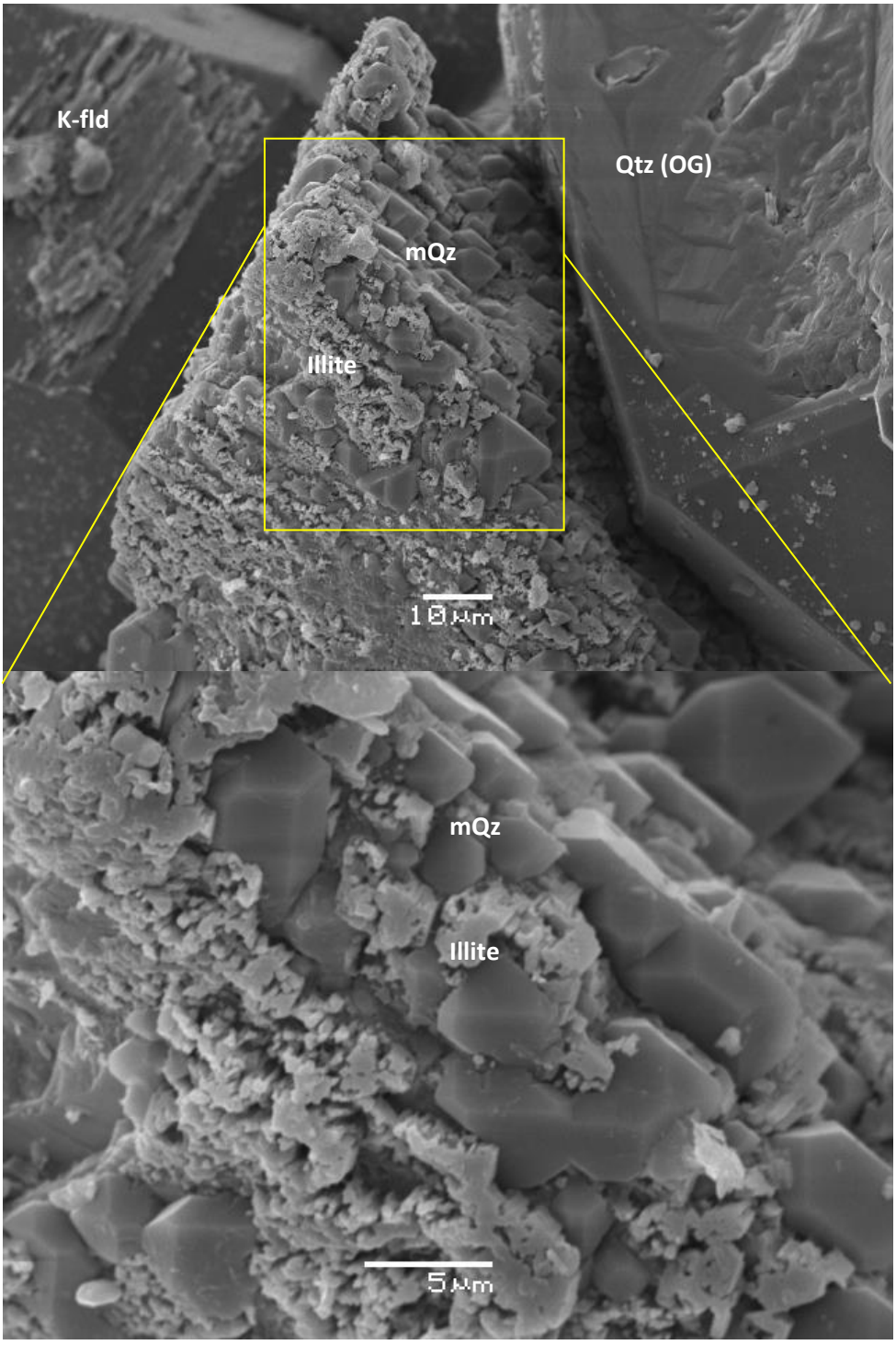

Figure 6.15: Microquartz (mQz) coating in the Nordmela Formation. Well 7220/7-1, depth 1922.47m.

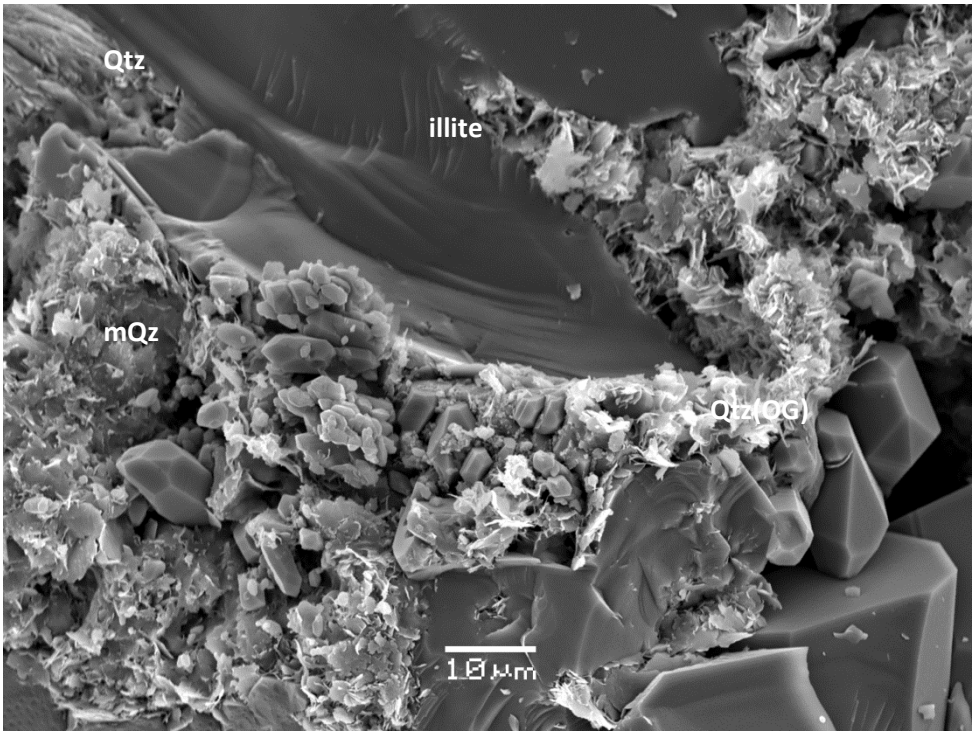

Figure 6.16: Illite and micro quartz (mQz) in between pores along with quartz overgrowth in the Stø Formation. Well 7219/8-1, Depth 4606.35m.

6.3.2 General Overview of Porosity from Both Wells

In order to have an overlook of porosity reduction due to quartz overgrowth and pore-filling authigenic clays, images and graphs have been taken from both wells. Porosity is high in well 7220/7-1 (1815.97m) due to low over overgrowth and pores are interconnected but on the other hand porosity is very low due to high quartz overgrowth and pores are isolated in well 7219/8-1(4601.64m).

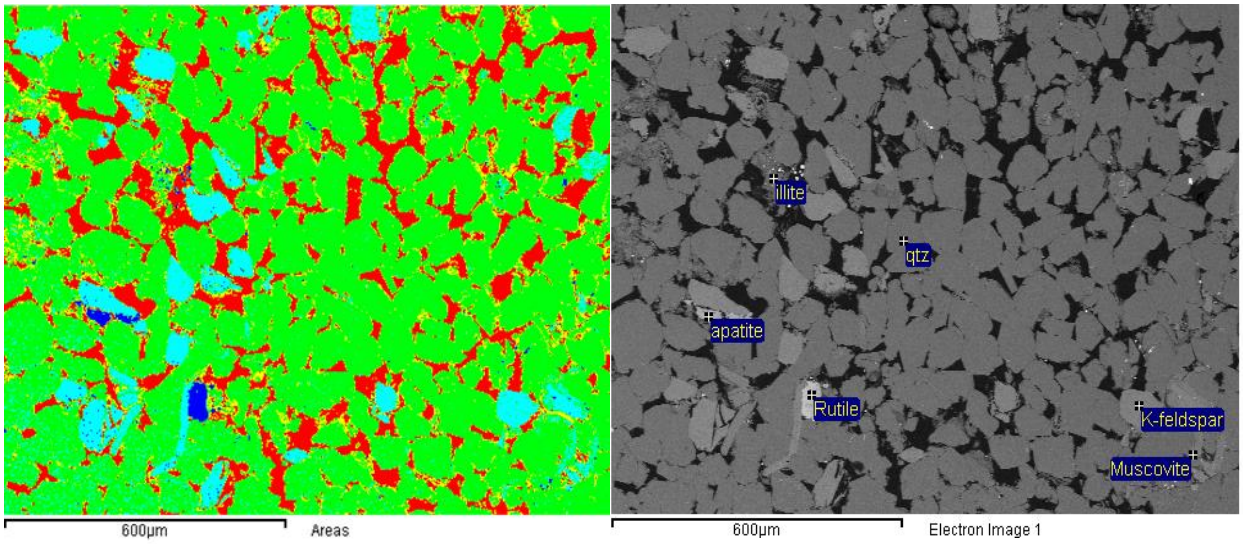

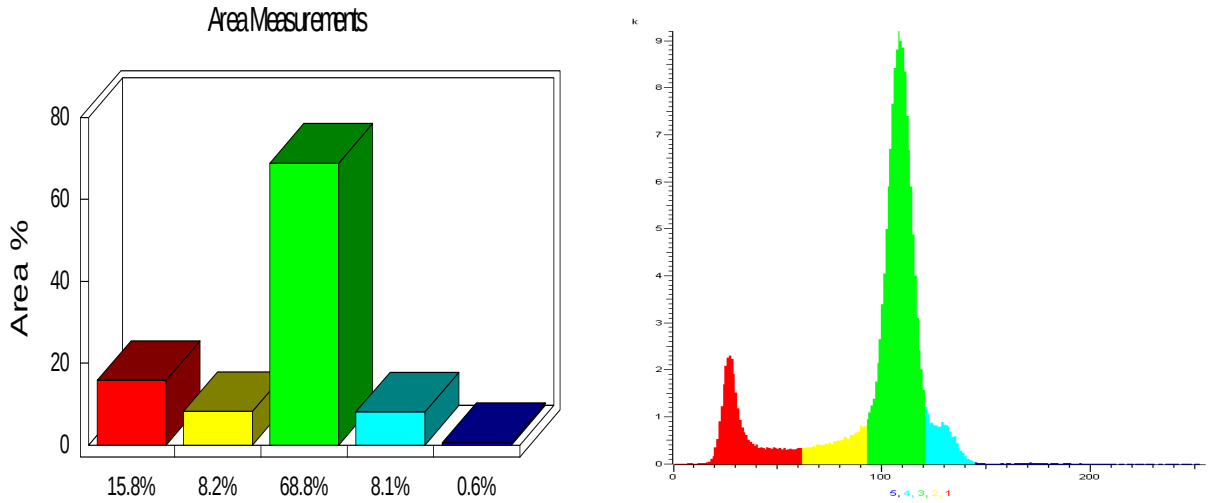

Figure 6.17: SEM image from well 7220/7-1, sample depth 1815.90m showing general overview of porosity and grains. Red: porosity, yellow: illite, Green: quartz, Pale Blue: K-feldspar and muscovite, Dark blue: heavy minerals.

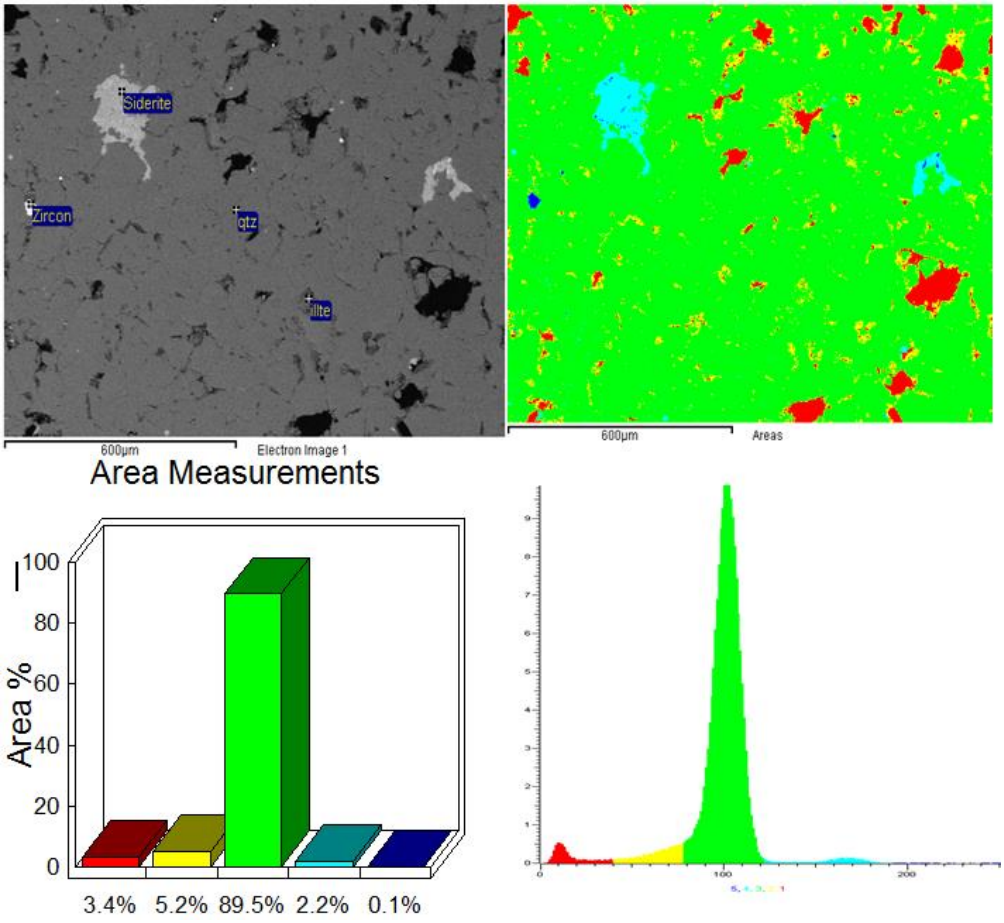

Figure 6.18: Histogram showing area measurement from well 7219/8-1(4601.64m). Red: porosity, Yellow: illite, Green: quartz, pale Blue: siderite, Dark blue: Heavy minerals respectively.

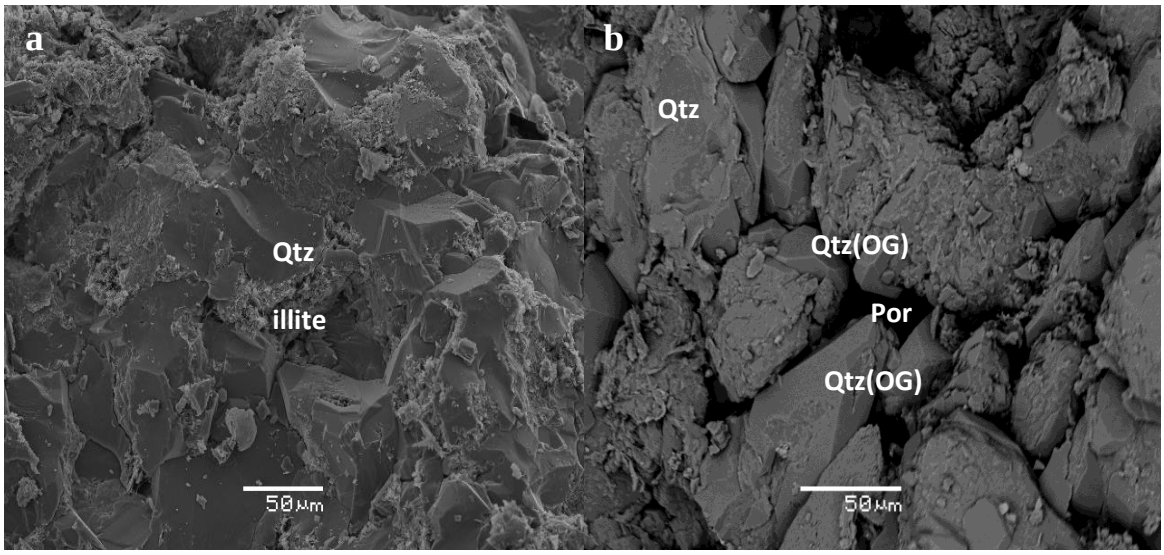

Figure 6.19: a) General overview of sample 4598.33m from well 7219/8-1 showing porosity reduction due to quartz over growth and pore-filling illite. b) 7220/7-1 1829.58 Quartz overgrowth, K-feldspar, illite and pyrite. Porosity overview along with overgrowth

6.3.3 Quartz overgrowth and Porosity

To relate our results from Point count analysis under the optical microscope, samples from Scanning electron microscopy (SEM) has also been studied. Being at shallow depth, both the Stø and Nordmela Formation have low quartz overgrowth and high porosity in well 7220/7-1 (Fig 6.19b). Under the normal circumstances, both parameters are inversely porportional to each other. The Stø Formation in the well 7219/8-1 has totally different characteristics. Overall the Stø Formation have very low porosity in well 7219/8-1 (Fig. 6.19a) because normally porosity decreases with increasing depth due to chemical compaction. The amount of quartz overgrowth calculated in point count analysis from well 7219/8-1 is quite low from the expected value because quartz cementation increases with increasing depth. In SEM, cathode ray luminescence (CL) images are used to differentiate detrital quartz grain from the authigenic quartz. Detrital grain appears more strongly but overgrowth has little bit dull illumination (Fig 6.20). The amount of quartz overgrowth observed in sample 4608.40m and 4611.05m from well 7219/8-1 around the detrital grain is not prominent (Fig. 6.24a). Grain dissolving Pressure solution at grain contacts is very visible in well 7219/8-1 (4608.40m).

Surface of quartz grains look homogeneous in back scattered image (Fig 6.22b) but close observation shows small quartz grains in between these homogenous grains.

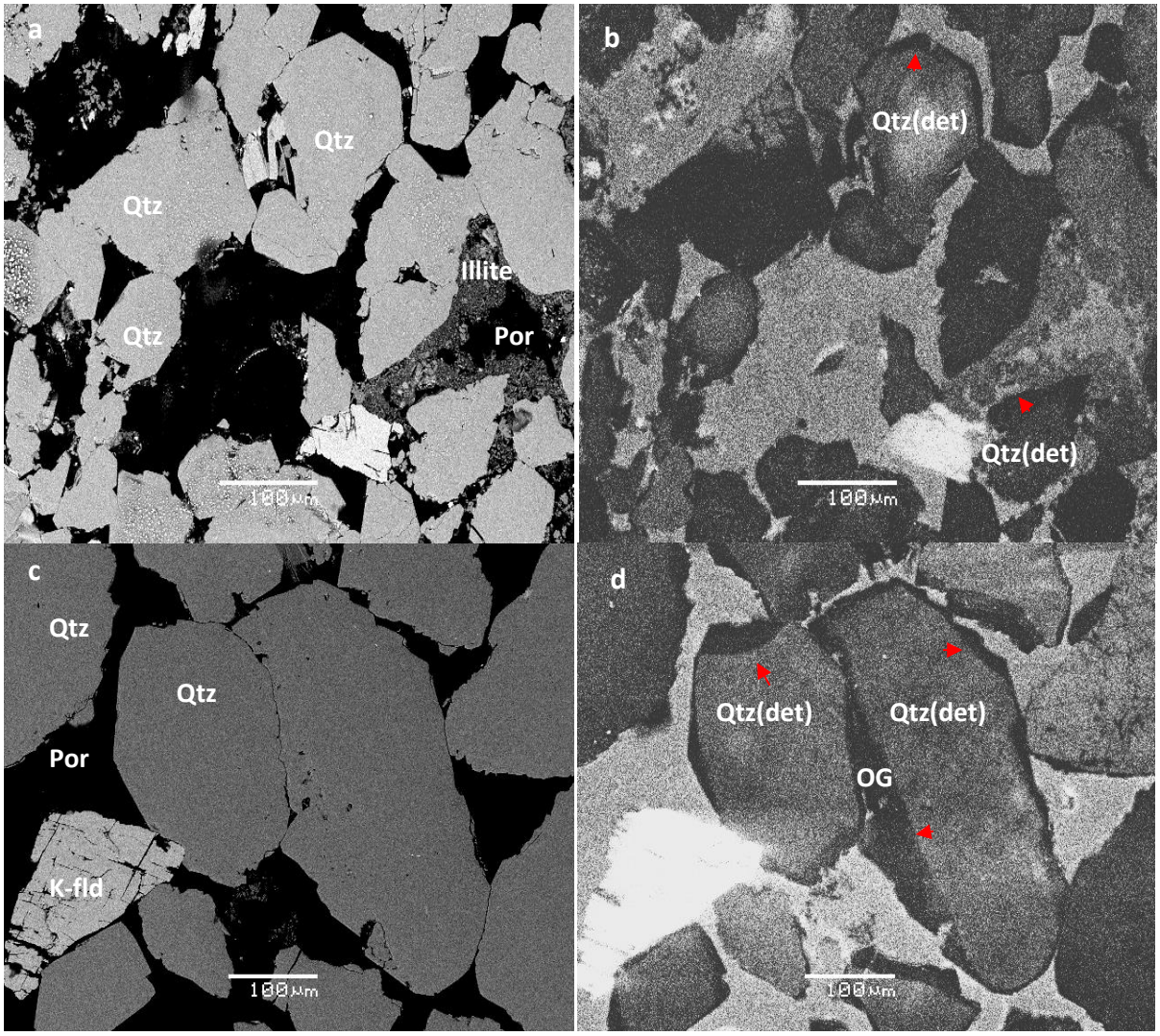

Figure 6.20: Carbon coated thin section from well 7220/7-1 (2017.25m) showing quartz overgrowth and illite in between the pores in the Nordmela Formation. a) is backscattered image and b) is cathode luminescence. c) Backscattered image of the Nordmela Formation in well 7220/7-1 (1972.23m) showing quartz grains along with K-feldspar d) Cathode luminescence image show detrital grain with high luminescence and overgrowth with dark black color around it.

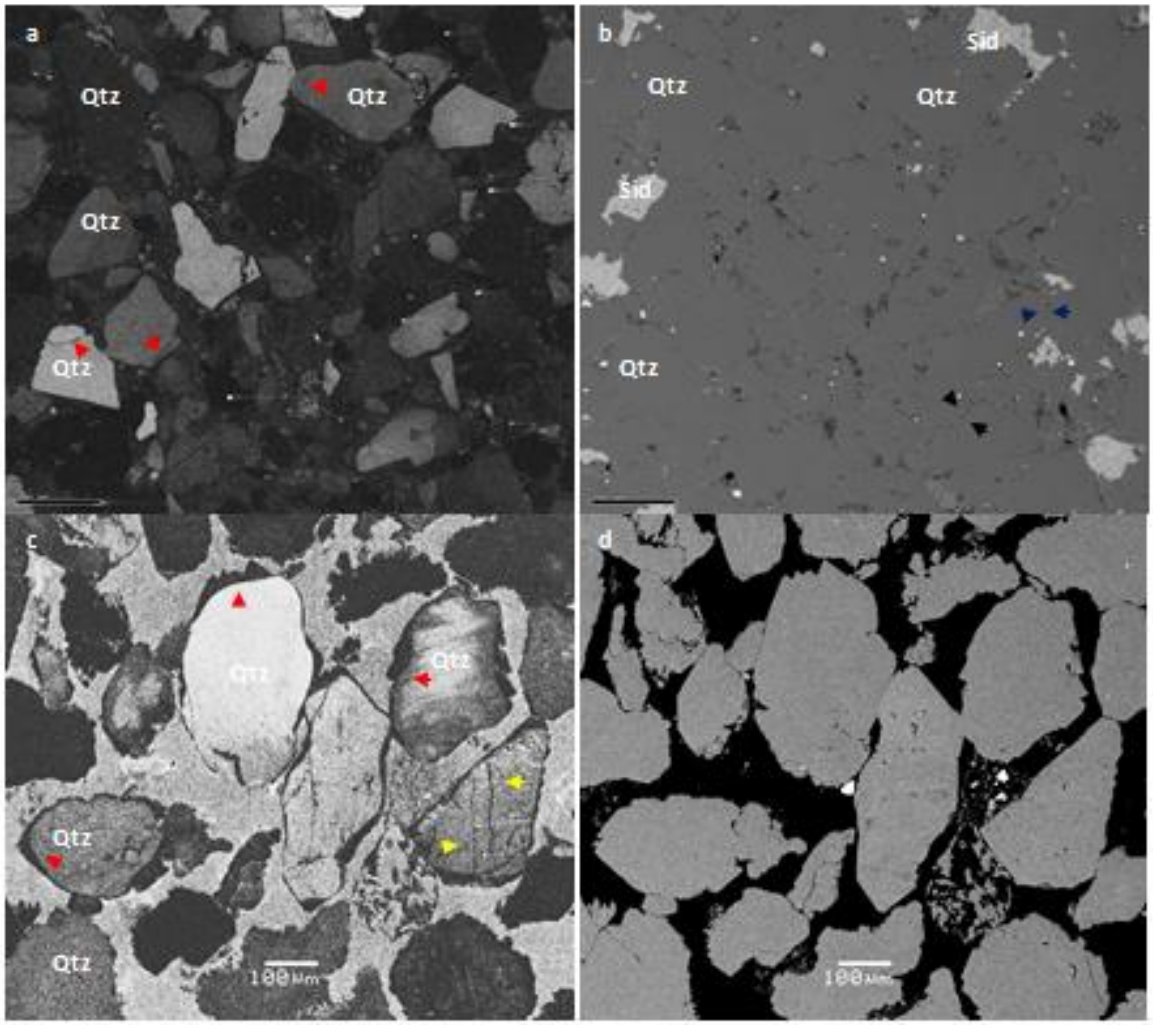

Figure 6.21: a) Cathode luminescence image in well 7220/7-1 (1972.23m) showing quartz overgrowth with siderite and pyrite b). Backscattered image of the same sample gives an overview of porosity reduction due to overgrowth. (➤) show pressure solution and (➔) show sutured contact. c) Cathode luminescence image of well 7219/8-1 (4611.05m) showing quartz overgrowth around the detrital grain along with mechanically crushed and fractured grain. d) Backscattered image gives an idea about the porosity reduction due to Pore filling illite along with the quartz overgrowth.

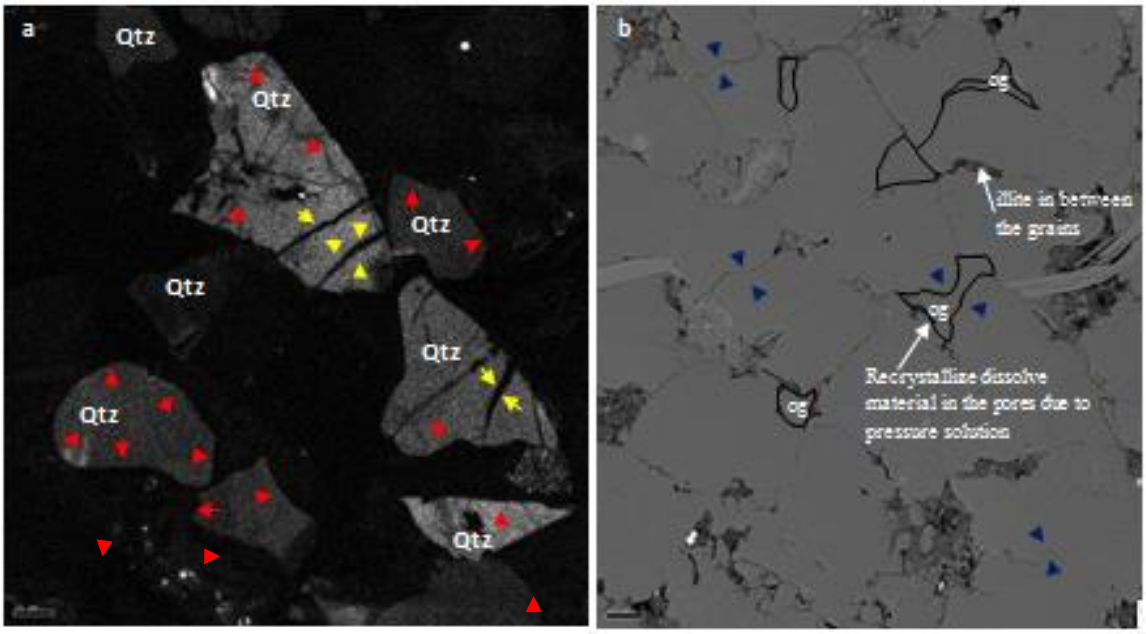

Figure 6.22: a) cathode luminescence image of well 7219/8-1 (4608.40m) showing quartz overgrowth( ) around the detrital grain (Qtz) along with healed fractured grain ( ). b) Backscattered image gives an idea about the porosity reduction due to Pore filling illite and pressure solution ( ) that dissolve the grain and reduce the IGV.

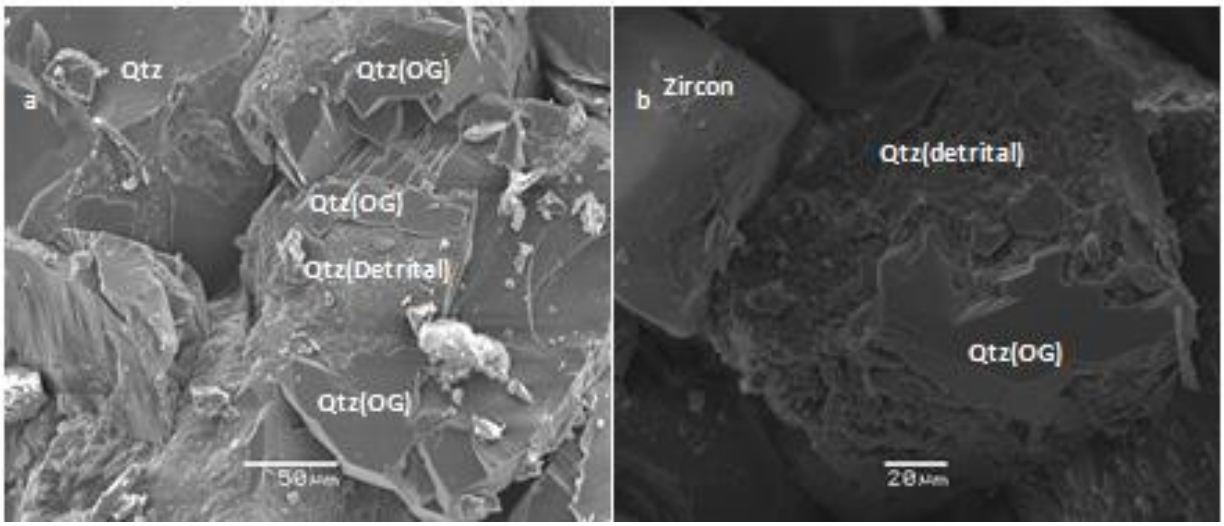

Figure 6.23: a) Partial quartz over growth on the detrital grain in the Stø Formation at a depth of 1851.90m in well 7220/7-1. b) Quartz overgrowth and illite transformation along with Zircon. 7220/7-1 1876.97

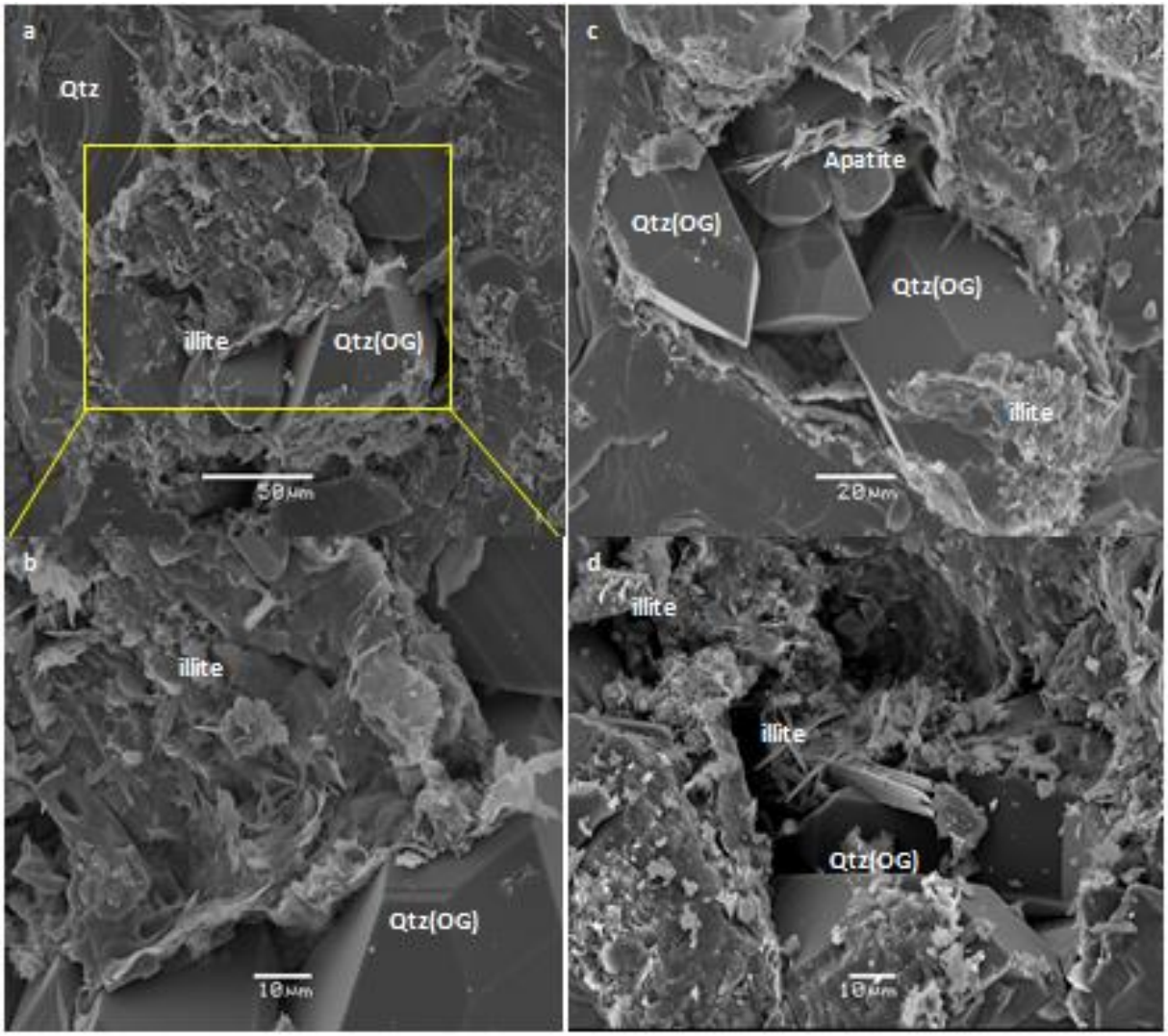

Figure 6.24: a) and b) Typical orthogonal quartz overgrowth and illite flakes filling the pores 7219/8-1 4598.33. c) Simultaneous growth of flaky illite on the surface of orthogonal quartz grain in well 7219/8-1 (4599.89m). d) Grain coated illite on quartz surface and orthogonal quartz overgrowth with illite needles in well 7219/8-1 (4606.35m).

6.3.4 Authigenic Clays and Porosity

Kaolinite and illite are the most prominent authigenic minerals found in these samples. Most of them are Pore filling (Fig 6.25). In well 7219/8-1, kaolinite is not observed but in well 7220/7-1, both illite and kaolinite have seen. This is also confirmed from XRD results. Kaolinite has very typical vermicular booklet shape (Fig 6.26) and illite have needle like and flakes like morphology. In well 7219/8-1, grain coated illite is also observed in the Stø Formation (Fig 6.24).

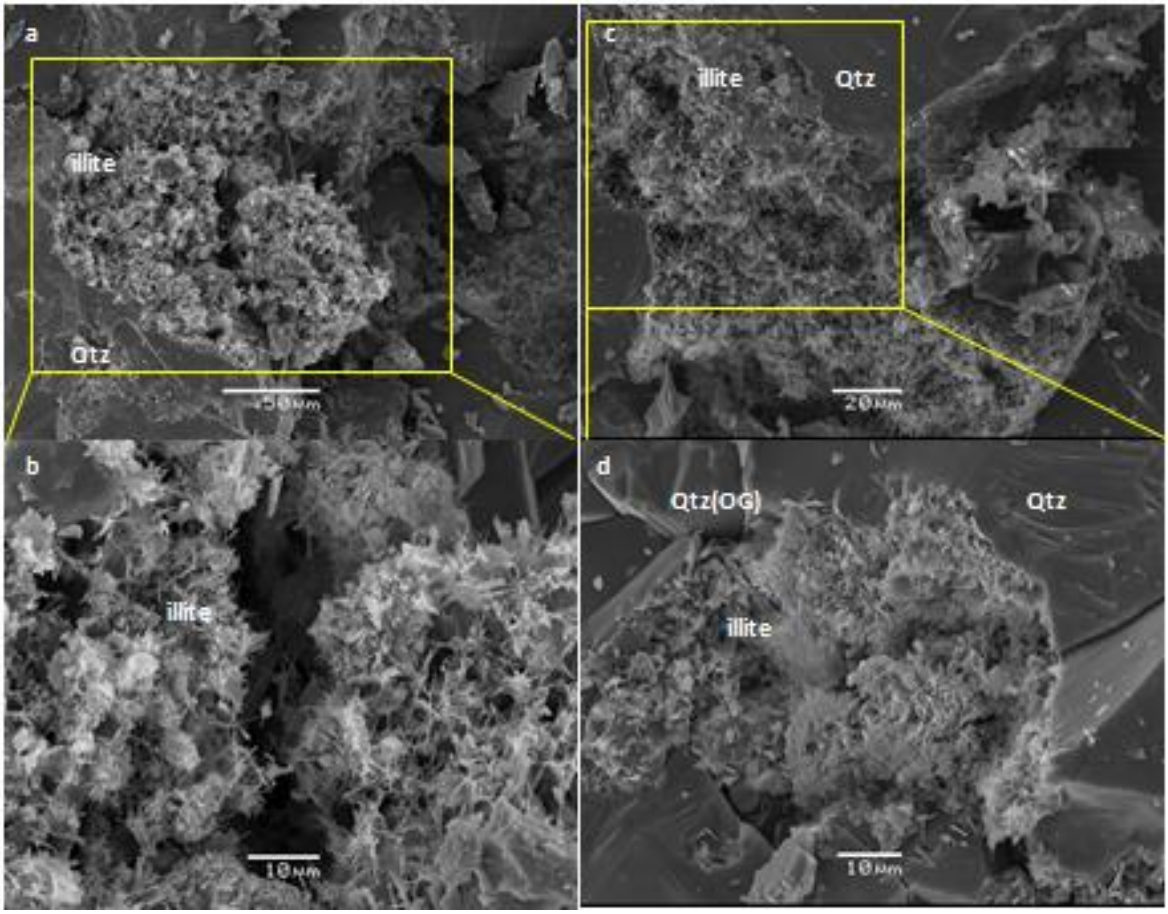

Figure 6.25: a) and b) Illite having needle and flakey like morphology in between quartz over growth in the Stø Formation.7219/8-1 4602.51. c) and d) Pore filling illite in between quartz overgrowth in the Stø Formation 7219/8-1 4603.91m.

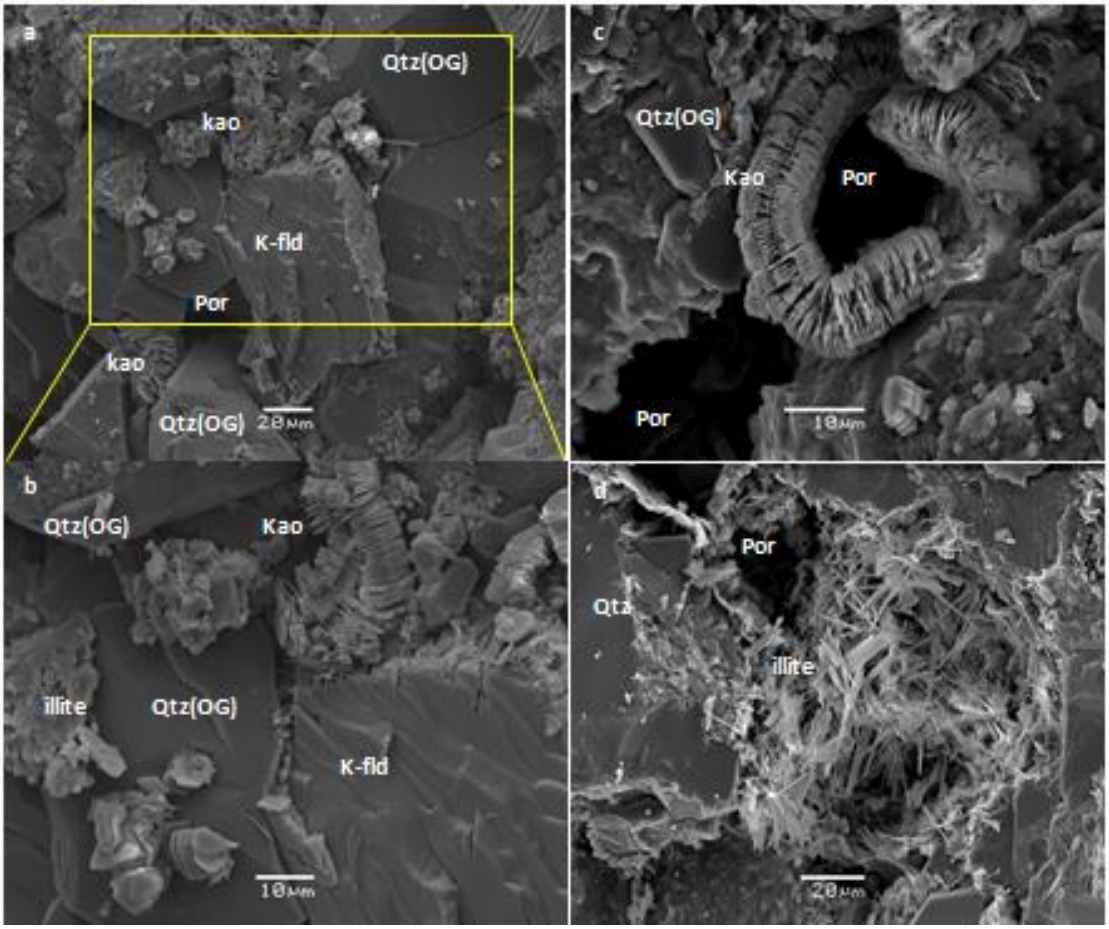

Figure 6.26:a) kaolinite with a vermicular booklet type morphology along with K-feldspar and quartz overgrowth in well 7220/7-1 (2017.25m). b) Vermicular booklet type kaolinite sitting in between quartz grain in well 7220/7-1 (1787.65m). c) Illite needles looks like smectite in between quartz overgrowth and pores are filled by this illite 7219/8-1 (4606.35m).

6.3.5 Carbonate Cement, Feldspar and Porosity

Carbonate also act as cement and reduce the porosity. In both wells siderite is the main carbonate cement (Fig. 6.27) along with that, calcite and ankerite are present in minute amount. Over all the amount of carbonate cement is not too much but two samples in both wells have abnormally very high values. At a sample depth of 1938.63m in well 7220/7-1, 17.85% siderite is present in XRD and 15.9% in point count. On the other hand in well 7219/8-1, 48% siderite is present in XRD and 39.3% in point count at a sample depth of 4607.6m.

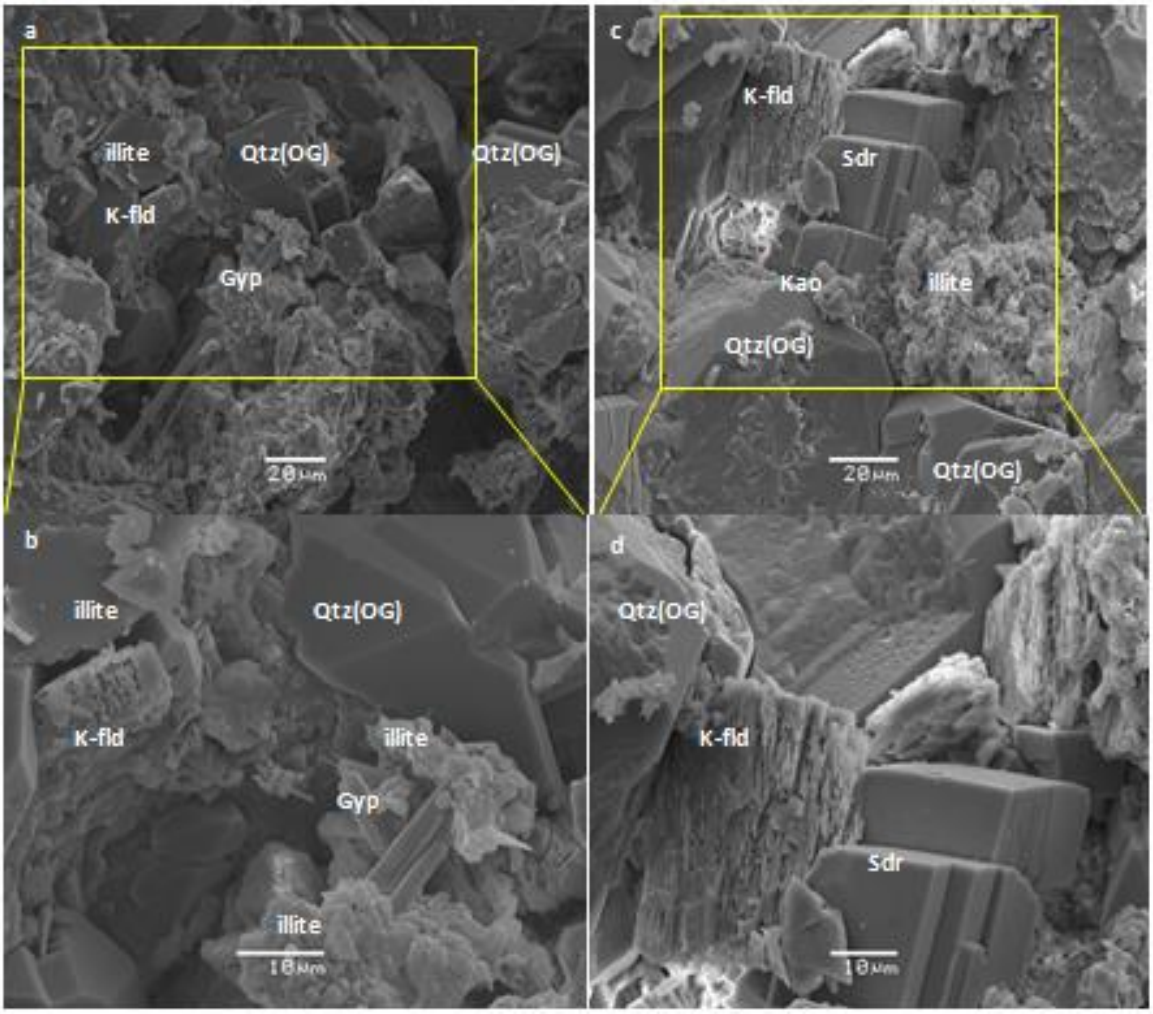

Figure 6.27: a) & b) Quartz overgrowth along with K-feldspar, illite and Gypsum in the Stø Formation. well 7220/7-1 (1851.40m). c) & d) Siderite and K- feldspar in between quartz overgrowth in the Nordmela Formation. Well 7220/7-1 (2015.25m).

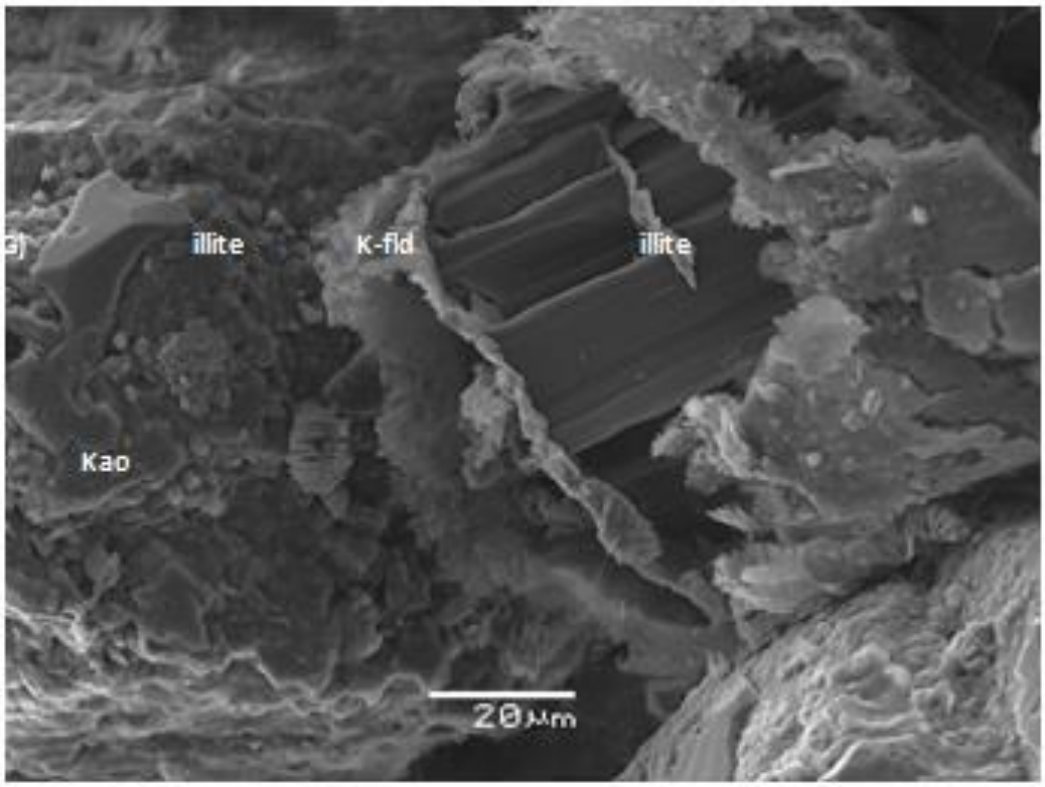

Figure 6.28: Quartz overgrowth at the surface of the detrital grain and illite along with kaolinite and K-feldspar.7220/7-1 (1876.97m).

6.3.6 Other Minerals

There are some minerals that are observed in minute amount apart from quartz, illite, K-feldspar and kaolinite. Pyrite, apatite and muscovite are the minerals that are also observed under the scanning electron microscope using stub mounted samples (Figure 6.28 and 6.29).

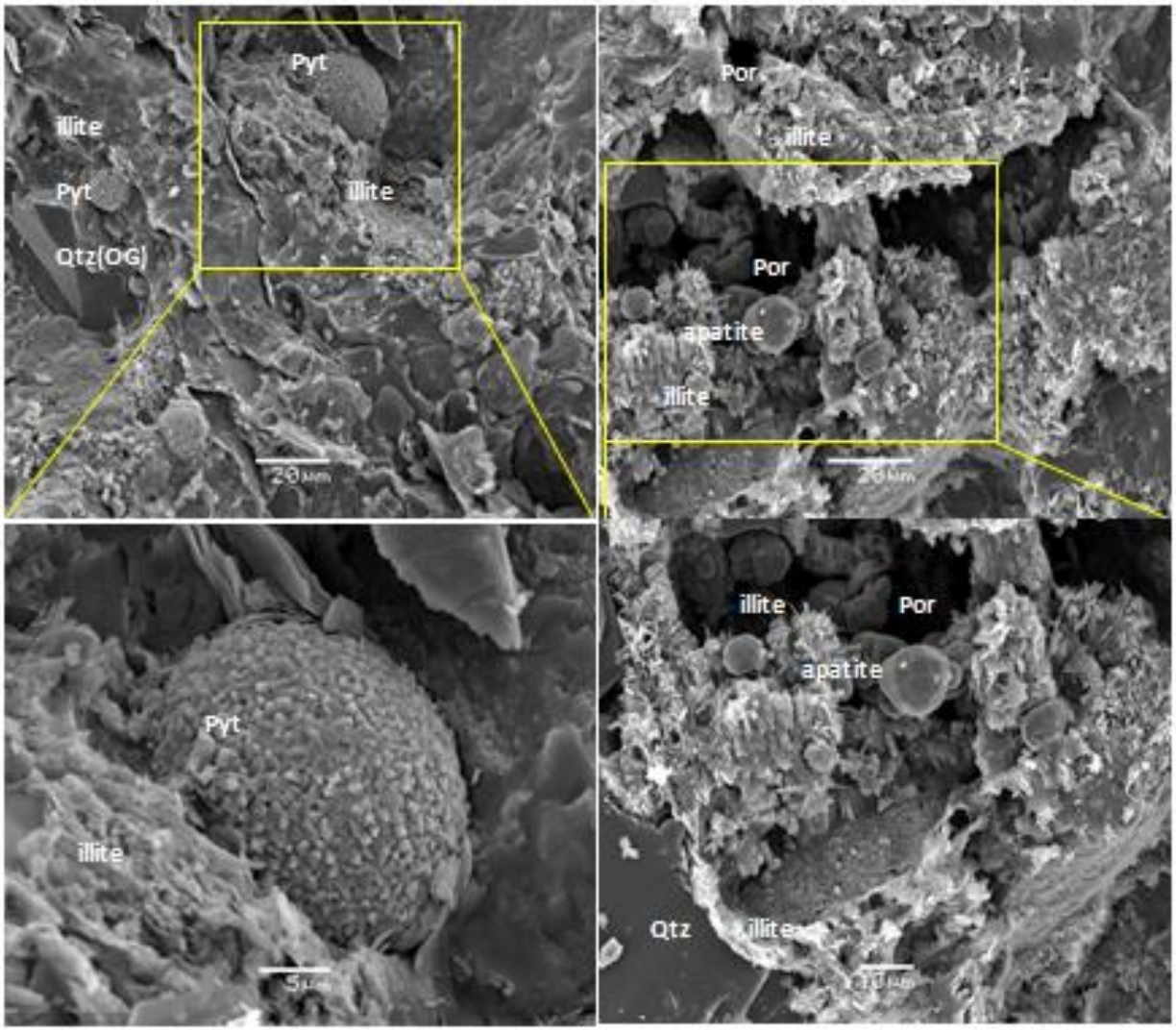

Figure 6.29: a) and b) In the Stø Formation, small pyrite nodules present on the surface of illite and quartz overgrowth. Well 7219/8-1 (4608.76m) c) and d) Apatite present along with illite(needle like) and quartz overgrowth in the Stø Formation. Well 7219/8-1 (4606.35m).

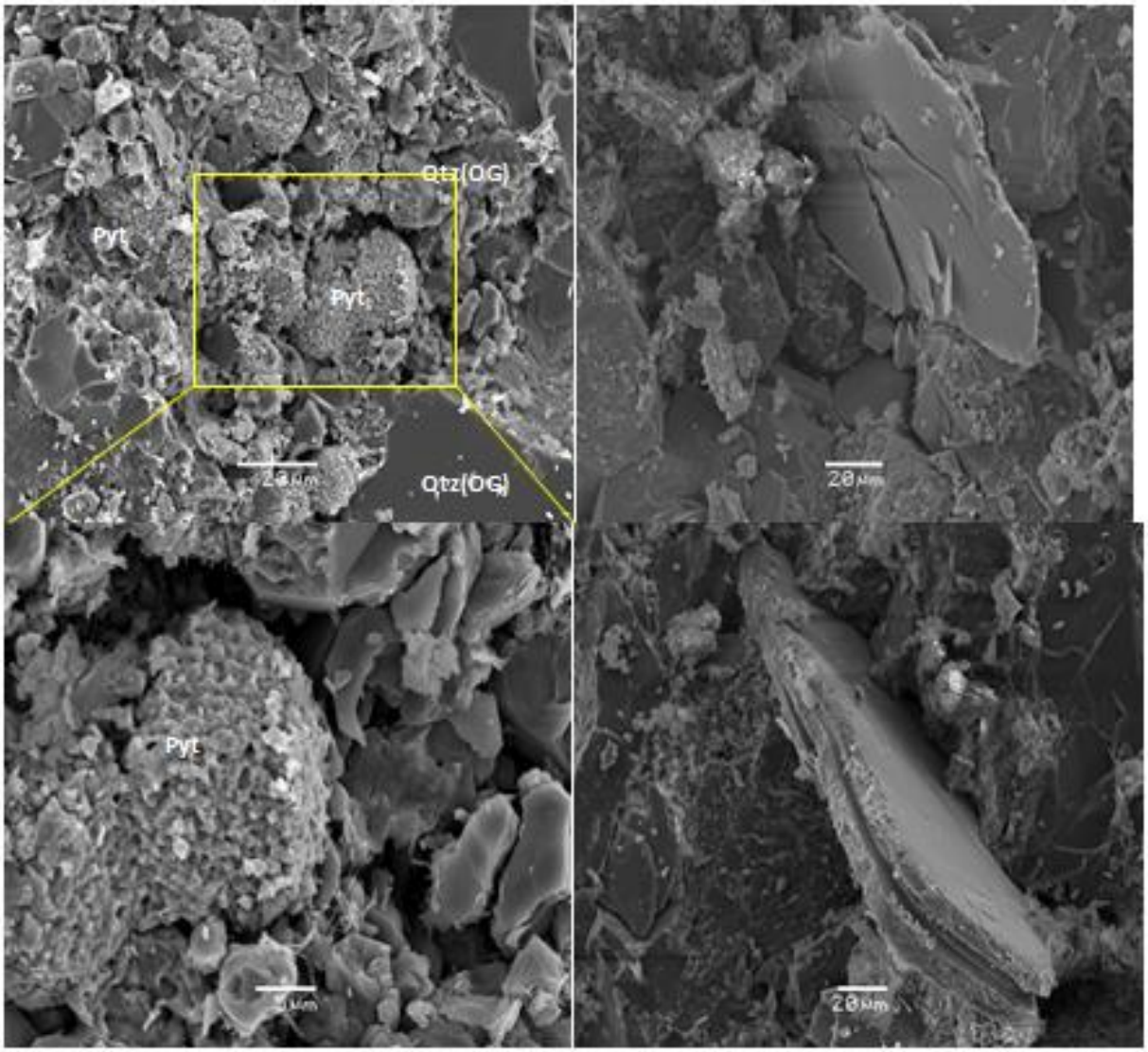

Figure 6.30: a) 7219/8-1, 4606.35m Pyrite, illite and Quartz. b) 7220/7-1, 1870.70m muscovite, pyrite, quartz and illite. c) 7219/8-1, 4608.40m Muscovite

6.4 X-Ray Diffraction (XRD) Analysis

XRD analysis on all the samples of the Stø and Nordmela Formation has been carried out. By using this technique we could have a better understanding of the mineralogy within the samples. Every mineral have its own angstrom value and particular peak height that is identified and semi-quantified to get a percentage value. Sample analyzed in XRD analysis does not give a true volume percentage of a particular mineral.

6.4.1 Bulk Analysis

Bulk analysis has been performed on samples of the Stø and Nordmela Formation from both wells. Results obtained from this analysis are shown in (Figure 6.30 and 6.31) and (Tables 6.8 and 6.9).

6.4.1.1 Well7219/8-1(Stø Formation)

Quartz is the most dominant mineral in all 20 samples from well 7219/8-1 with an average XRD% of 91. Illite and Siderite have almost similar XRD% of 3.81 and 3.74. In a sample depth of 4607.6m, 48% siderite is present which is quite high. Rests of the minerals are in minute amount (Table 6.8).

Table 6.8: All the minerals from XRD analysis and their percentages

Well	Formation	Depth	Quartz XRD %	K- Feldspar XRD %	Plageoclase XRD %	Illite XRD %	Calcite XRD %	Siderite XRD %	Pyrite XRD %	Sphalerite XRD %	Gypsum XRD %	Augite XRD %	NaCl (Halite) XRD %	Barite XRD %
7219/8-1	Stø	4597.23	95.083			3.758	0.364	0.19	0.604					
		4598.33	94.679			3.566	0.223	1.398	0.084	0.050				
		4598.93	94.49			3.889	0.241	1.041	0.247					
		4599.84	93.34			2.845	0.395	2.591	0.778	0.053				
		4600.15	94.39			4.018	0.198	1.157	0.076	0.061			0.097	
		4601.64	94.58			3.046		1.636	0.297		0.402		0.039	
		4602.51	94.04			3.15		2.224	0.21		0.378			
		4602.87	97.12		0.985	1.226		0.279			0.368		0.019	
		4603.17	98.129			1.578		0.292						
		4603.91	96.97		0.93	1.842		0.258						
		4604.26	96.35		1.106	2.045		0.027		0.043			0.051	
		4604.68	96.868			2.359		0.408			0.364			
		4605.76	89.29		1.384	6.285		1.874	0.289	0.046	0.724		0.109	
		4606.35	92.73	0.69		4.369		1.425	0.266		0.374		0.152	
		4607.6	49.6			2.19		48	0.208					
		4608.4	89.65	0.22	1.31	5.141		1.783	0.249		0.606	0.922	0.116	
		4608.76	93.08			5.59		0.429	0.226	0.069			0.039	
		4609.57	90.31			6.55		1.884	0.375		0.66		0.07	0.15
		4610.1	88.87			8.3		1.715	0.278	0.072	0.643		0.127	
		4611.05	86.43	1.22		4.469		6.365	0.666		0.635			0.216

Table 6.9: All the minerals from XRD analysis and their percentages.

Well	Formation	Depth	Quartz XRD %	K-Feldspar XRD %	Plageoclase XRD %	Kaolinite XRD %	Illite XRD %	Calcite XRD %	Siderite XRD %	Ankerite XRD %	Pyrite XRD %	Sphalerite XRD %	Gypsum XRD %	Marcasite XRD %	NaCl (Halite) XRD %
7220/7-1	Stø	1787.65	91.83	1.28	1.23	3.27	1.933						0.45		
		1792.85	82.42	1.4	1.97	3.82	3.48			0.68	4.98	0.159	1.08		
		1807.7	85.14	4.35	1.58		3.88				3.61	0.114	0.93	0.38	
		1814.37	87.62	3.89	3.34	2.16		2.308			0.66				
		1815.9	87.88	4.14			5.36				2.50	0.109			
		1829.58	99.29	0.71											
		1842.32	97.52	1.93							0.50	0.048			
		1848.9	97.87	1.79						0.068	0.27				
		1851.4	95.81	1.57			1.905				0.33		0.37		
	Nordmela	1861.4	98.88	0.87							0.25				
		1876.97	99.45				0.55								
		1883.35	90.36	2.21		2.86	4.22				0.34				
		1890.4	80.38	5.24	7.42	3.46	2.91				0.59				
		1905.4	92.24	1.53	4.52	1.68						0.028			
		1922.47	85.65	6.85		4.41	2.037			0.224	0.41	0.411			
		1938.63	72.4	3.85		4.91	0.86		17.85			0.116			
		1948.73	93.3	2.06		2.06				2.5		0.087			
		1972.23	98.59			0.59		0.751							0.055
		1975.37	94.62	1.71		2.89	0.658					0.112			
		2017.25	78.12	6.7		7.33	7.85								

6.4.1.2 Well 7220/7-1 (Stø and Nordmela Formations)

Total of 9 samples from Stø and 11 from the Nordmela Formation has been analyzed. Quartz being the most dominent minerals in both Formations. From the Stø Formation, it has an average XRD% of 91.7 and 89.45% from the Nordmela Formation. In the Stø Formation, Kaolinite,illite, K-feldspar, albite, pyrite and calcite have mean XRD percentages ranging from 2-4%. Other minerals are in minute amount with less than 1% XRD value. Nordmela Formation has high amount of albite with 6% XRD value. 17.85% siderite is present in a sample depth of 1938.63m. Kaolinite, muscovite and K-feldspar are in a range of 2-4%.

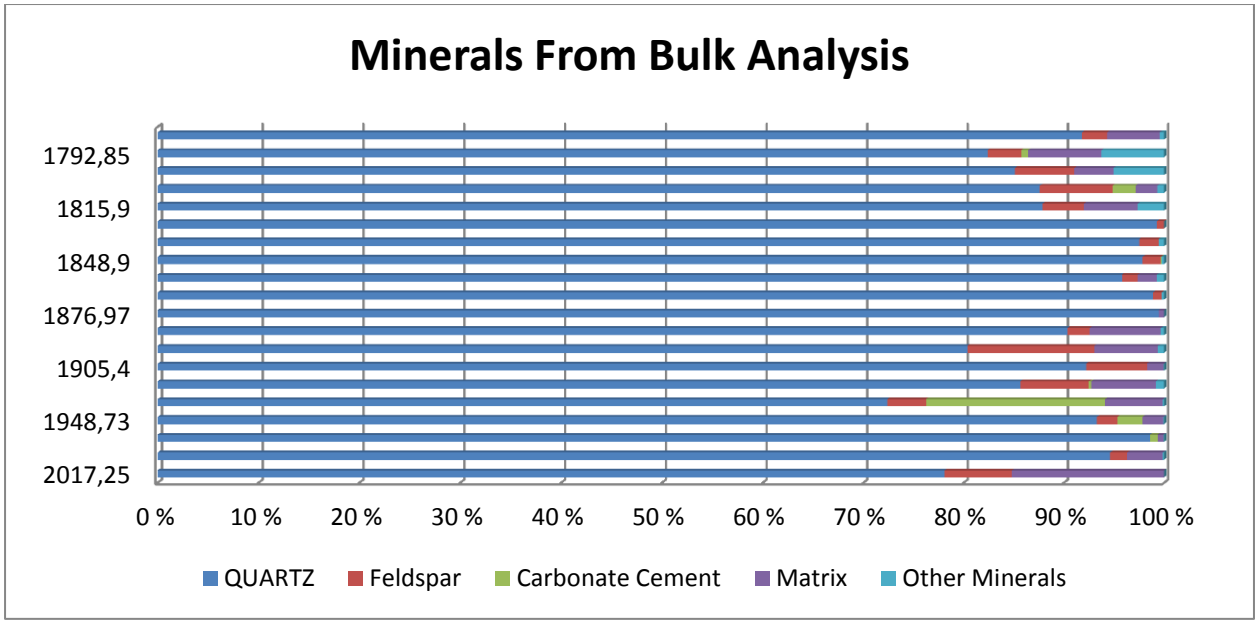

Figure 6.31: Minerals that are identified from Bulk Analysis in XRD. Well 7220/7-1.

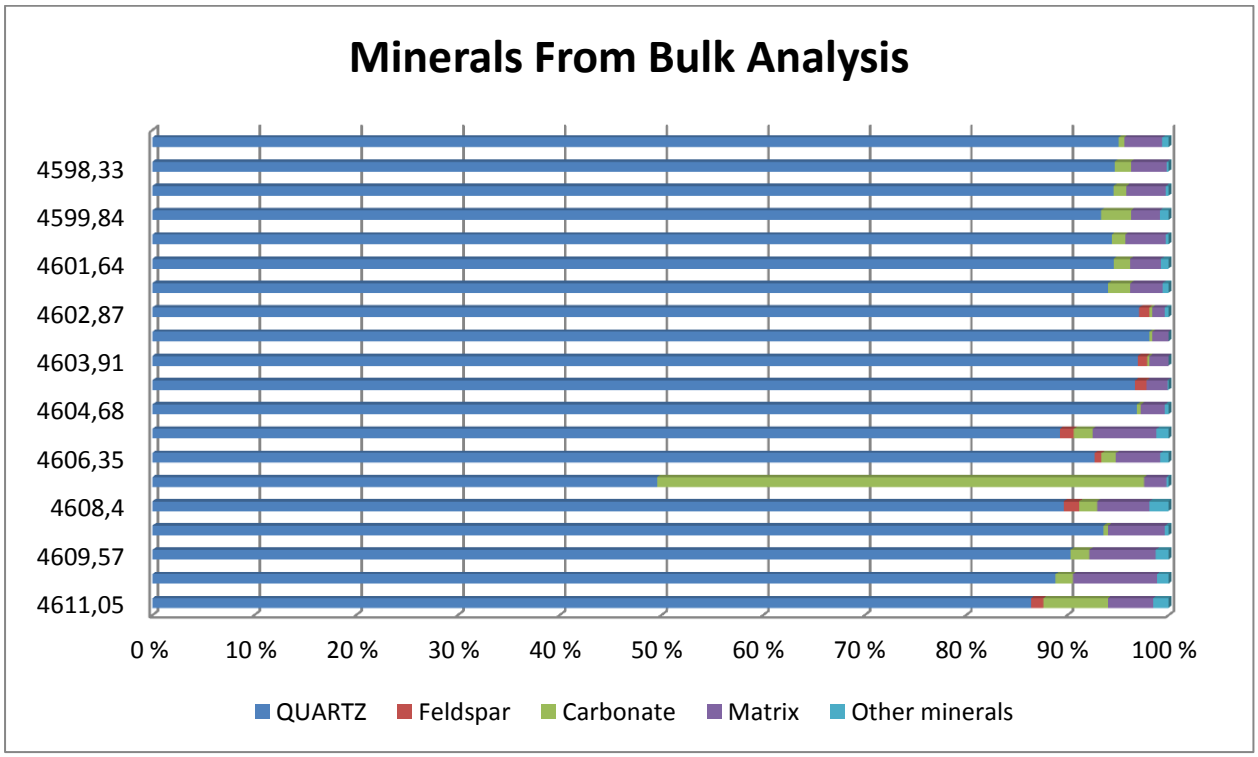

Figure 6.32: Minerals that are identified from bulk analysis in XRD. Well 7219/8-1.

7 DISCUSSION

7.1 Mineralogy

Monocrystalline quartz are the most dominant detrital grain found in both the Stø and Nordmela Formation along with that, some polycrystalline quartz are also present (Fig 6.6). Both Kaolinite and K- feldspar are observed in well 7220/7-1 (Table 6.9) but there is no evidence of these two minerals in well 7219/8-1 (Table 6.8). Illite, lithic fragments and muscovite are the other observed minerals. Both Quartz and Carbonate cements are present within the Stø and Nordmela Formation but quartz being the most dominant among them. Calcite, siderite and ankerite are the carbonate minerals present in minute amount. From both wells, all samples of the Stø Formation are fine to medium grain sized, well sorted apart from the sample (4599.84m) that is moderately sorted (Table. 6.1). In well 7220/7-1, samples from Nordmela Formation are well to moderately sorted (Table 6.2). High amount of siderite is observed in sample (4607.6m) from the Stø Formation and that is 39.3%. On the other hand 15.9% siderite is also observed in sample (1938.63m) from the Nordmela Formation.

7.2 Sedimentology

Both the Stø and Nordmela Formations contains insignificant amount of clay content and are not able to satisfy the criteria of/for textural immaturity by (Folk, 1951). Grains should be well sorted and subangular in their shape in order to be texturally mature. Almost all the samples from the Stø Formation are well sorted and subangular , subrounded and rounded in shape but the Nordmela Formations are well to moderately sorted (Fig 6.15a,b) and shape is subangular to subrounded. Both formations are texturally mature according to Folk, 1951 (Table 6.7).

Stø Formation is considered as a good reservoir rock but the reservoir quality of the Nordmela Formation is poor. On the bases of depositional environments, both the Stø and Nordmela Formations is sub divided into upper and lower intervals (Fig 5.2).

In the lower part of the Stø Formation, the sand is very clean with good reservoir properties. This may be due to the wave and tidal energy reworking of the sediments. Grains are well sorted and fine to medium in size. Upper part of the Stø Formation has low reservoir qualities as compared to the lower part and the deposition is influenced by middle to upper shore face environment. It is silty sandstone however a well sorted, bioturbated, and composed of fine to medium sized grain. According to (Olaussen et al., 1984) the depositional environment of the Stø Formation is upper near shore and inner shelf.

The reservoir quality of lower part of the Nordmela formation is poor. It is a fine to medium sized, well sorted silty sandstone with mudstone. Upper part of the Nordmela Formation is fine to medium grain sandstone with moderate reservoir quality. Lenticular to flaser bedding is common. Based on the gamma ray, upper part is more sandy and having a low gamma ray value as compared to the lower part and better reservoir quality as well (Figure 5.2) .The depositional environment of the Nordmela Formation is coastal plain/tidal flat sequence (Olaussen et al., 1984).

7.3 Detrital Grain Petrography

In order to find out the sandstone composition, all the detrital grains observed during point counting are divided into three categories; quartz, feldspar and lithic fragments and are plotted in a QFL ternary diagram of petrographical classification (Fig 6.7a, b). Both the Stø and Nordmela Formations contain matrix less than 15% and have quite good amount of detrital grain. Almost all of the samples from Stø Formation are quartz arenite based on the classification of Pettijohn (1975). Quartz arenite is the sandstones having more than 95% of quartz and it is considered as mineralogically mature sandstone (Adams et al., 1984). Nordmela Formation is also quartz arenite with some exceptions of subfeldspathic arenite (fig 6.7a). According to sandstone petrography of (Dickinson 1985), provenance of both Stø and Nordmela Formation is interpreted as cratonic interior (6.8a, b). Detrital mineral composition plot by (Dickinson 1985) for both the Stø and Nordmela Formation show cratonic interior or recycled orogenic origin (fig 6.9a, b).

7.4 Carbonate Cement

Carbonate cement is derived mostly from biogenic carbonate, particularly from the aragonite bearing organisms and due to the dissolution and reprecipitation of biogenic carbonate (Bjørlykke and Jahren, 2010). Overall the amounts of carbonate cement observed in both wells are quite low apart from two sample depths. This is mainly due to the presence of high amount of siderite. Calcite and ankerite are the other two minerals types forming carbonate cement but they are in very small amount. In well 7219/8-1, siderite is 39% from sample depth of 4607.6m and 15.9% from a sample depth of 1938.63m in well 7220/7-1 (Figure 6.13). This may be the cause for an unusual increase in IGV values in these two samples**.** In well-sorted sands, intergranular volume is around 40-45% approximately at the sediment-water interface (Paxton et al., 2002). In the reservoirs, precipitation of quartz along with the carbonate during the early and late stages of diagenesis is the main reason for porosity loss and is indicated by high IGV values of the sandstones (Letamendi et al., 2007).

At low temperature (20-40°C) early diagenetic siderite formed from mixed marine/meteoric waters during the early diagenetic history (Girard, 1998). In the fluvial sandstones, early diagenetic siderite is precipitated near the sediment/water interphase and in transitional sandstone it is formed due to the mixing of the meteoric and marine water. During late diagenesis, dissolution of feldspar and carbonate cements may be the main processes of forming secondary porosity. At deeper depth and higher temperature, siderite may be replaced by ankerite or recrystallized (Letamendi et al., 2007).

During the early diagenesis siderite was acting as a detrital grain and preserving porosity from mechanical compaction and then it dissolved and recrystallized during the late diagenesis. That may be why siderite is present in high amount and also influence the IGV values.

7.5 Quartz Cementation

At temperature of around 60 to 80°C, quartz cement in sandstones take over kinetic restrictions and starts to precipitate on available surface of quartz grain based on the time , temperature, quartz grain, surface area and nucleation domain size (Ajdukiewicz and Lander, 2010).

Mechanical compaction seize further effectively in most cases by only 2-4% quartz cement in sandstone and then compaction is further controlled chemically by rate of mineral dissolution and precipitation (Bjørlykke and Jahren, 2010). The amount of quartz cement in well 7220/7-1 is around 0.3-1.8% (Table 6.2). The depth interval of the Stø and Nordmela Formations is from 1781m to 2023m but it is uplifted around 1000m (Fig 7.1 and Appendix C). Well 7219/8-1 has a quartz cementation that is ranging from 5-8% (Table 6.1) which is still quite low being at this burial depth. Both the Stø and Nordmela Formations in both wells are under chemical compaction zone. Depth as a function of velocity cross plot in (Fig 5.6a) shows that both the Stø and Nordmela Formations in well 7220/7-1 are just below the transition zone where chemical compaction starts taking place. A sudden shift in velocity trend starts from the Stø Formation and the velocity ranges from 3400m/s - 3940m/s. Velocity values in well 7219/8-1 for the Stø Formation are quite high, ranging from 14700 ft/s (4480m/sec) to 17700 ft/s (5394.96m/s) as shown in the depth versus velocity cross plot in (Fig 5.6b). High velocity in the Stø Formation is due to high density (Fig 5.5b). Chemical compaction plays a vital role in rock stiffing at greater burial depth. Rocks get more compacted at a faster rate by quartz cementation rather than by increase in vertical stress from the over burden (Bjørlykke and Jahren, 2010).

In many reservoir sandstones, quartz cement is the most dominant porosity reducing agent. Grain size, sorting, clay content, mechanical compaction, early cementation and authigenic clay minerals are other factors that also play an important role in destroying porosity in reservoir sandstones. (Storvoll et al., 2002). In well 7220/7-1, porosity is preserved in both the Stø and Nordmela Formations because quartz cementation has just started at this point and the amount of quartz overgrowth is not enough to fill the voids (Fig 6.21). At 2.5 to 3.5 km of burial depth, beginning of quartz cementation significantly influenced the porosity reduction along with the start of pressure solution and stylolitization (Bjørlykke et al., 1989). Both bulk-rock volume and porosity is reduced dynamically as a result of intergranular pressure solution (Houseknecht, 1988).

Normally at deeper depth, quartz cementation is high but in well 7219/8-1 point count values for quartz cementation are low from the expected values. This might have also influenced the overall IGV values. This ambiguity may be to some extent related to underestimation of quartz overgrowth during point count analysis. Identification of the quartz overgrowth around the detrital grain rims was not an easy task.

Due to illite coating on the grains, porosity in deep reservoir may be preserved because illite coating inhibits the quartz overgrowth. During compaction illite in between the grains also causes the material to dissolve at the site of grain contacts and quartz crystallizes on the surface of detrital quartz grains and also in the open pore spaces. So the net flow of material

is from high gradient area to the low gradient area. Illite coating in the deep well was poor (Fig 6.26). This could likely be due to the illite coating between the grains were dissolved to form the quartz cement. IGV in the Stø Formation in deep well is low because grains are cemented (Fig 6.24b).

Stylolites in the core log are also observed in the form of irregular sutured structure at different intervals (Appendix B).Material that dissolve at the site of stylolite is redistributed, if the volume is available in between the stylolites. There seems a volume loss at the site of stylolite and this dissolved material is reinforced in the volume available around it. This is a passive infilling so it does not affect the IGV.

Cathode luminescence was employed in order to identify the detrital from authigentic quartz grains (Götze et al., 2001). The amount of quartz overgrowth around the detrital grains was not also distinctly distinguished due to bad resolution under Cathode luminescence (Fig 6.24a). In the back scattered image pressure solution along with sutured grains contacts are observed (Fig 6.24b). Grain coated with illite around the detrital quartz grain in well 7219/8-1 is observed at three different sample depths: 4598.33m, 4599.89m and 4606.35m (Fig 6.26).

Quartz overgrowth is inhibited by clay coatings and therefore maintaining small grain contact areas where stress can act more effectively rather than on those contacts that have been filled by overgrowth precipitation (Houseknecht, 1988). At grain contacts, grain-to-grain'pressure' dissolution starts where the critical depth achieved during the burial. Illite grain coatings are known to catalyze pressure solutions. As a result of this the process is named as clay influenced dissolution process rather than presure solution. Illite coatings can form as far as there is a species generating K and Al which are one of the essential elements for illite growth (Worden and Morad, 2009). Smectite may be the source for grain coated illites. Volcano-clastic materials could form smectite at low temperatures and therefore the grain coating illite may be developed from this smectite (Storvoll et al., 2002).

Why intergranular pressure solution takes place due to the presence of clay coating.

- Silica movement may also be more rapid away from the sites of pressure solution because clays give an efficient medium of silica diffusion and therefore increase an intergranular pressure solution. (Houseknecht, 1988)

Chemical compaction in the Stø Formation is mainly influenced by quartz cementation along with pressure solution process. Presence of grain coated illite along with dissolved grain contacts gives an idea of pressure solution in well 7219/8-1. Grains come closed into each other due to pressure solution at grain contacts and the dissolved material crystallized in the open pore space (Fig 6.24b) causing porosity and overall volume reduction. Due to this compaction from pressure solution, IGV is reduced and the Stø Formation has low IGV and also quartz cementation while the density is high in well 7219/8-1(Fig 5.5b). This together with possible underestimation of quartz cement explains the low IGV and quartz cement from point counting and the high Vp.

7.6 Intergranular volume (IGV)

IGV is about 40 percent at the depositional surface in well sorted sands. Compaction processes can only reduce the IGV about 30 percent. The IGV can possibly be reduced by mechanical compaction and rest is controlled by chemical compaction where the most important specific process is intergranular pressure solution. Intergranular porosity of a sandstone tells us how much IGV is conserved and how much is occupied by cement. Intergranular porosity = IGV - Cement (Houseknecht, 1988).

In well 7220/7-1, mean Intergranular volume in the Stø Formation is 29.56% and in the Nordmela Formation 30.82 (Table 6.6). Their IGV is controlled by high porosity and low quartz cementation. Due to shallow burial depth the cementation process was very low therefore the porosity was preserved. On the other hand average IGV of the Stø Formation in well 7219/8-1 is 18.74%. Usually at deeper depth, porosity is reduced due to quartz cementation. Point count analysis revealed low porosity values. In addition overgrowth values are also not very high that actually disturb the whole IGV values of the Stø Formation from this deep well.

There are two samples from both wells in which IGV values are quite high from the normal values. In well 7219/8-1, IGV value of sample from depth 4607.6m is 52.2% (Table 6.1) and 44.4% IGV is in well 7220/7-1 from sample depth 1938.63m (Table 6.2). The reasons for such high IGV values in both wells are the presence of high amount of carbonate cement particularly siderite. 39.3% siderite is present in sample 4607.6m and 15.9% in 1938.63m from both wells.

7.7 Reservoir Quality with Depth

There are three factors that are affecting the quality of sandstone reservoirs at any degree.

1. Sorting, grain size, shape and sand/mud ratio based depositional porosity and permeability.
2. Extent of mechanical and chemical compaction
3. Type and amount of pore filling cement(Worden and Morad, 2000).

Both the Stø and Nordmela Formations in well 7219/8-1 and 7220/7-1 are well to moderately sorted, mature quartz arenite sandstones. Very little matrix and lithic fragments are present. Both wells are under chemical compaction zone (Fig 5.6a, b) and cementation is the main factor that is controlling the reservoir quality. Porosity of the Stø Formation in well 7220/7-1 is good and cementation is just at its initial stage so pores are well preserved and presence of kaolinite and K-feldspar also indicate that illitization is also not taking control in the clean sandstone of the Stø Formation. Nordmela Formation in this well has the same properties but its siltier and having interbedded mudstone layers that is affecting the permeability. So it is not considered as a good reservoir. Reservoir quality of the Stø Formation in well 7219/8-1 is very poor. Because of the deep burial, quartz cementation, intergranular pressure solution and pore-filling illite destroyed the porosity. Along with quartz cementation, illitization is probably the most important reason for reduction of reservoir properties (Bjørlykke et al.,

1992). At burial depths of about 3.7 to 4 Km (120°C-140°C) illitization starts only if kaolinite and k-feldspar are present together in reservoir (Chuhan et al., 2000).

7.8 Uplift/Exhumation

From Paleocene to Pliocene - Pleistocene, different stages of uplift and erosion in the Barents sea causes reduction of hydrocarbon accumulation and lateral redistribution of remaining hydrocarbon in the region. According to (Ohm et al., 2008) tentative uplift map of the southwestern Barents Sea, the estimated uplift in the study area is in between 1000m to 1200m. In order to compare the uplift in our study area, kaolinite : silt (50:50) compaction curve from (Mondol, 2009) has been used. Present depth is plotted against Vp (Fig 7.1a) and the trend line does not match with the velocity data. After reconstructing the measurements by adding 1000m to the present burial depth, the trend line matches with the data set in the exhumed depth Vs Vp crossplot (Fig 7.1b). Uplift calculated from (Mondol, 2009) and (Ohm et al., 2008) have the similar average values.

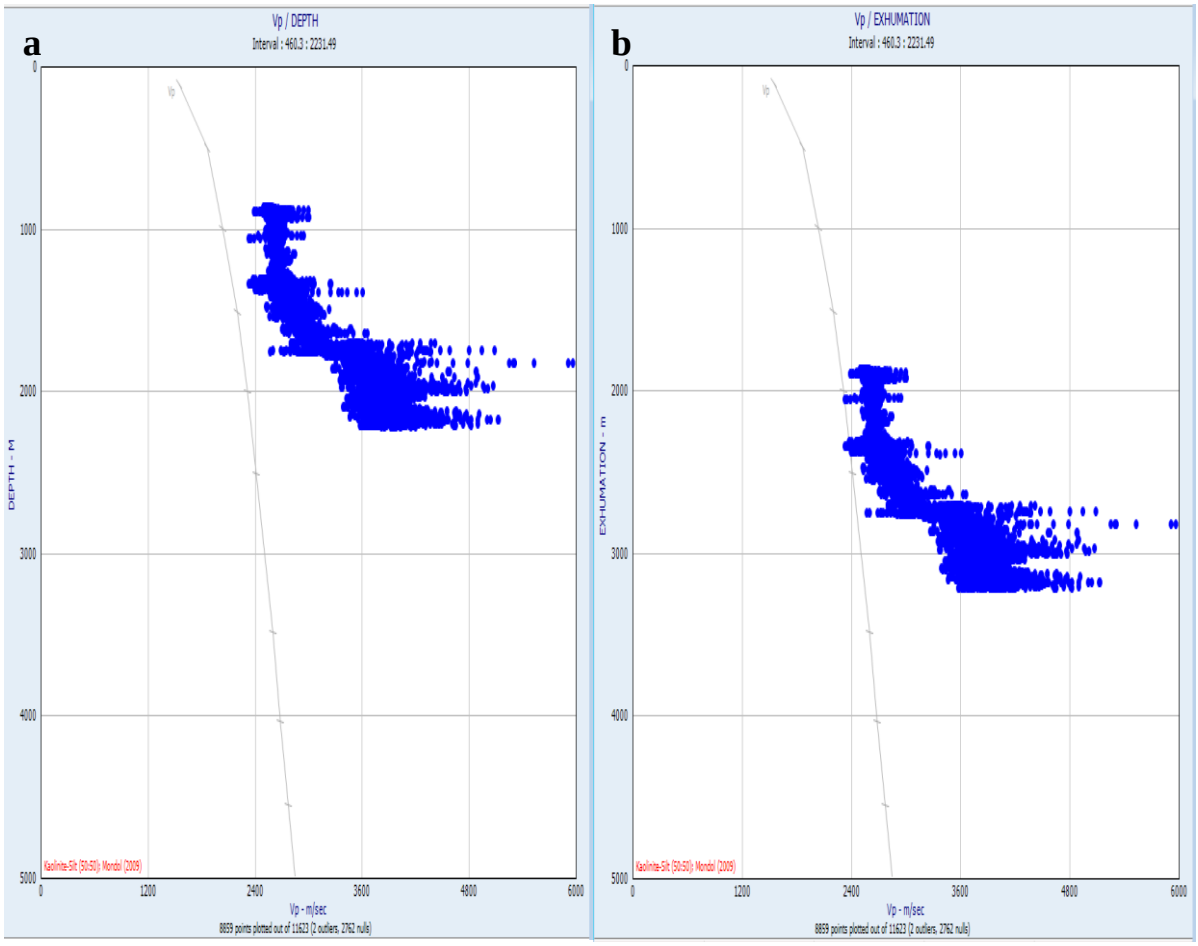

Figure 7.1: kaolinite: silt (50:50) compaction curve from estimation of uplift. a) Present day depth versus velocity. b) Exhumed depth versus velocity

7.9 Core Analysis

Depositional environments of different units within the Stø and Nordmela Formations are interpreted on the basis of lithology variation and sedimentary structures observed while doing core logging (Appendix A). Fine to medium grained, well sorted clean sandstone of the Stø Formation is having cross lamination and deposited in beach shore line where sediments are reworked. The upper part of the Stø Formation is light gray silty sand with vertical bioturbation and some burrows.

The lower part of the Nordmela Formation consist of interbedded silty sandstone and mudstone with mud drapes, cross lamination and lenticular to flaser bedding. The upper part of the Nordmela formation is silty sand with mud drapes, cross lamination and lenticular to flaser bedding. Lower part is deposited in tidal flat to flood plain environment and upper part is more influenced by fluvial tidal channel.

7.10 Relationship between Core Sedimentology, Petrography and Petrophysical analysis

In order to strengthen our results obtained from different analysis, correlation has been made among them. Values gathered from XRD, SEM and point count analysis were related with the values taken from petrophysical analyses and core logs. Stø Formation in deep well (7219/8-1) is having high Vp values as shown in depth versus velocity cross plot (Fig 5.6b). Velocity is a function of density. Mean density of the Stø formation in density histogram is 2.52g/cc (Fig 5.5b) which indicates that porosity should be very low. Higher the velocity, greater would be the density and low porosity. Porosity values in the Stø Formation are very low and ranging from 2-8 percent in point count analysis and mean porosity is 4% (Fig 6.1). Stø Formation in deep well (7219/8-1) is a more clean sandstone with low clay and silt (A2). The histogram for gamma ray of the Stø Formation shows low gamma ray mean value around 33.89 API (Fig 5.3a). Sand with low clay content has low gamma ray value.

Depth versus velocity cross plot of the Stø and Nordmela Formations in shallow well (7220/7-1) have values ranging from 3410 m/sec to 4200 m/sec (Fig 5.6a) which is not as high as in deep well for Stø Formation because the porosity here is quite high (Fig 6.2). Mean Porosity in point count analysis for the Stø Formation is 24.74% and Nordmela Formation has 23.19% (Table 6.3). Mean density for both formations in density histogram is 2.37g/cc (Fig 5.5a).Velocity is dependent on density and density is directly related to porosity. Low density and low velocity values in both formations are explained by high porosity values. In shallow well, sandstone of the Stø Formation is clean with some silt and have a low gamma ray value (Fig 5.3b) but gamma ray of the Stø Formation in deep well is lower than the Stø in shallow well. Nordmela Formation is silty sand with interbedded mudstone and has high gamma ray value then the Stø Formation (Fig 5.1).

7.11 Reservoir Quality

Reservoir quality of the Stø Formation in deep well is very poor. This may be because of the low porosity but the density and velocity values are very high which means that the Stø Formation is highly compacted due to chemical compaction. On the other hand the Stø and Nordmela Formation in shallow well are having good porosity but low density and velocity. Reservoir quality of the Nordmela Formation is poor due to the presence of mudstone interbedded with silty sandstone which affects the permeability. Low gamma ray values of the Stø Formation in deep well indicate that the sandstone is clean. Gamma ray values of the Stø Formation in the shallow well are comparatively less than the Nordmela Formation because sandstone of Stø formation is clean and having a good reservoir quality. Based on petrophysical, petrographical and core analysis the reservoir quality of the Stø Formation in shallow well is very good whereas in deeper well it is very poor.

7.12 Burial History Curve

In shallow well (7220/7-1) present day bottom hole temperature is 72°C and surface temperature is considered as 4°C. Total depth is 2230m and water depth is 365m. According to this given data geothermal gradient of this well is 36.48°C. If we add 1000m of uplift then reservoir attained maximum temperature of about 100°C during late tertiary prior to uplift. Quartz cementation starts at about 1.9km depth and reaches to its maximum value at about 2.3km depth. After reaching the maximum burial depth, the reservoir was uplifted and quartz cementation was perhaps stopped. At present day the reservoir is in mechanical compaction zone.

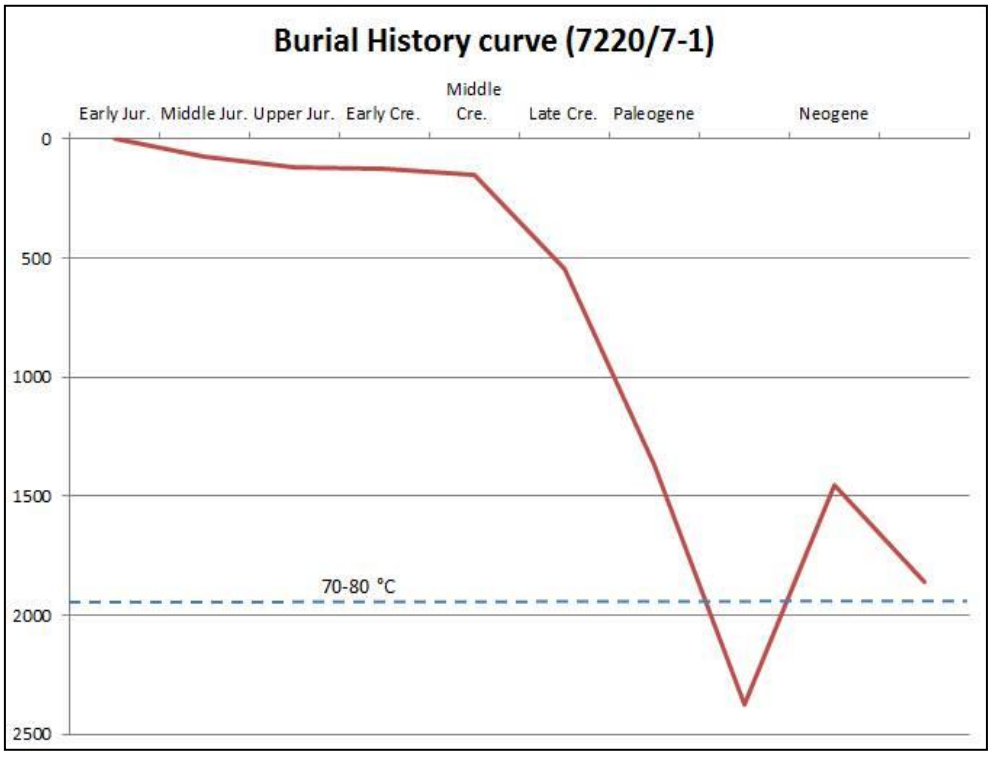

Figure 7.2a: Burial history curve within 7220/7-1.

In the deeper well, the present day temperature is 165°C and surface temperature is 4°C. Geothermal gradient is 39.3°C presently. After adding 1000m uplift then maximum burial goes to around 204°C which is quite high. The rate of quartz cementation increases by 1.7/10°C. At 165°C, rate of quartz cementation is around 28 but at 204°C it is around 37 which were quite high. At this point rate of quartz cementation and time temperature integral is quite high which causes high rate of cementation in a shorter period of time. Time does not explain itself anything about the mechanism of cementation but it is just an indicative that lot of cementation is expected. Low porosity and very high values of Vp and density also indicate that the Stø Formation is highly compacted due to cementation. Quartz cementation starts at a burial depth of around 1.9Km in the Early to Middle Cretaceous and reaches to its maximum at a burial depth of 4.8Km during Late Tertiary. The reservoir attained maximum temperature of around 200°C at this depth and starts uplift in Late Tertiary where the temperature is around 165°C. The reservoir remained in the chemical compaction regime after uplift at a burial depth of around 4.2Km.

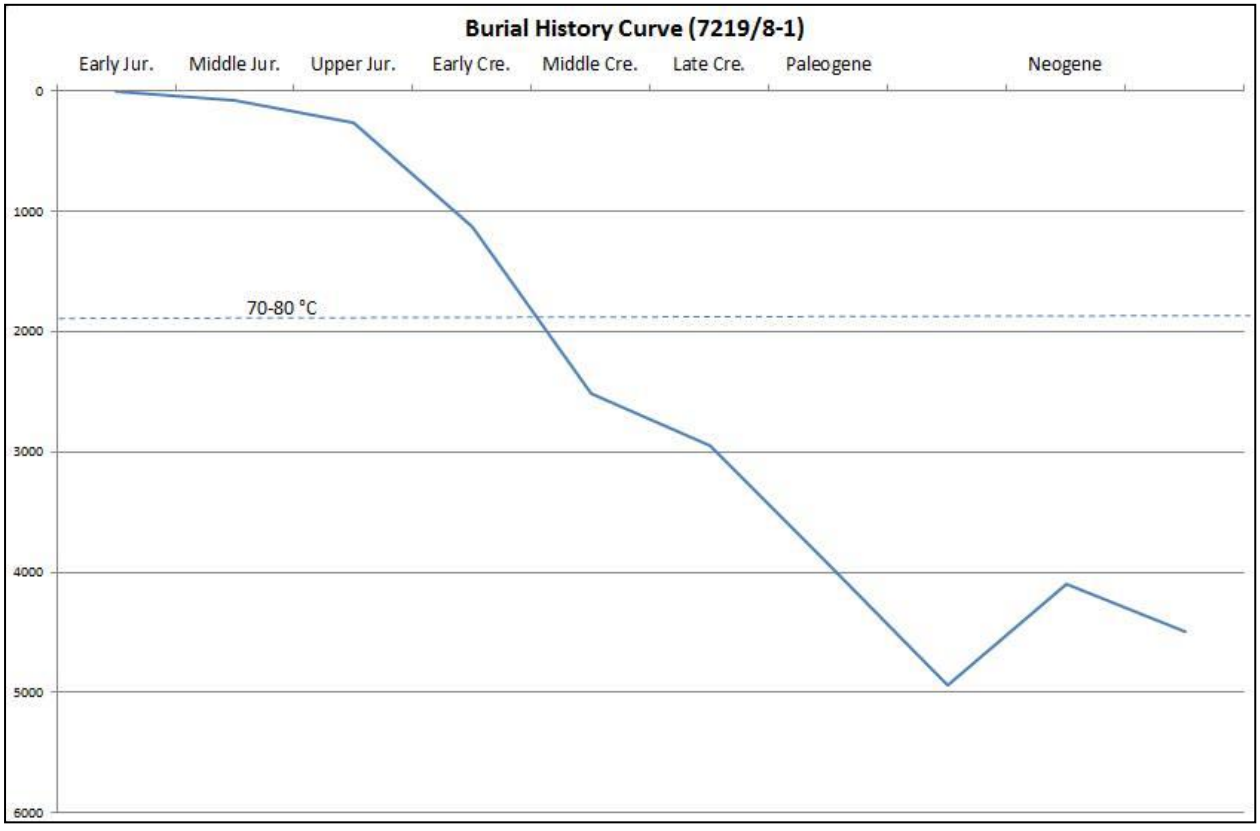

Figure 7.2b: Burial history curve within well 7219/8-1.

8 CONCLUSION

- The Stø and Nordmela Formation in both wells have sandstones that were mineralogically mature but the sandstones of the Nordmela Formation were less sorted.
- Abnormally high intergranular volume in two samples from deep and shallow well were observed. This may be mainly due to the presence of siderite as a detrital grain during the early diagenesis and then dissolution and recrystallization during late diagenesis.
- In the shallow well, the Stø and Nordmela Formations had well preserved porosity but porosity in the deeper well was totally destroyed due to quartz cementation and intergranular pressure solution.
- In deep well the presence of illite and absence of Kaolinite and K-feldspar may suggest that both minerals due to their unstable nature at high temperature (thermodynamically) were converting into illite.
- In deep well (7219/8-1), low porosity is may be due to the presence of quartz cementation, intergranular pressure solution and pore-filling illite.
- Presence of small amount of quartz overgrowth and pore-filling kaolinite and illite does not affect the porosity of the Stø and Nordmela Formation in the shallow well.
- In deep well, chemical compaction in the Stø Formation was controlled by quartz cementation and intergranular pressure solution but chemical compaction in the shallow well was only influenced by quartz cementation in the Stø and Nordmela Formation.
- The Stø Formation in the deeper well has both grain coated and pore-filling illite. The Stø and Nordmela Formation however, only have pore-filling illite in the shallower well.

9 REFERENCES

AAGAARD, P., EGEBERG, P., SAIGAL, G., MORAD, S. & BJORLYKKE, K. 1990. Diagenetic Albitization of Detrital K-Keldspars in Jurassic, Lower Cretaceous and Tertiary Clastic Reservoir Rocks from Offshore Norway, II. Formation Water Chemistry and Kinetic Considerations. *Journal of sedimentary Research,* 60. 575-581.

ADAMS, A. E., MACKENZIE, W. S. & GUILFORD, C. 1984. *Atlas of sedimentary rocks under the microscope,* Longman; Wiley.

AJDUKIEWICZ, J. M. & LANDER, R. H. 2010. Sandstone reservoir quality prediction: The state of the art. *AAPG bulletin,* 94**,** 1083-1091.

BARRÈRE, C., EBBING, J. & GERNIGON, L. 2009. Offshore prolongation of Caledonian structures and basement characterisation in the western Barents Sea from geophysical modelling. *Tectonophysics,* 470**,** 71-88.

BERGLUND, L., AUGUSTSON, J., FÆRSETH, R., GJELBERG, J. & RAMBERG-MOE, H. 1986. The evolution of the Hammerfest Basin. *Habitat of hydrocarbons on the Norwegian continental shelf***,** 319-338.

BJØRLYKKE, K. & JAHREN, J. 2010. Sandstones and sandstone reservoirs. *Petroleum Geoscience.* Springer.

BJØRLYKKE, K., NEDKVITNE, T., RAMM, M. & SAIGAL, G. C. 1992. Diagenetic processes in the Brent Group (Middle Jurassic) reservoirs of the North Sea: an overview. *Geological Society, London, Special Publications,* 61**,** 263-287.

BJØRLYKKE, K., RAMM, M. & SAIGAL, G. C. 1989. Sandstone diagenesis and porosity modification during basin evolution. *Geologische Rundschau,* 78**,** 243-268.

BLOCH, S., LANDER, R. H. & BONNELL, L. 2002. Anomalously high porosity and permeability in deeply buried sandstone reservoirs: Origin and predictability. *AAPG bulletin,* 86**,** 301-328.

BREIVIK, A. J., FALEIDE, J. I. & GUDLAUGSSON, S. T. 1998. Southwestern Barents Sea margin: late Mesozoic sedimentary basins and crustal extension. *Tectonophysics,* 293**,** 21-44.

CHUHAN, F. A., BJØRLYKKE, K. & LOWREY, C. 2000. The role of provenance in illitization of deeply buried reservoir sandstones from Haltenbanken and north Viking Graben, offshore Norway. *Marine and Petroleum Geology,* 17**,** 673-689.

CHUHAN, F. A., KJELDSTAD, A., BJØRLYKKE, K. & HØEG, K. 2003. Experimental compression of loose sands: relevance to porosity reduction during burial in sedimentary basins. *Canadian Geotechnical Journal,* 40**,** 995-1011.

CLARK, S., GLORSTAD- CLARK, E., FALEIDE, J., SCHMID, D., HARTZ, E. & FJELDSKAAR, W. 2014. Southwest Barents Sea rift basin evolution: comparing results from backstripping and time- forward modelling. *Basin Research,* 26**,** 550-566.

DALLAND, A., WORSLEY, D. & OFSTAD, K. 1988. *A Lithostratigraphic Scheme for the Mesozoic and Cenozoic and Succession Offshore Mid-and Northern Norway,* Oljedirektoratet.

DORÉ, A. 1995. Barents Sea geology, petroleum resources and commercial potential. *Arctic***,** 207-221.

FALEIDE, J., VÅGNES, E. & GUDLAUGSSON, S. Late Mesozoic–Cenozoic evolution of the southwestern Barents Sea. Geological Society, London, Petroleum Geology Conference series, 1993a. Geological Society of London, 933-950.

FALEIDE, J. I., BJØRLYKKE, K. & GABRIELSEN, R. H. 2010. Geology of the Norwegian continental shelf. *Petroleum Geoscience.* Springer.

FALEIDE, J. I., GUDLAUGSSON, S. T. & JACQUART, G. 1984. Evolution of the western Barents Sea. *Marine and Petroleum Geology,* 1**,** 123-150.

FALEIDE, J. I., VÅGNES, E. & GUDLAUGSSON, S. T. 1993b. Late Mesozoic-Cenozoic evolution of the south-western Barents Sea in a regional rift-shear tectonic setting. *Marine and Petroleum Geology,* 10**,** 186-214.

FOLK, R. L. 1951. Stages of textural maturity in sedimentary rocks. *Journal of Sedimentary Research,* 21.

GABRIELSEN, R. 1984. Long-lived fault zones and their influence on the tectonic development of the southwestern Barents Sea. *Journal of the Geological Society,* 141**,** 651-662.

GABRIELSEN, R. H., FAERSETH, R. B., JENSEN, L. N., KALHEIM, J. E. & RIIS, F. 1990. Structural elements of the Norwegian Continental Shelf. Part 1: The Barents Sea Region. *Norwegian Pertoleum Directorate,* Bulletin no. 6**,** 1-33.

GERNIGON, L., BRÖNNER, M., ROBERTS, D., OLESEN, O., NASUTI, A. & YAMASAKI, T. 2014. Crustal and basin evolution of the southwestern Barents Sea: from Caledonian orogeny to continental breakup. *Tectonics,* 33**,** 347-373.

GIRARD, J. P. 1998. Carbonate Cementation in the Middle Jurassic Oseberg Reservoir Sandstone, Oseberg Field, Norway: A Case of Deep Burial–High Temperature Poikilotopic Calcite. *Carbonate Cementation in Sandstones: Distribution Patterns and Geochemical Evolution***,** 285-307.

GÖTZE, J., PLÖTZE, M. & HABERMANN, D. 2001. Origin, spectral characteristics and practical applications of the cathodoluminescence (CL) of quartz–a review. *Mineralogy and Petrology,* 71**,** 225-250.

HOUSEKNECHT, D. W. 1988. Intergranular pressure solution in four quartzose sandstones. *Journal of Sedimentary Research,* 58.

JOHNSON, R. H. 1920. The cementation process in sandstone. *AAPG Bulletin,* 4**,** 33-35.

LETAMENDI, J. E., PÉREZ, R. M., HUERTAS, A. D. & I BASTARDAS, A. P. 2007. The Impact of carbonate cements on the reservoir quality in the Napo Fm sandstones (Cretaceous Oriente Basin, Ecuador). *Geologica Acta,* 5**,** 89.

LONGIARU, S. 1987. Visual Comparators for Estimating the Degree of Sorting from Plane and Thin Section: RESEARCH METHOD PAPER. *Journal of Sedimentary Research,* 57.

MONDOL, N. H. Porosity and permeability development in mechanically compacted silt-kaolinite mixtures. SEG Technical Program Expanded Abstracts, 2009.

NPD. 2012. *Norwegian continental shelf* [Online]. Available: http://www.npd.no/Global/Engelsk/3-Publications/Norwegian-Continental-Shelf/No-1-2012/Norsk-sokkel-engelsk-nr-1-2012-small.pdf [Accessed 4 April 2015].

NPD. 2014. Petroleum resources on the Norwegian continental shelf 2014 Fields and Discoveries. Available: http://www.npd.no/Global/Engelsk/3-Publications/Resource-report/Resource-report-2014/Resources-2014-nett.pdf.

OHM, S. E., KARLSEN, D. A. & AUSTIN, T. 2008. Geochemically driven exploration models in uplifted areas: Examples from the Norwegian Barents Sea. *AAPG bulletin,* 92**,** 1191-1223.

OLAUSSEN, S., DALLAND, A., GLOPPEN, T. & JOHANNESSEN, E. 1984. Depositional environment and diagenesis of Jurassic reservoir sandstones in the eastern part of Troms I area. *Petroleum Geology of the North European Margin.* Springer.

PAXTON, S., SZABO, J., AJDUKIEWICZ, J. & KLIMENTIDIS, R. 2002. Construction of an intergranular volume compaction curve for evaluating and predicting compaction and porosity loss in rigid-grain sandstone reservoirs. *AAPG bulletin,* 86**,** 2047-2067.

SAIGAL, G. & BJØRLYKKE, K. 1987. Carbonate cements in clastic reservoir rocks from offshore Norway—relationships between isotopic composition, textural development and burial depth. *Geological Society, London, Special Publications,* 36**,** 313-324.

SAIGAL, G. C., MORAD, S., BJORLYKKE, K., EGEBERG, P. K. & AAGAARD, P. 1988. Diagenetic albitization of detrital K-feldspar in Jurassic, Lower Cretaceous, and Tertiary clastic reservoir rocks from offshore Norway, I. Textures and origin. *Journal of Sedimentary Research,* 58.

SMELROR, M. 1994. Jurassic stratigraphy of the western Barents Sea region: A review. *Geobios,* 27**,** 441-451.

STILWELL, H. 2012. New Insights on Stratigraphy of Triassic/Jurassic Sequences in the Barents Sea.

STORVOLL, V., BJØRLYKKE, K., KARLSEN, D. & SAIGAL, G. 2002. Porosity preservation in reservoir sandstones due to grain-coating illite: a study of the Jurassic Garn Formation from the Kristin and Lavrans fields, offshore Mid-Norway. *Marine and Petroleum Geology,* 19**,** 767-781.

TAYLOR, T. R., GILES, M. R., HATHON, L. A., DIGGS, T. N., BRAUNSDORF, N. R., BIRBIGLIA, G. V., KITTRIDGE, M. G., MACAULAY, C. I. & ESPEJO, I. S. 2010. Sandstone diagenesis and reservoir quality prediction: Models, myths, and reality. *AAPG bulletin,* 94**,** 1093-1132.

WALDERHAUG, O. 1996. Kinetic modeling of quartz cementation and porosity loss in deeply buried sandstone reservoirs. *AAPG bulletin,* 80**,** 731-745.

WORDEN, R. & MORAD, S. 2000. Quartz cementation in oil field sandstones: a review of the key controversies. *Quartz cementation in sandstones, Special publications of international association of sedimentologists,* 29**,** 1-20.

WORDEN, R. & MORAD, S. 2009. *Quartz cementation in oil field sandstones: a review of the key controversies*, Blackwell Publishing Ltd.

10 APPENDICES

APPENDIX A: Sedimentary logs.

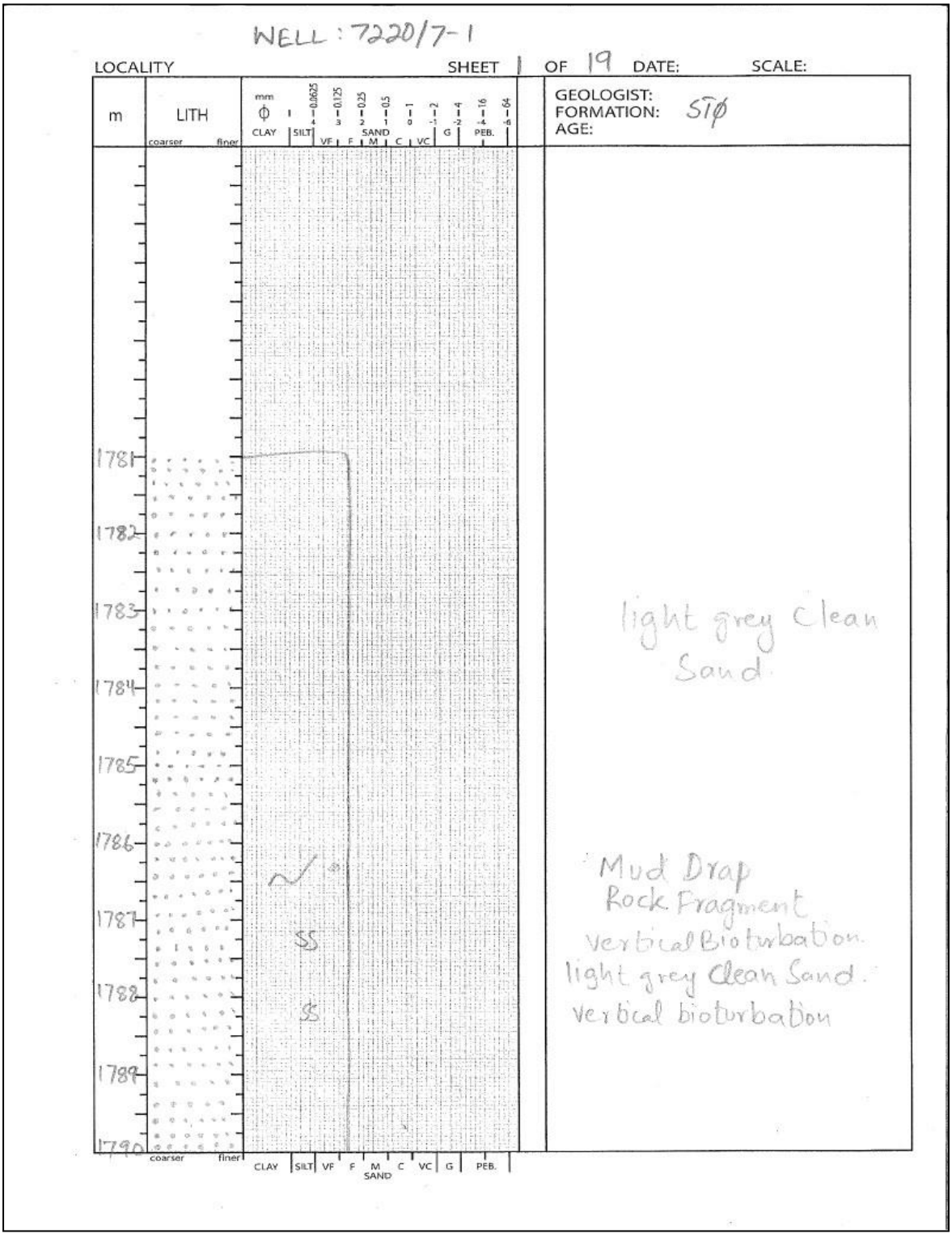

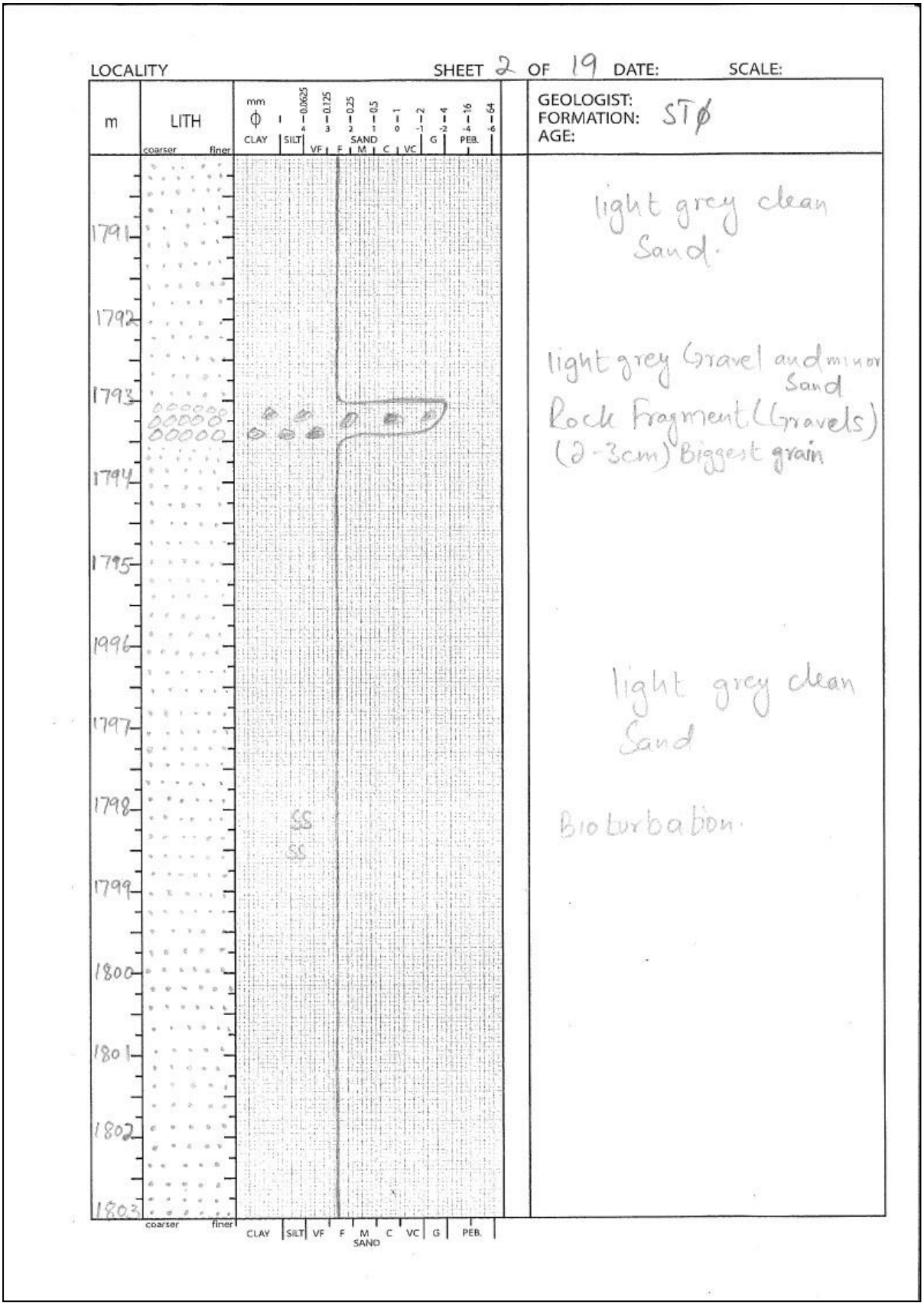
LOCALITY
SHEET 2 OF 19 DATE:
SCALE:
m
LITH
coarser
finer
mm
ϕ
CLAY
SILT
VF
F
M
C
VC
G
PEB.
SAND
GEOLOGIST:
FORMATION: STϕ
AGE:
1791
1792
1793
1794
1795
1996
1797
1798
1799
1800
1801
1802
1803
light grey clean Sand.
light grey Gravel and minor Sand
Rock Fragment (Gravels) (2-3cm) Biggest grain
light grey clean Sand
Bioturbation.
SS
SS

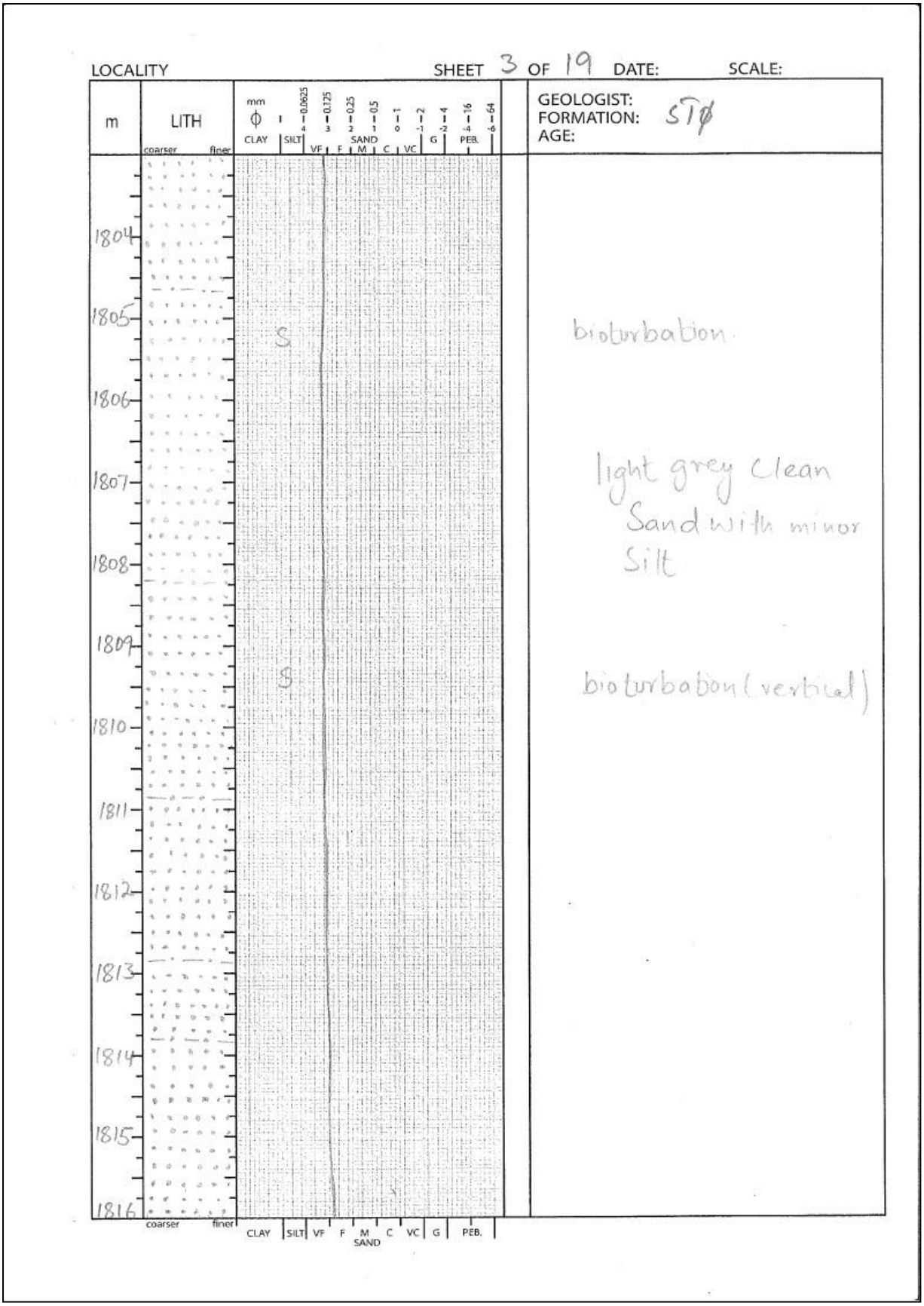
LOCALITY
SHEET 3 OF 19
DATE:
SCALE:
m
LITH
coarser
finer
mm
ϕ
CLAY
SILT
SAND
VF
F
M
C
VC
G
PEB.
GEOLOGIST:
FORMATION: STϕ
AGE:
1804
1805
1806
1807
1808
1809
1810
1811
1812
1813
1814
1815
1816
bioturbation
light grey clean Sand with minor Silt
bioturbation (vertical)

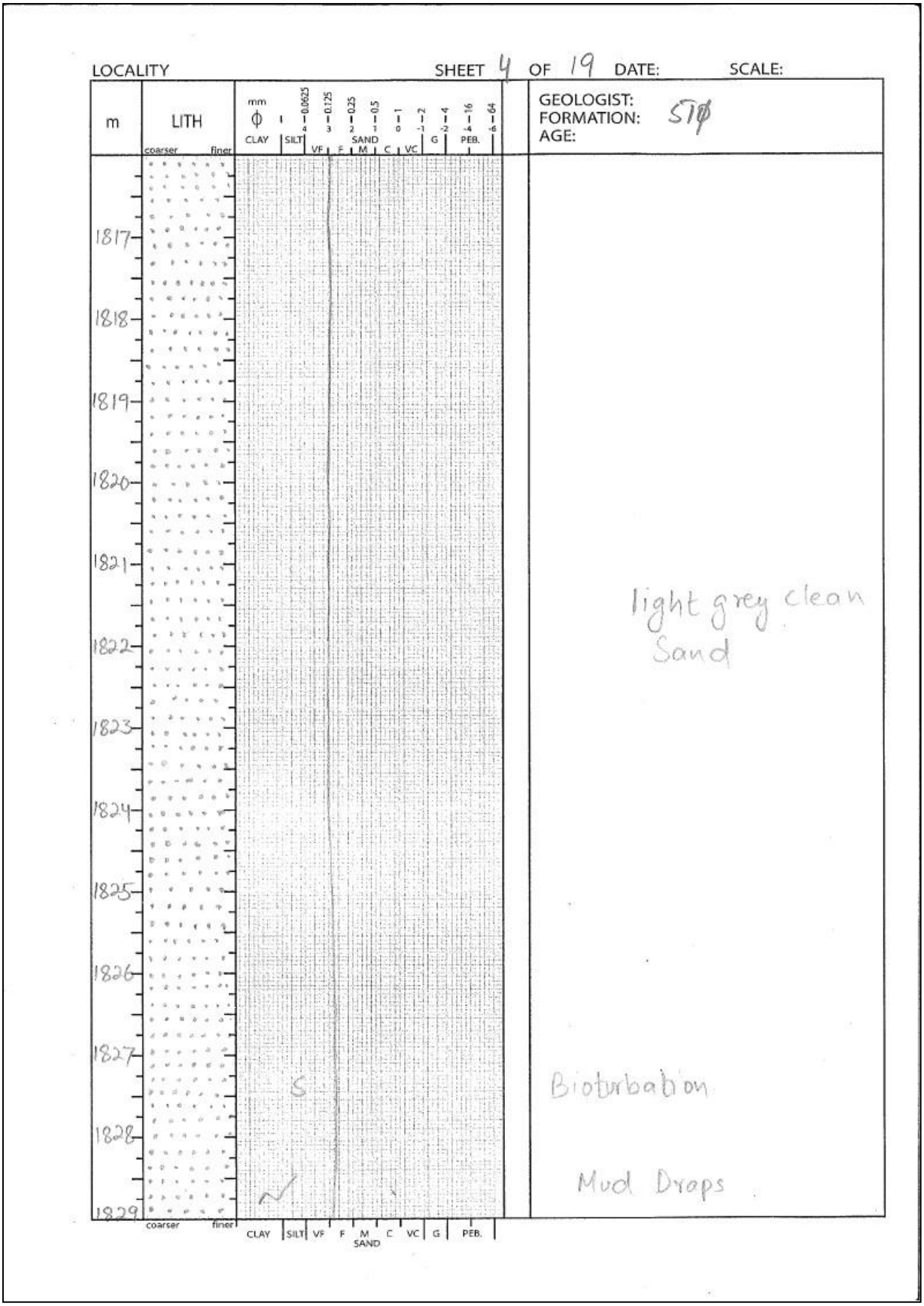
LOCALITY
SHEET 4 OF 19 DATE:
SCALE:
m
LITH
coarser
finer
mm
ϕ
CLAY
SILT
SAND
VF
F
M
C
VC
G
PEB.
GEOLOGIST:
FORMATION: STP
AGE:
1817
1818
1819
1820
1821
1822
1823
1824
1825
1826
1827
1828
1829
light grey clean Sand
Bioturbation
Mud Drops

LOCALITY SHEET 5 OF 19 DATE: SCALE:

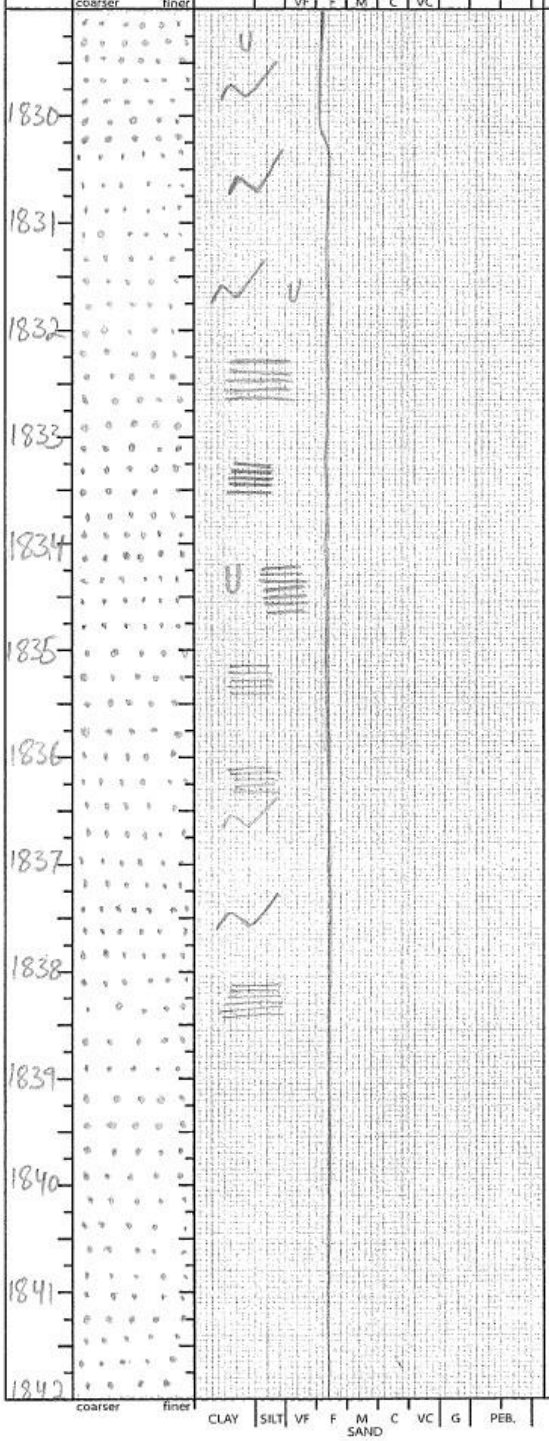

GEOLOGIST:
FORMATION: STP
AGE:

light grey clean Sand

Parallel lamination.
Clean
Brown Parallel lamination
Sand

Parallel lamination
Mud Drap

Mud Drap.
Parallel lamination.

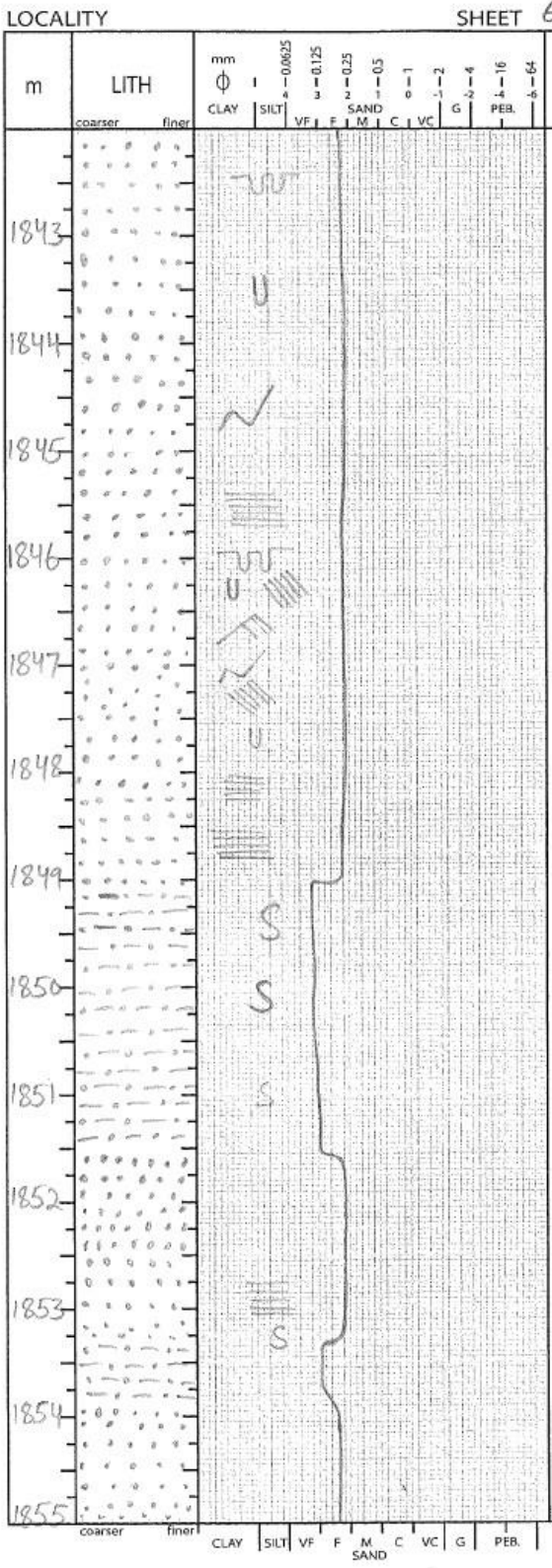
LOCALITY
SHEET 6 OF 19
DATE:
SCALE:
m
LITH
coarser
finer
mm
ϕ
CLAY
SILT
VF
F
M
C
VC
G
PEB.
SAND
GEOLOGIST:
FORMATION: SID
AGE:
1843
1844
1845
1846
1847
1848
1849
1850
1851
1852
1853
1854
1855
load Cast
burrow
Mud drop
Brown Clean
Sand
load cast
Cross lamination.
ripple marks
Mud Drop
Cross lamination
Burrows.
light Brown to Black
Silty Sand
Bioturbation
Brown clean Sand
Parallel lamination
vertical & diagonal Bioturbat
ion. Silty Sand
Brown Clean Sand

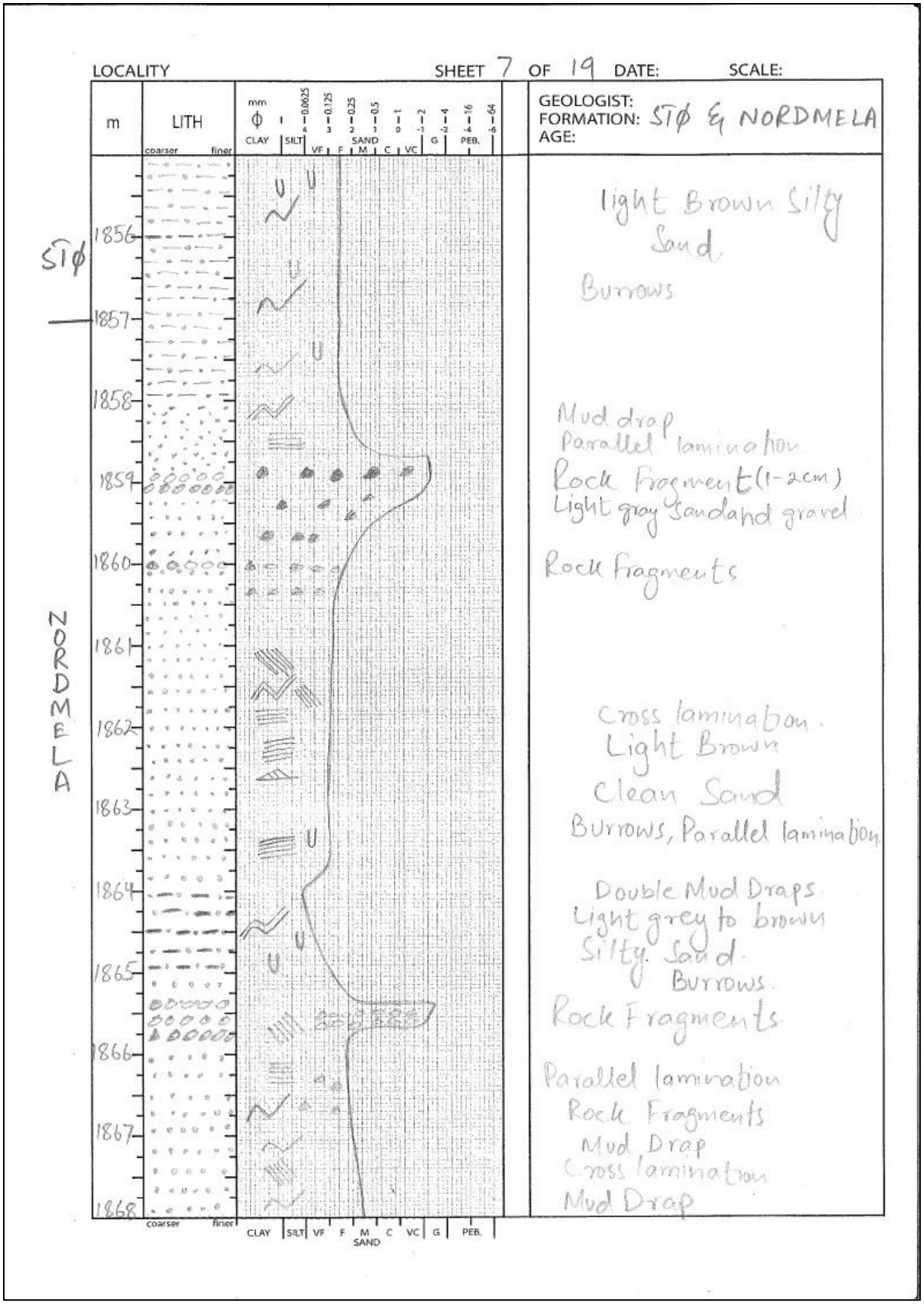
LOCALITY
SHEET 7 OF 19
DATE:
SCALE:
m
LITH
coarser
finer
mm
ϕ
CLAY
SILT
SAND
VF
F
M
C
VC
G
PEB.
GEOLOGIST:
FORMATION: STØ & NORDMELA
AGE:
STØ
NORDMELA
1856
1857
1858
1859
1860
1861
1862
1863
1864
1865
1866
1867
1868
light Brown Silty Sand
Burrows
Mud drop
Parallel lamination
Rock Fragment (1-2cm)
Light gray Sand and gravel
Rock Fragments
Cross lamination
Light Brown
Clean Sand
Burrows, Parallel lamination
Double Mud Draps
Light grey to brown
Silty Sand
Burrows
Rock Fragments
Parallel lamination
Rock Fragments
Mud Drap
Cross lamination
Mud Drap

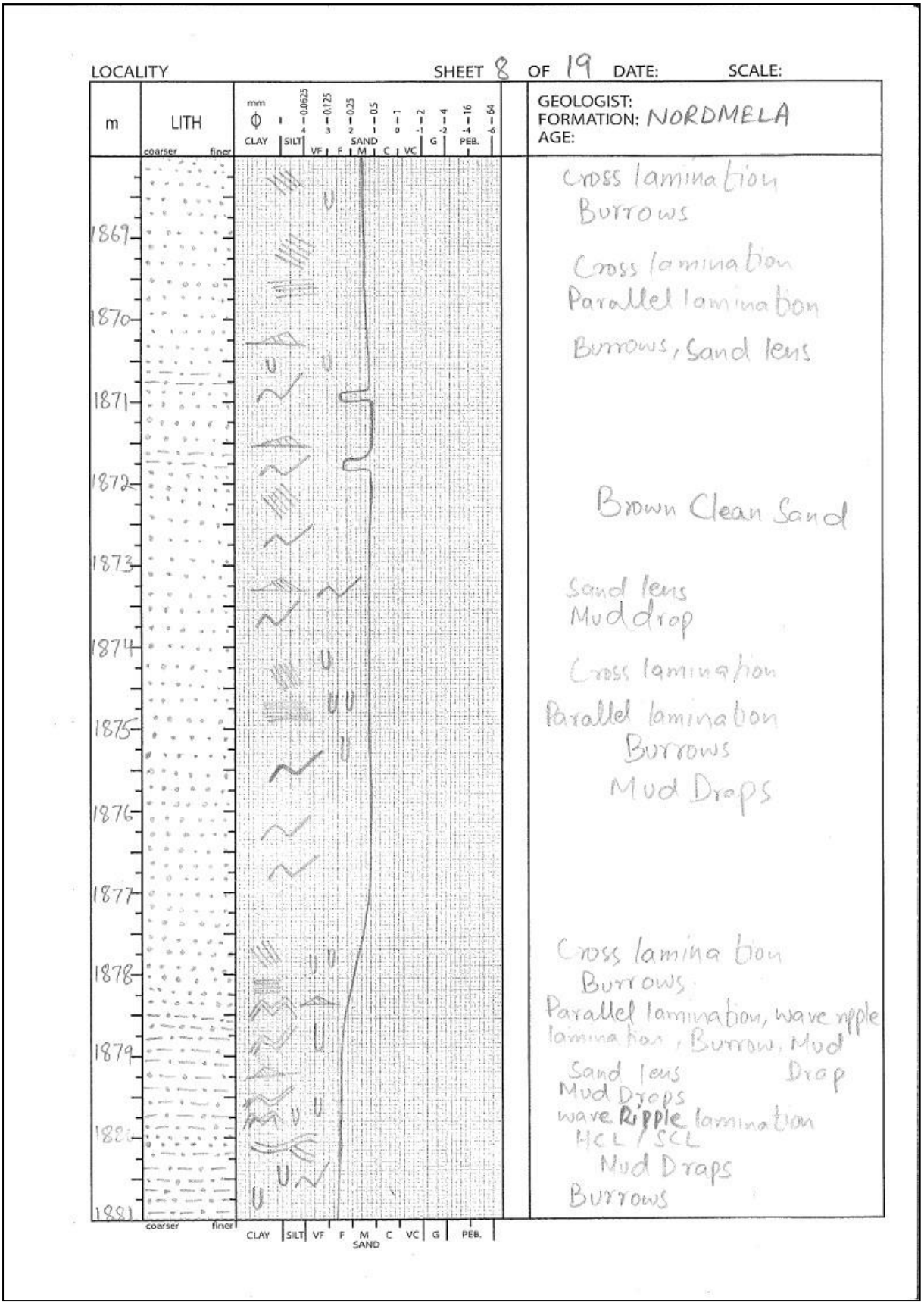
LOCALITY
SHEET 8 OF 19 DATE: SCALE:
m
LITH
coarser finer
mm
Φ
CLAY SILT VF F M C VC G PEB.
SAND
GEOLOGIST:
FORMATION: NORDMELA
AGE:
1869
1870
1871
1872
1873
1874
1875
1876
1877
1878
1879
1880
1881
Cross lamination
Burrows
Cross lamination
Parallel lamination
Burrows, Sand lens
Brown Clean Sand
Sand lens
Mud drop
Cross lamination
Parallel lamination
Burrows
Mud Drops
Cross lamination
Burrows
Parallel lamination, wave ripple lamination, Burrow, Mud
Sand lens
Drop
Mud Drops
wave Ripple lamination
HCL / SCL
Mud Drops
Burrows

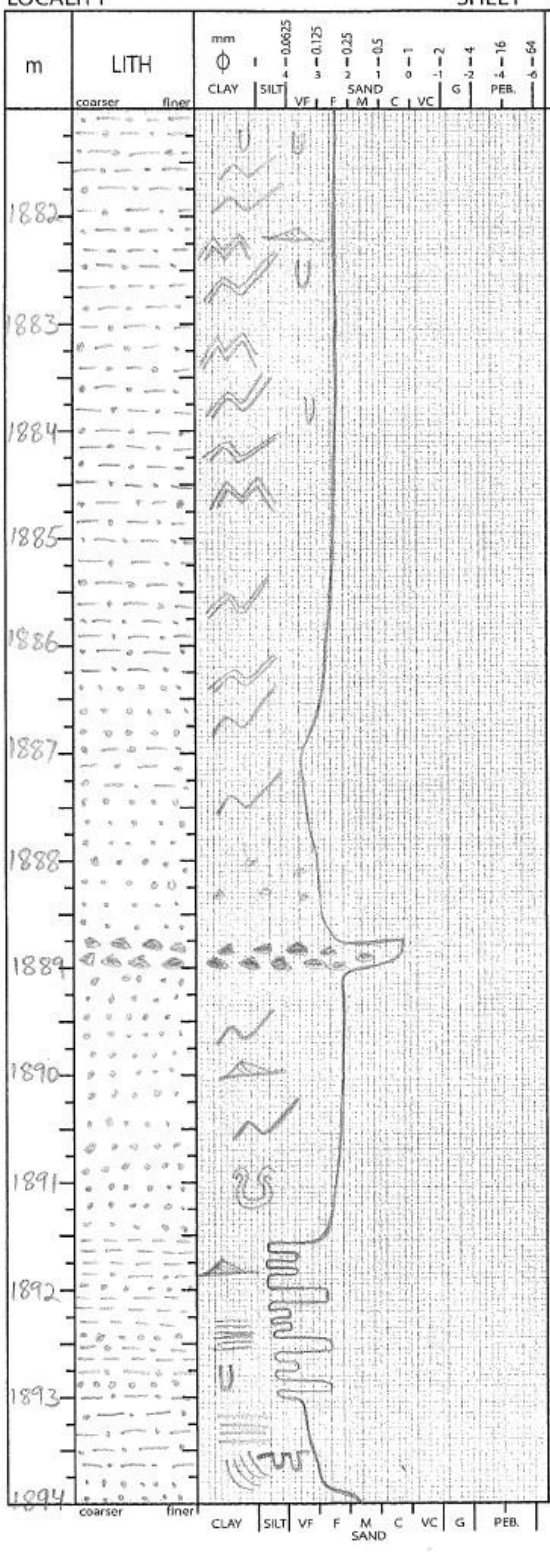
LOCALITY
SHEET 9 OF 19 DATE:
SCALE:
m
LITH
coarser
finer
mm
CLAY
SILT
SAND
VF
F
M
C
VC
G
PEB.
GEOLOGIST:
FORMATION: NORDMELA
AGE:
1882
1883
1884
1885
1886
1887
1888
1889
1890
1891
1892
1893
1894
Burrows
Mud Drap
Sand lens
Light grey to
Brown Silty
Sand.
Mud Drap
wave Ripple lamination.
Double Mud Draps
Mud Draps.
Light grey clean Sand
with Some silt
Rock Fragments Gravel
Sand lens
Mud Drops
Slump Structure
Light grey to Brown interbedd
ed Clean Sand and Silty Mud
Burrows, Parallel lamination
Trough Cross lamination
Light grey to Brown
Silty Sand Parallel lamination

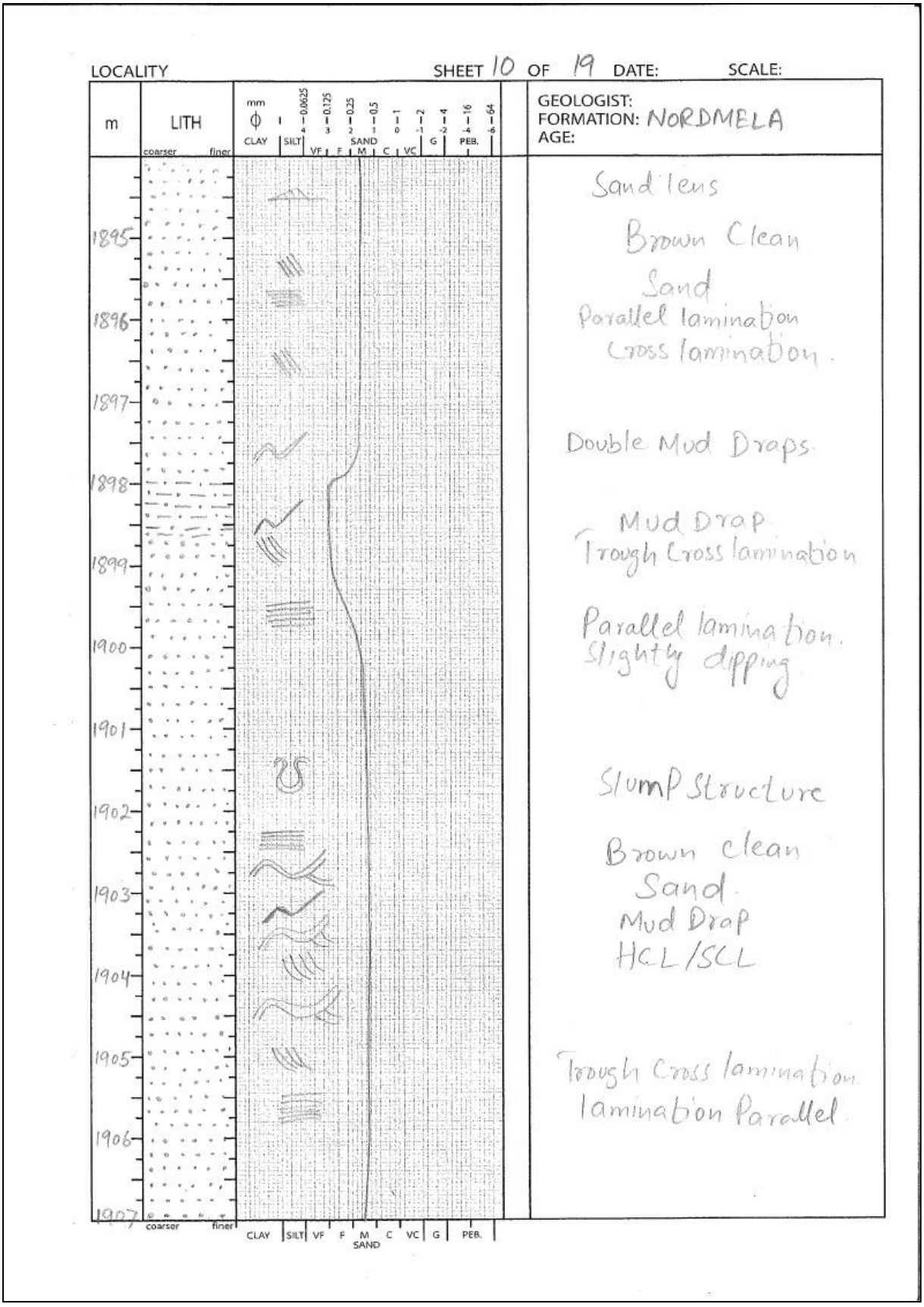
LOCALITY
SHEET 10 OF 19
DATE:
SCALE:
m
LITH
coarser
finer
mm
ϕ
CLAY
SILT
SAND
VF
F
M
C
VC
G
PEB.
GEOLOGIST:
FORMATION: NORDMELA
AGE:
1895
1896
1897
1898
1899
1900
1901
1902
1903
1904
1905
1906
1907
Sand lens
Brown Clean
Sand
Parallel lamination
Cross lamination.
Double Mud Draps.
Mud Drap
Trough Cross lamination
Parallel lamination.
Slightly dipping
Slump Structure
Brown clean
Sand.
Mud Drap
HCL/SCL
Trough Cross lamination
lamination Parallel

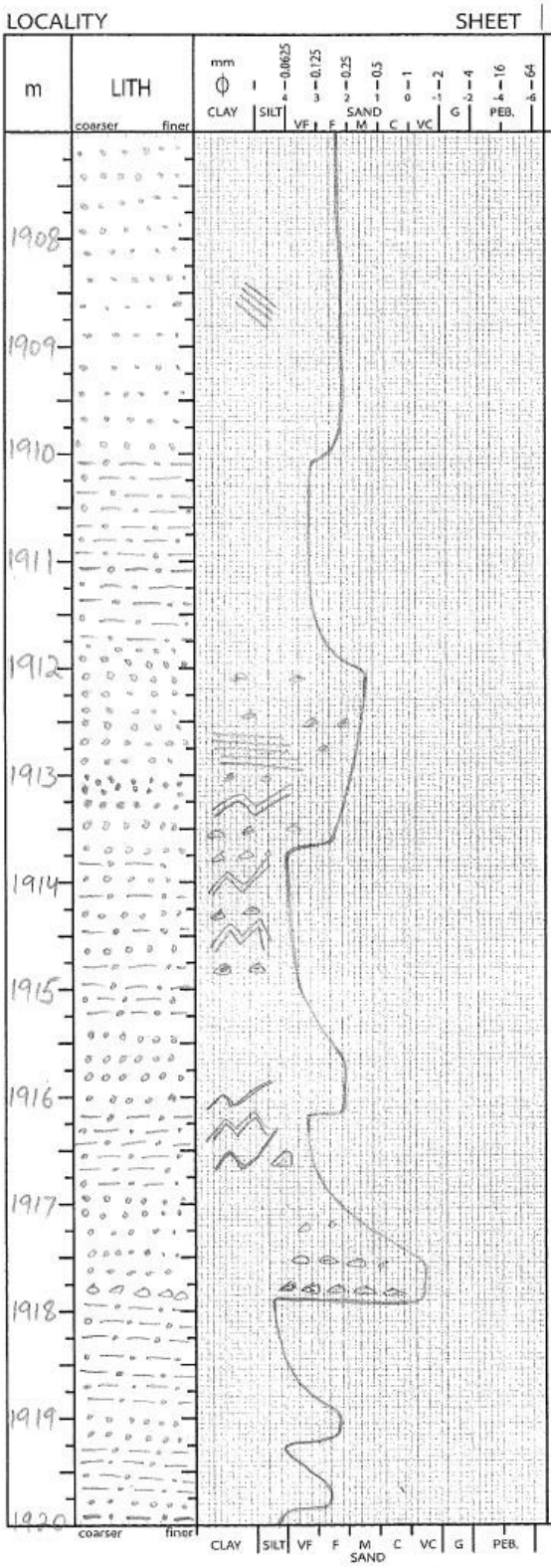

Brown Clean Sand.

light grey to Brown Silty Sand.

Fragments laminated Sand but slightly Dipping.
Double Mud drops
Rock Fragments

Wave Ripple lamination
Rock Fragments

wave ripple lamination
Fragments Silty Sand Mud Drap
Coarse grain
Light to Dark Brown
Sand & gravels
Gravels/Rock Fragments

Light Brown
Silty Sand

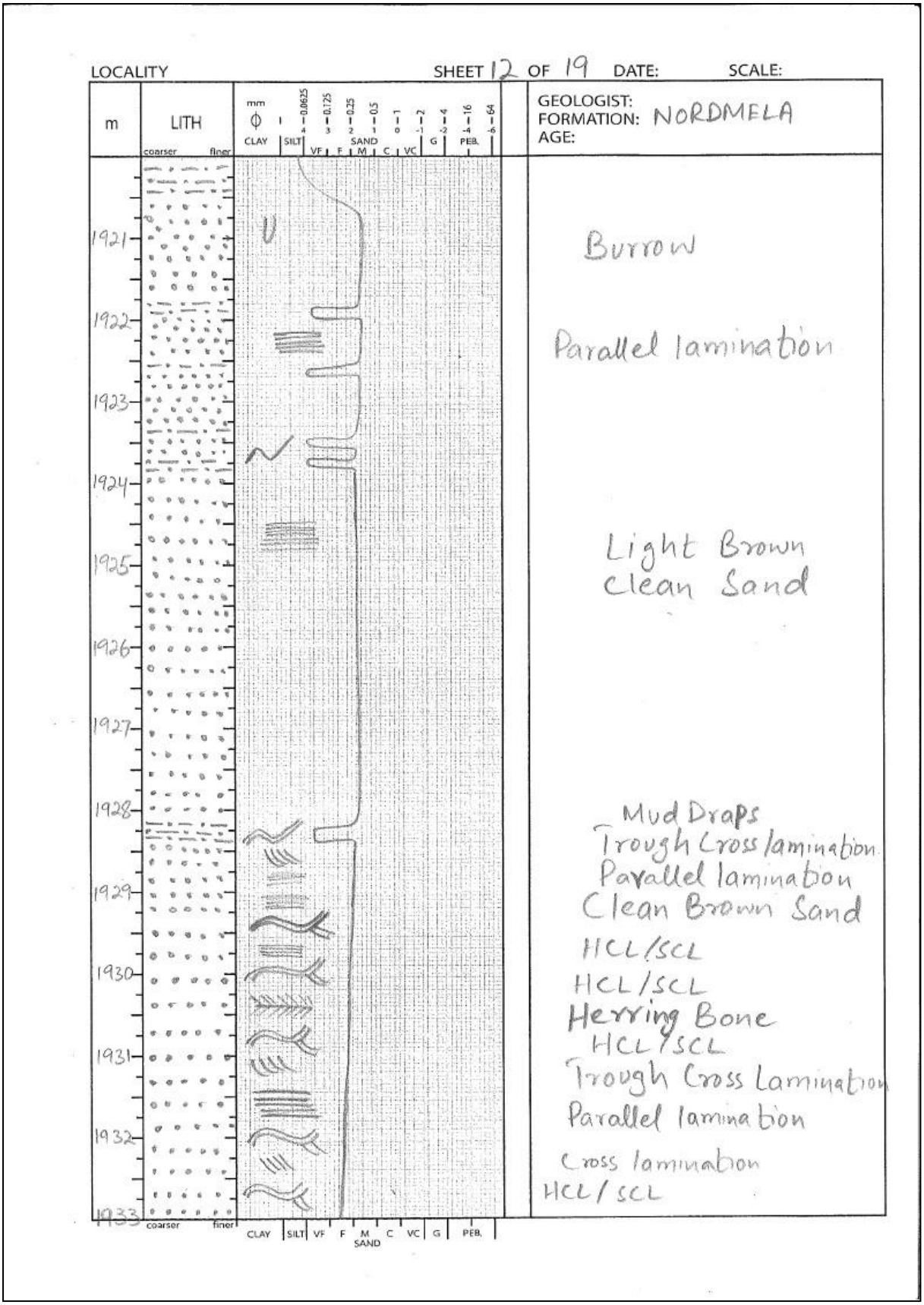
LOCALITY
SHEET 12 OF 19
DATE:
SCALE:
m
LITH
coarser
finer
mm
CLAY
SILT
SAND
VF
F
M
C
VC
G
PEB.
GEOLOGIST:
FORMATION: NORDMELA
AGE:
1921
1922
1923
1924
1925
1926
1927
1928
1929
1930
1931
1932
1933
Burrow
Parallel lamination
Light Brown
Clean Sand
Mud Draps
Trough Cross lamination
Parallel lamination
Clean Brown Sand
HCL/SCL
HCL/SCL
Herring Bone
HCL/SCL
Trough Cross Lamination
Parallel lamination
Cross lamination
HCL/SCL

LOCALITY SHEET 13 OF 19 DATE: SCALE:

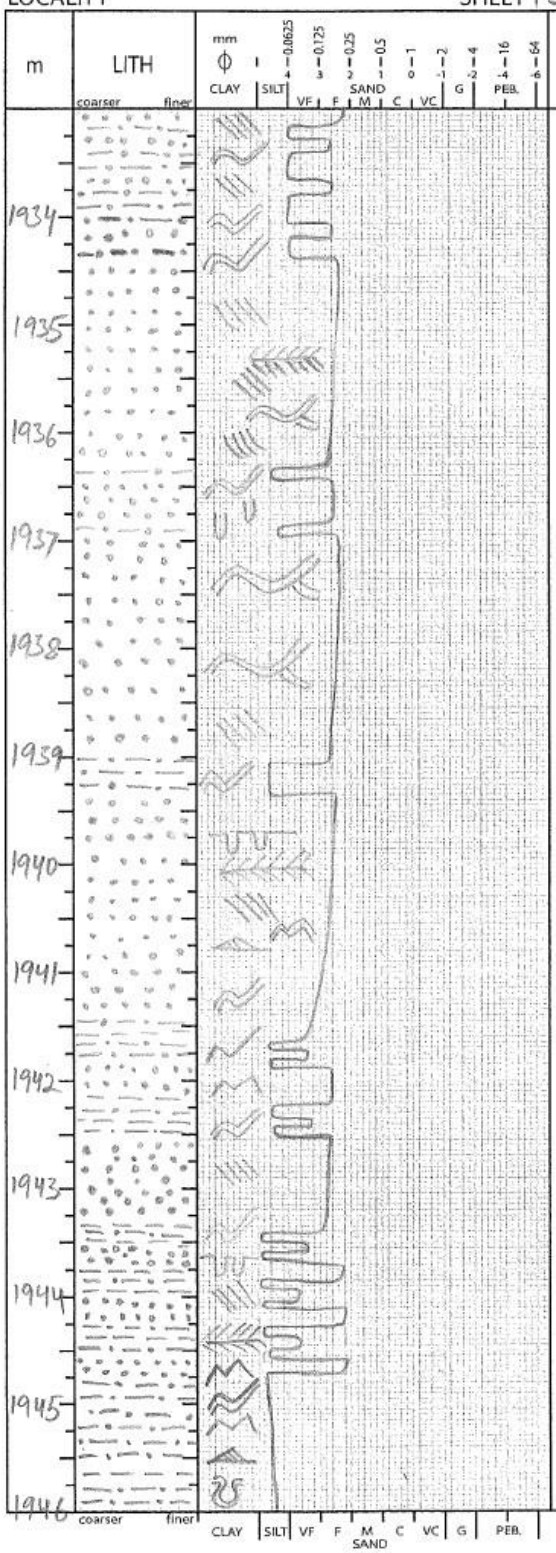

GEOLOGIST:
FORMATION: NORDMELA
AGE:

Cross Lamination
Double Mud Draps

HCL/SCL, Herring Bone
Cross lamination
Trough Cross lamination.

Burrows, Double Mud Drap
Brown Clean Sand
with light grey to
Black. Silty Mud.
HCL/SCL
Cross lamination.
Double Mud Draps.
load Cast
Herring Bone
Cross lamination
Wave Ripple lamination
Sand lens
Mud drops

wave ripple lamination
Cross lamination
load Cast, Mud Draps.
Cross lamination
Interbedded Brown
Clean Sand with Silty Mud
Herring Bone.
light grey Silty Sand with
Mud stone.
Wavy Ripple lamination
Mud draps, Sand lens.
Slump Structure, Sand lense

LOCALITY SHEET 14 OF 19 DATE: SCALE:

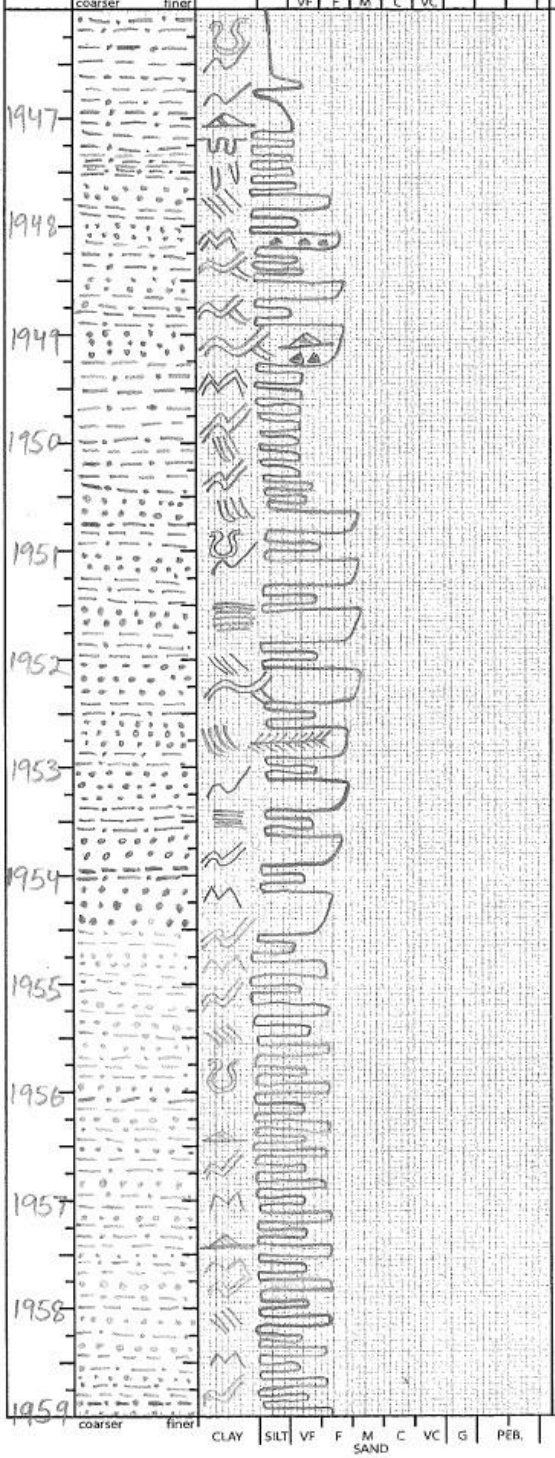

GEOLOGIST:
FORMATION: NORDMELA
AGE:

Light grey silty Sand with Mud stone. Slump

Sand lens. Mud Drop load Casts

Cross lamination, Burrows

Coal Fragments.

Wave Ripple lamination

HCL / SCL

Coal Fragments

HCL/SCL, Sand lense

wave ripple lamination

Cross lamination.

Double Mud draps

Slump Structure

Interbedded Clean Brown Sand with Black to Grey Silty Mud.

HCL/SCL, Cross lamination

Trough Cross lamination

herring Bone structure.

Mud draps, Parallel lamination

wave ripple lamination

Slump structure

Light grey to Black Silty Sand with Mud stone, slightly dipping

Parallel lamination

wave ripple lamination

Cross lamination

Double Mud draps

LOCALITY SHEET 15 OF 19 DATE: SCALE:

GEOLOGIST:
FORMATION: NORDMELA
AGE:

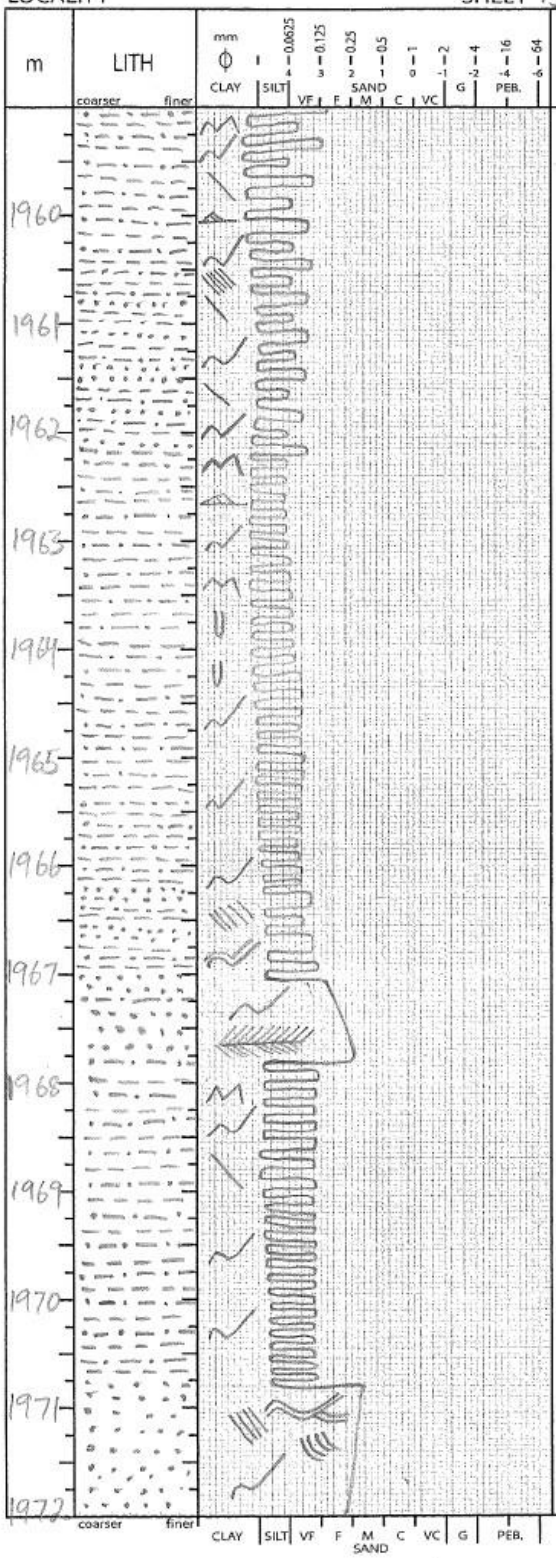

Cross lamination.
Sand lens
Thin laminated
Silty Sand and
Mudstone
Slightly dipping

Sand lens.
Thin laminated Mud
Stone and Silty Sand
Black to grey Color
Burrows.
Mud drops

Herring Bone cross lamination
Clean Brown Sand
wave ripple Lamination
Interbedded Mudstone
& Silty Sand
Slightly dipping
Mud drops.

HCL/SCL
Brown Clean Sand
Cross lamination.
Mud drap
Trough Cross Lamination.

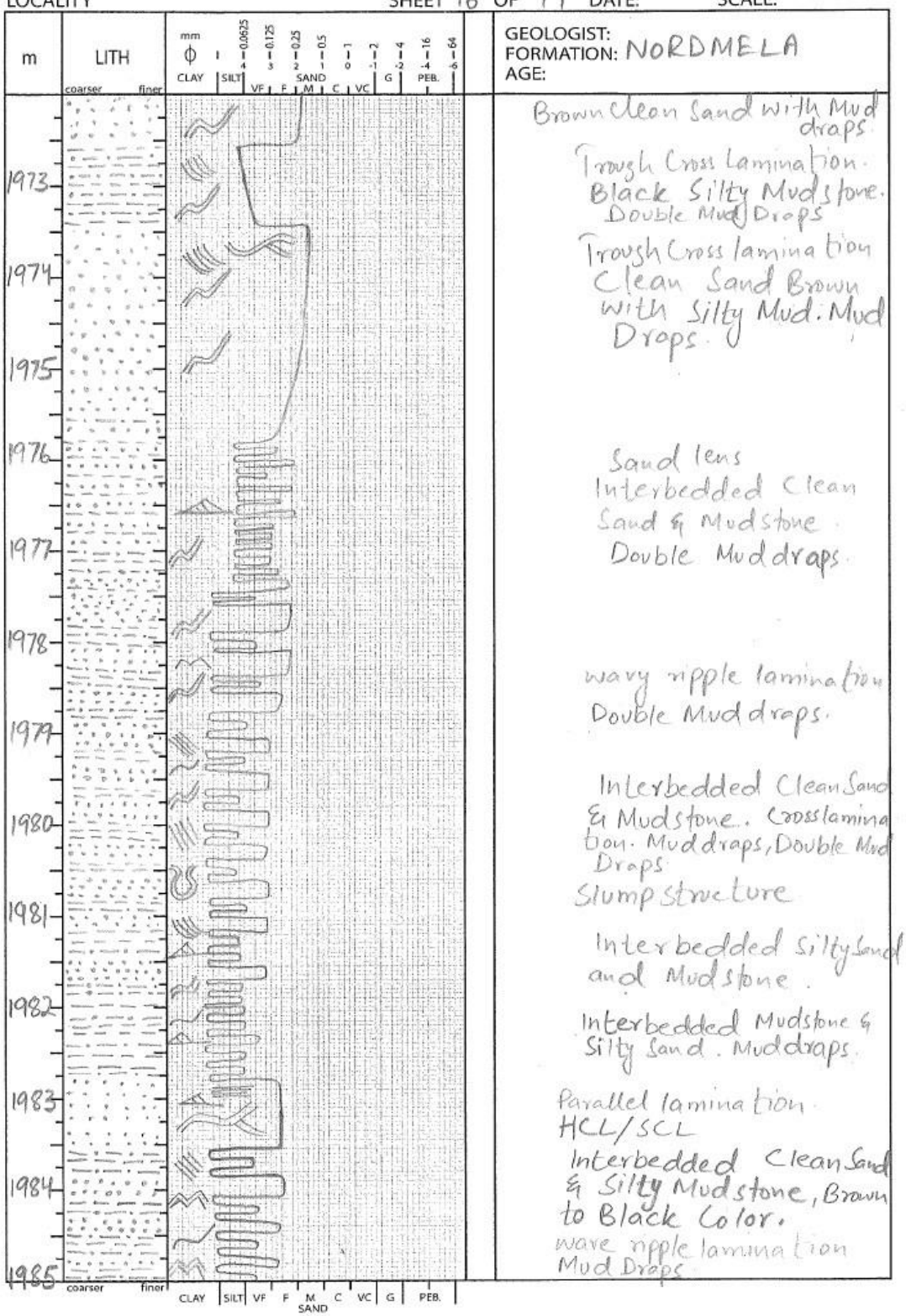
LOCALITY
SHEET 16 OF 19
DATE:
SCALE:
m
LITH
coarser
finer
mm
ϕ
CLAY
SILT
SAND
VF
F
M
C
VC
G
PEB.
GEOLOGIST:
FORMATION: NORDMELA
AGE:
1973
1974
1975
1976
1977
1978
1979
1980
1981
1982
1983
1984
1985
Brown clean Sand with Mud draps
Trough Cross lamination.
Black Silty Mudstone.
Double Mud Draps
Trough Cross lamination
Clean Sand Brown
with Silty Mud. Mud
Draps.
Sand lens
Interbedded Clean
Sand & Mudstone.
Double Mud draps.
wavy ripple lamination
Double Mud draps.
Interbedded Clean Sand
& Mudstone. Cross lamina
tion. Mud draps, Double Mud
Draps.
Slump structure
Interbedded Silty Sand
and Mudstone.
Interbedded Mudstone &
Silty Sand. Mud draps.
Parallel lamination.
HCL/SCL
Interbedded Clean Sand
& Silty Mudstone, Brown
to Black Color.
wave ripple lamination
Mud Draps

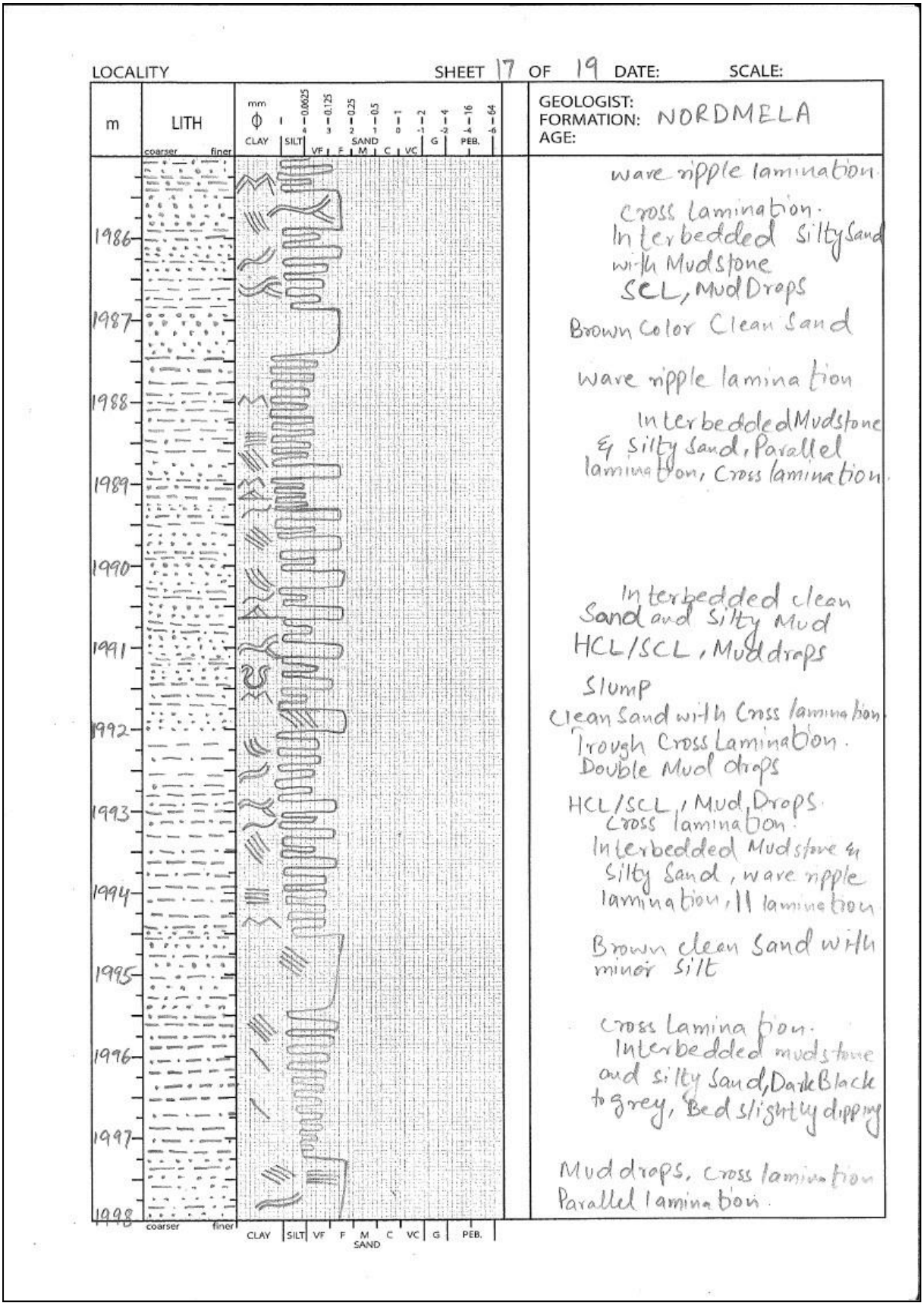
LOCALITY
SHEET 17 OF 19 DATE: SCALE:
m
LITH
coarser finer
mm
ϕ
CLAY SILT VF F M C VC G PEB.
SAND
GEOLOGIST:
FORMATION: NORDMELA
AGE:
1986
1987
1988
1989
1990
1991
1992
1993
1994
1995
1996
1997
1998
wave ripple lamination.
Cross lamination.
Interbedded Silty Sand with Mudstone SCL, Mud Drops
Brown Color Clean Sand
wave ripple lamination
Interbedded Mudstone & Silty Sand, Parallel lamination, Cross lamination.
Interbedded clean Sand and Silty Mud HCL/SCL, Mud drops
Slump
Clean Sand with Cross lamination. Trough Cross Lamination. Double Mud drops
HCL/SCL, Mud Drops. Cross lamination.
Interbedded Mudstone & Silty Sand, wave ripple lamination, II lamination
Brown clean Sand with minor Silt
Cross Lamination. Interbedded mudstone and silty Sand, Dark Black to grey, Bed slightly dipping
Mud drops, Cross lamination Parallel lamination.

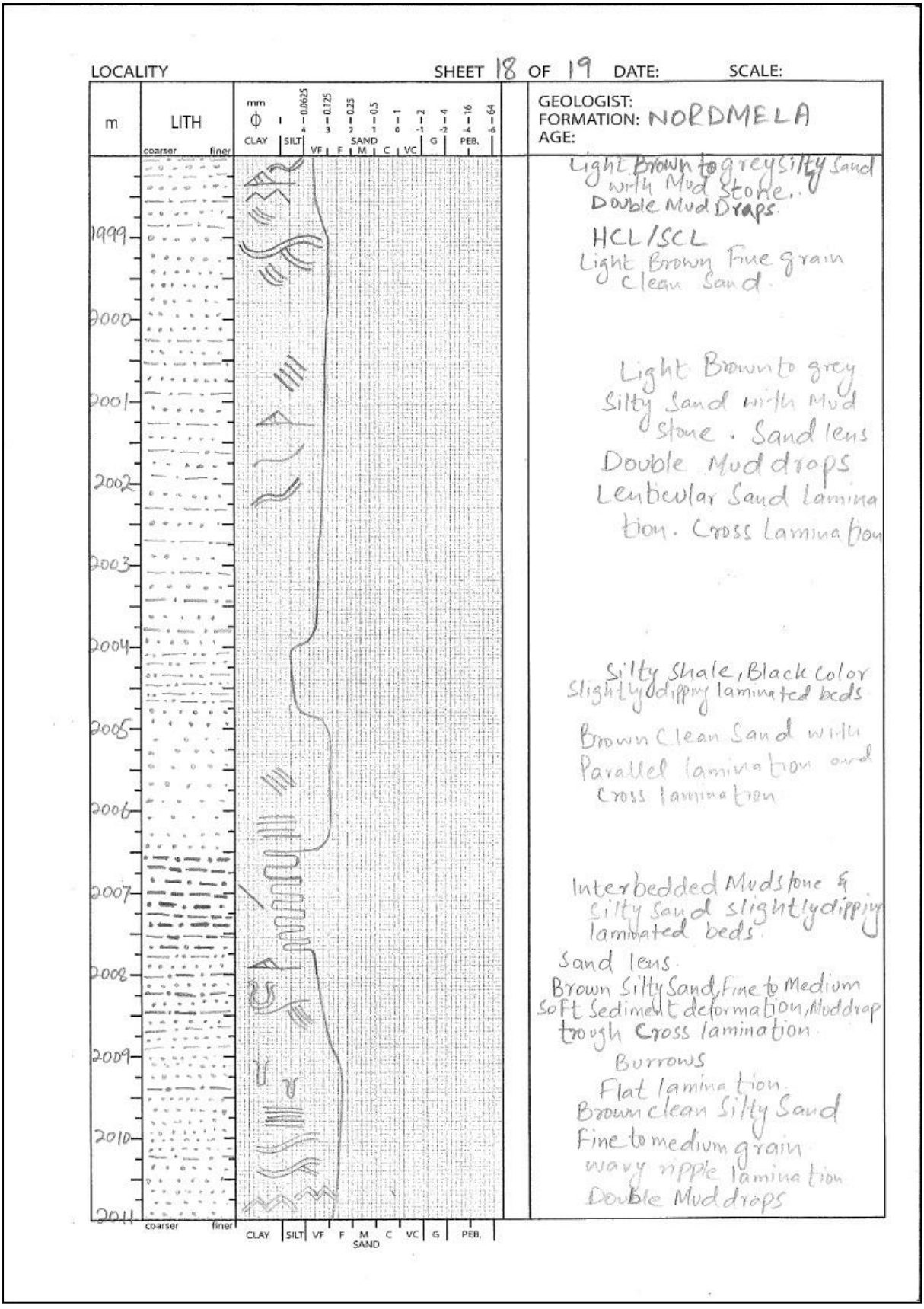
LOCALITY
SHEET 18 OF 19
DATE:
SCALE:
m
LITH
coarser
finer
mm
ϕ
CLAY
SILT
SAND
VF
F
M
C
VC
G
PEB.
GEOLOGIST:
FORMATION: NORDMELA
AGE:
1999
2000
2001
2002
2003
2004
2005
2006
2007
2008
2009
2010
2011
Light Brown to grey silty Sand with Mud Stone.. Double Mud Draps.
HCL/SCL
Light Brown Fine grain clean Sand.
Light Brown to grey Silty Sand with Mud stone. Sand lens Double Mud drops Lenticular Sand Lamination. Cross Lamination
Silty Shale, Black Color Slightly dipping laminated beds
Brown Clean Sand with Parallel lamination and Cross lamination
Interbedded Mudstone & Silty Sand slightly dipping laminated beds.
Sand lens.
Brown Silty Sand, Fine to Medium Soft Sediment deformation, Mud drop trough Cross lamination.
Burrows
Flat lamination.
Brown clean Silty Sand
Fine to medium grain
wavy ripple lamination
Double Mud drops

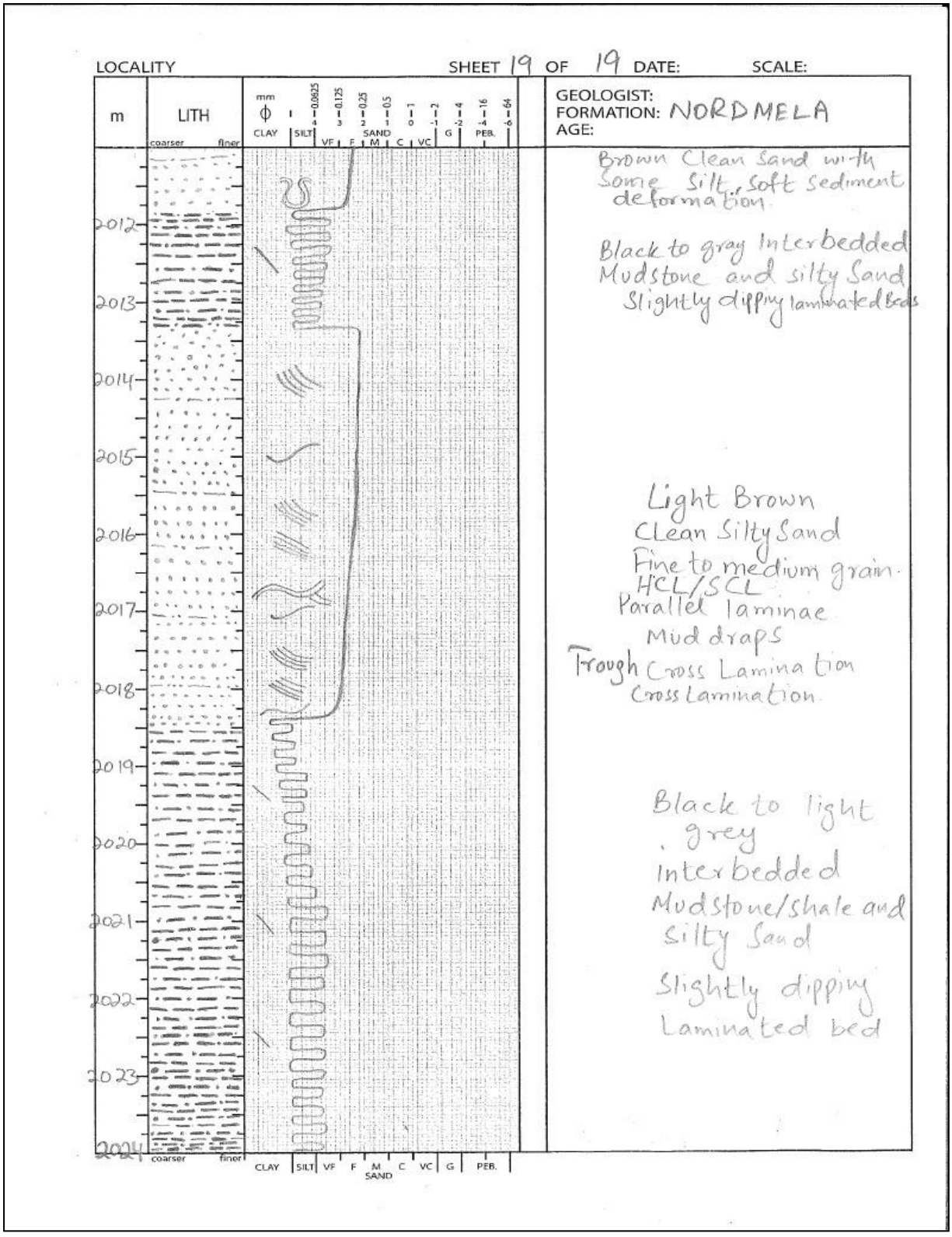

A1. Sedimentary core log of well 7220/7-1.

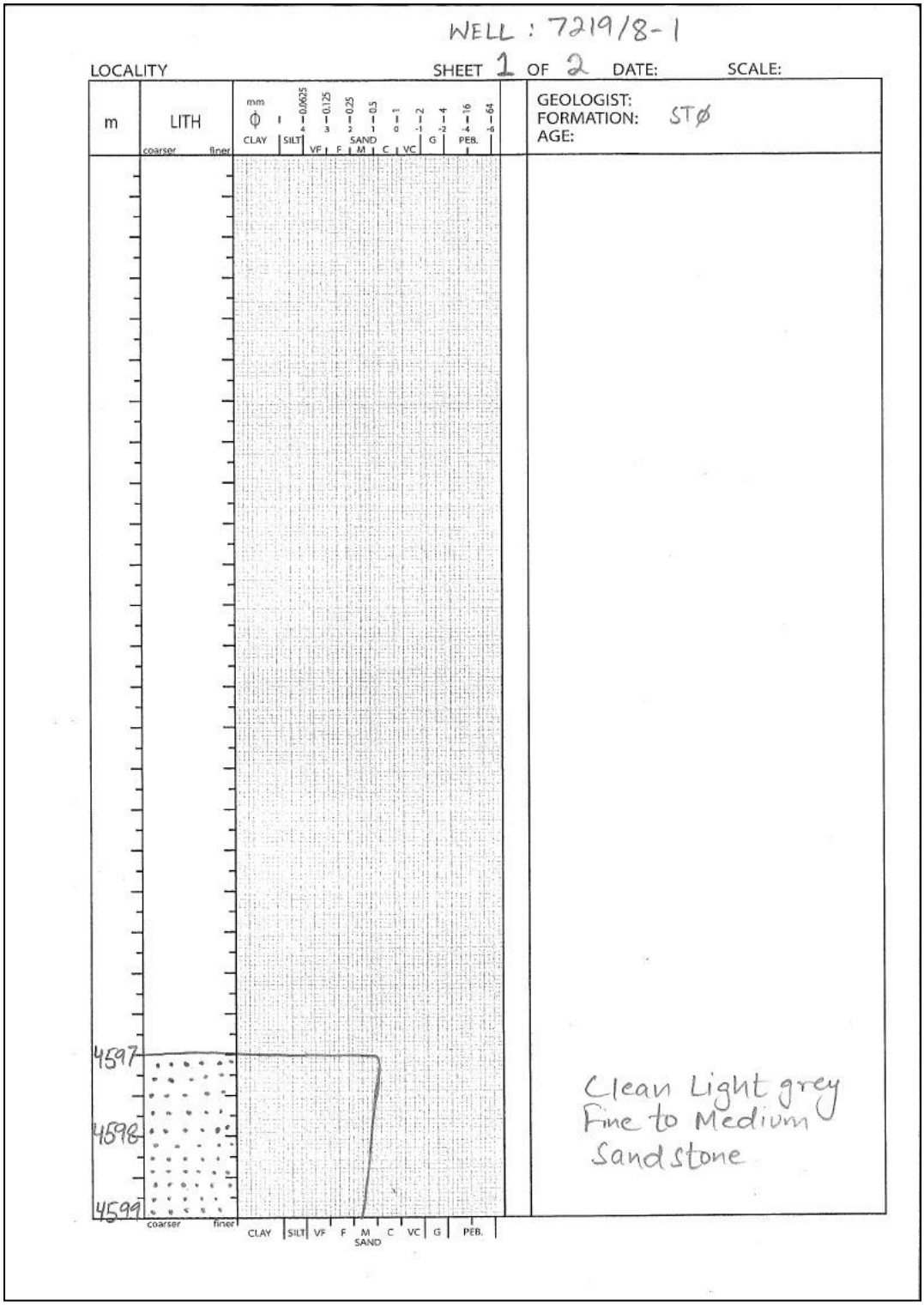
WELL : 7219/8-1
LOCALITY
SHEET 1 OF 2
DATE:
SCALE:
m
LITH
coarser
finer
mm
Φ
4
3
2
1
0
-1
-2
-4
-6
0.0625
0.125
0.25
0.5
1
2
4
16
64
CLAY
SILT
VF
F
M
C
VC
G
PEB.
SAND
GEOLOGIST:
FORMATION: STØ
AGE:
4597
4598
4599
Clean Light grey
Fine to Medium
Sandstone

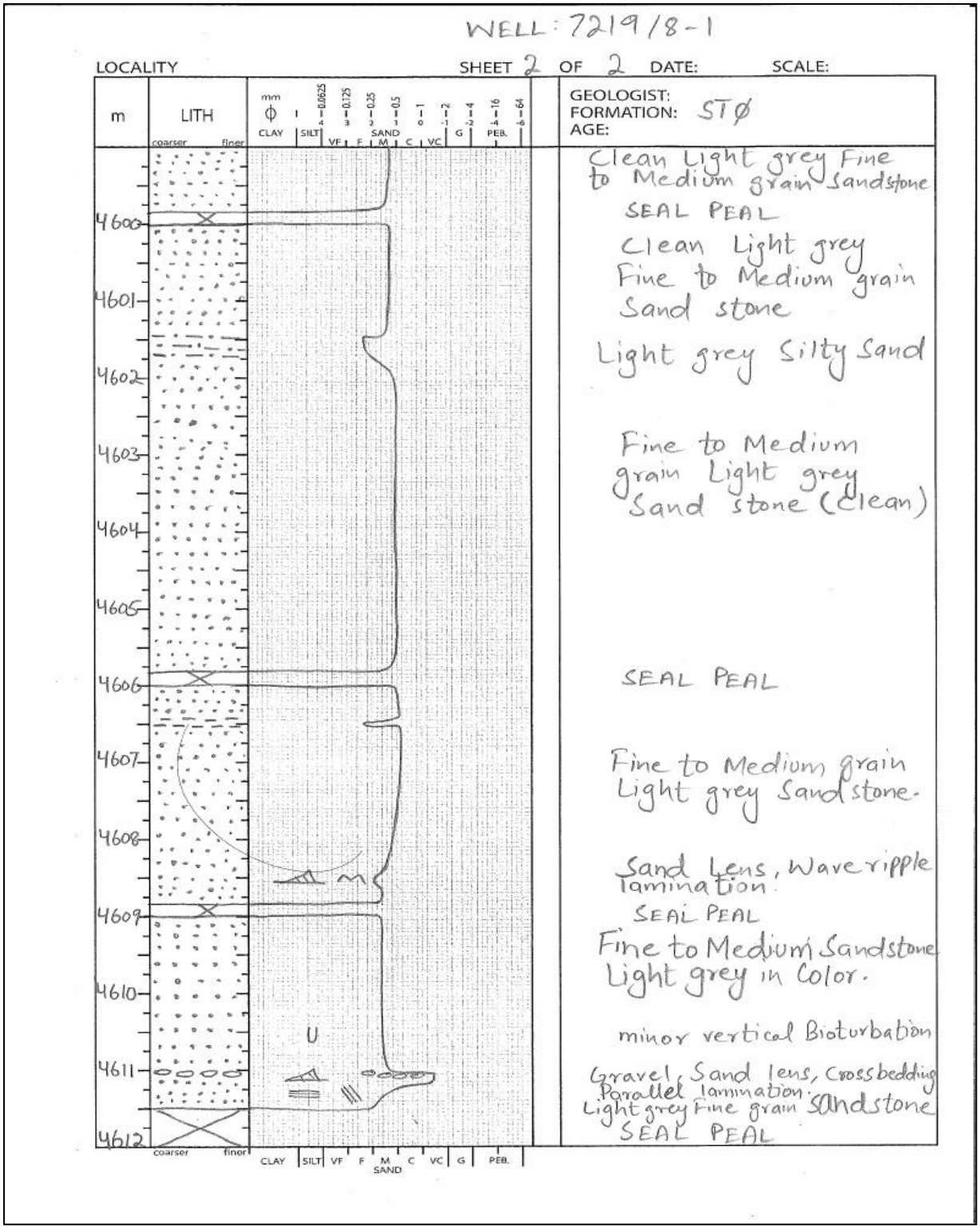

A2. Sedimentary core log of well 7219/8-1.

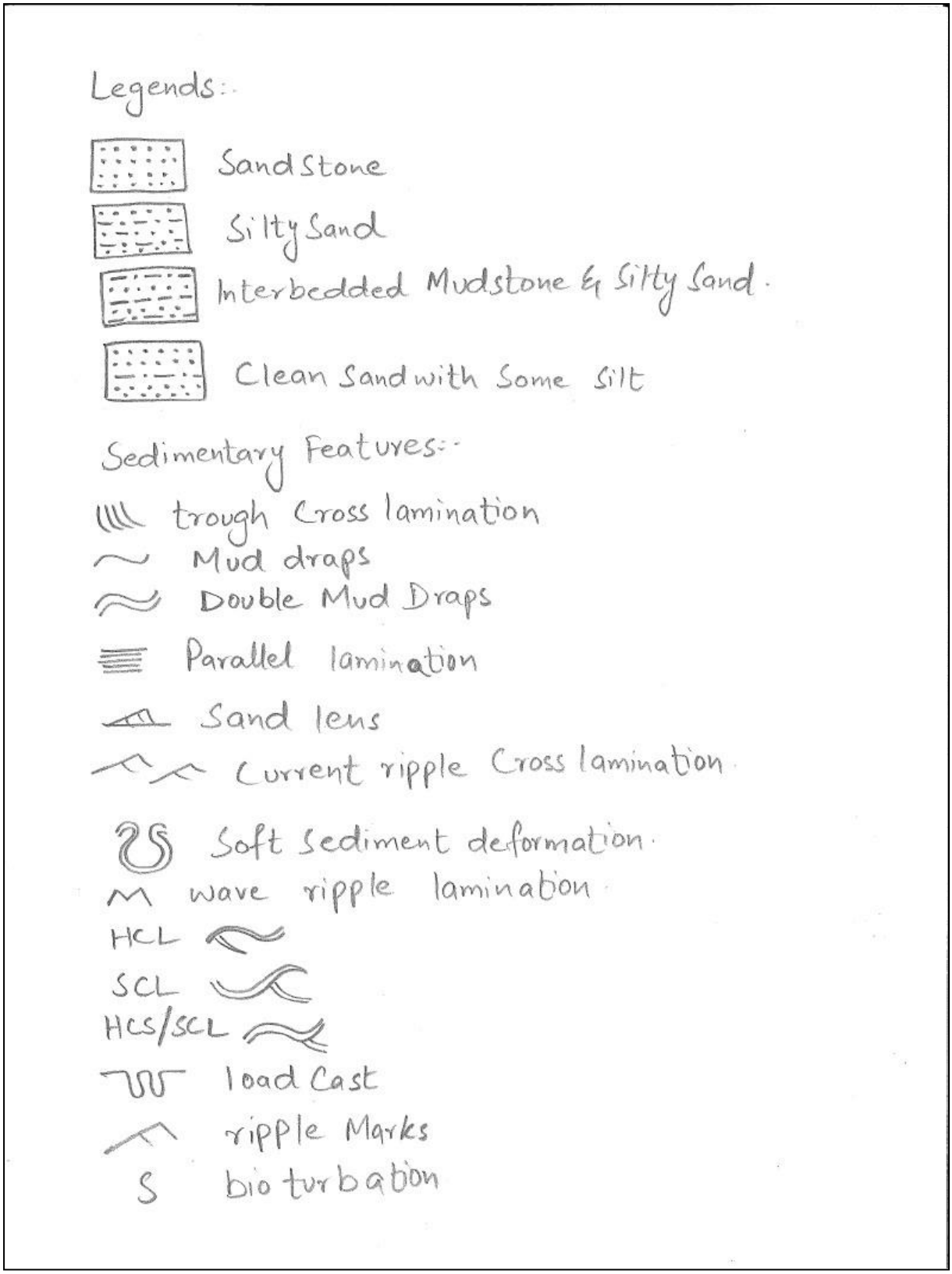

A3. Legends and sedimentary structures in sedimentary log.

Appendix B: Stylolites within Stø Formation in well 7219/8-1.

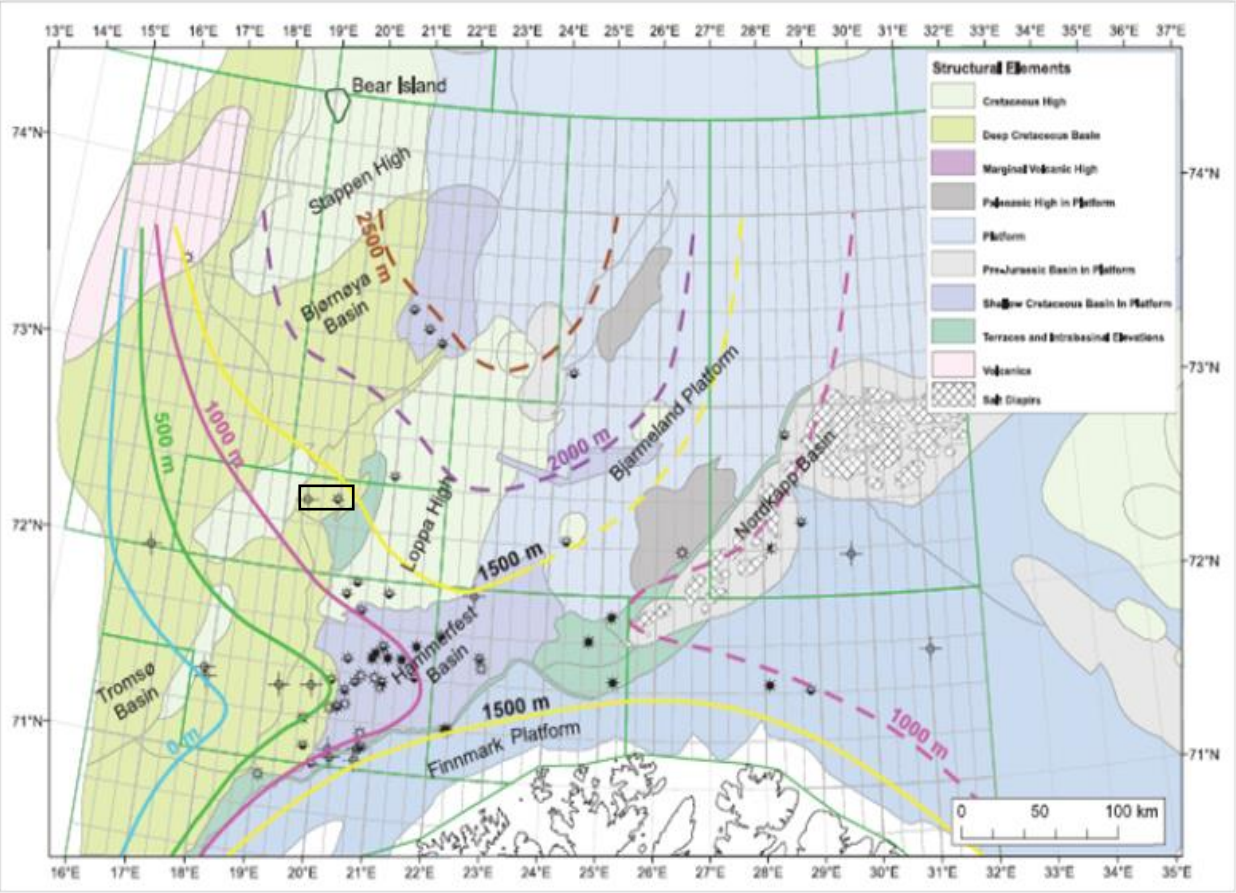

Appendix C: Experimental map showing total amount of upliftment on the basis of vitrinite data. Study area is indicated b (Ohm et al., 2008).